STUDIES OF ULTRA HIGH TEMPERATURE CERAMIC COMPOSITE COMPONENTS: SYNTHESIS AND CHARACTERIZATION OF HfO_xC_y AND Si OXIDATION IN ATOMIC OXYGEN CONTAINING ENVIRONMENTS

By

Mekha Raichie George

Dissertation

Submitted to the Faculty of the

Graduate School of Vanderbilt University

in partial fulfillment of the requirements

for the degree of

DOCTOR OF PHILOSOPHY

in

CHEMICAL ENGINEERING

AUGUST, 2008

Nashville, Tennessee

APPROVED:

Professor Bridget Rogers

Professor Clare McCabe

Professor Douglas Levan

Professor Kane Jennings

Professor Sharon Weiss

To my amazing parents, Mereen George and George Abraham Kollamana,
who instilled the value of education and selflessly supported me through my long academic career.

ACKNOWLEDGEMENTS

This work was supported through the Air Force Office of Scientific Research (contract No. FA9550-04-1-0448).

I would like to thank my advisor Dr Bridget Rogers who has shown considerable patience and bonhomie throughout my five years here. She constantly emphasized the importance of developing skills not just for my graduate career but also my future professional career and I am extremely grateful for her taking the time to do so.

I am deeply indebted to the three PIs out at SRI International, Menlo Park, CA: Dr Jochen Marschall, Dr Dusan Pejakovic and Dr Yigal Blum, for allowing me to work with them on their projects and for their mentoring during my time at SRI International.

I also had the privilege to work with a research group that always worked as a team, provided humor, warmth and considerable support. I owe a lot to Dr Robert D Geil for doing RBS runs whenever I requested and to Benjamin Schmidt for listening to my theories for hours on end and for the help with XPS. I would also like to thank Dr Zhe Song, James Burst and Nirav for their help as well.

I want to thank the following professors and students within the chemical engineering department: Dr Grant Glover and Dr Douglas Levan for the occasional loan of equipment; Dr Peter Cummings for setting up introductions with other computational scientists for the silicon oxidation work; Andrea Hafeman and Dr Scott Guelcher for the use of the SDT analysis software.

I would like to thank my committee members: Dr Clare McCabe, Dr Sharon Weiss, Dr Douglas Levan, Dr Kane Jennings, for making this happen.

Graduate School was a major networking event for me when it came to using equipment. I would like to thank: Dr Eugene Leboeuf for letting me use the SDT instrument in his lab; Rosanne Delapp, his research assistant, for being the most accommodating person I have ever worked with; Dr Richard Haglund and his graduate students Joyeeta Nag and Eugene Donev for letting me use the PLD system and providing assistance whenever I requested; Dr John Rozen in Dr Leonard Feldman's lab, for the use of the tube furnace; Dr Bo Choi for performing the annealing runs.

I am also grateful to Mark Holmes and Robin Midgett for always providing a quick, simple and innovative remedy to all my technical problems.

I want to thank Mary Gilleran and Margarita Talavera for the many conversations that helped me to unwind and temporarily forget my graduate student world, for their warmth, support and genuine care.

I would not even be in graduate school if it was not for Mr George Eapen inspiring me to take up the challenge. I am grateful to Mr Mammen Thomas, my mentor, who always offered advice and ideas, and the only member of my family who actually understands my work.

There are several people who were part of my support system and to whom I owe a lot: the Rosetta Stone group at the Blakemore United Methodist Church, Nashville, TN, and my second set of parents, Tana and John Kimbro. My best friends Nadia Hissin, Fatma Ahu Akin and Sumeetha Jacob who have been there for me through all my ups and downs.

I would not have achieved anything without my family: my brother Manoo for always providing the humor and being a calming presence, my sister Manju and brother-in-law Arun for opening up their home during my fellowship in Menlo Park and their gentle advice and constructive criticism.

All that I am and all that I have achieved today would not have been possible without my parents. My mum, who taught me to be a strong, resilient person, and my dad, who taught me to aspire for more and to remain humble and kind towards others as success is achieved. I feel honored and privileged to have parents who spent so many years, working selflessly, to provide the best for their children, without once placing their expectations on us. This degree is really for them and their hard work.

To all the people above……THANK YOU!

TABLE OF CONTENTS

Page

LIST OF TABLES

Table Page

LIST OF FIGURES

LIST OF DEFINITIONS

Active Oxidation: In this context, active oxidation regime refers to when an oxide layer is removed from a substrate surface due to evaporation of volatile by-products of oxidation. Typically occurs at low oxygen pressures and high temperatures.

Anneal: is heating a material and thus causing changes in microstructure due to elemental diffusion

Creep: is a measure of change in strain when a material is subjected to a constant stress eg. high temperatures or high pressures

Crystalline: when atoms are arranged in regular, repeating patterns in a lattice

Glass: a uniform amorphous solid produced formed when a molten material is cooled very rapidly to below its glass transition temperature, thereby not being able to form a crystal lattice.

Glass transition temperature: Temperature below which molecules in a material have little relative mobility

Hot-pressing: process of sintering reactant powders through applied pressure and heating in vacuum or inert environment.

Passive Oxidation: the formation of thin oxide layer, usually at high oxygen pressures and low temperatures, that adheres to the substrate surface. Often it prevents further oxidation of the underlying material.

Pressureless sintering: process of making powder composites by heating and applying no pressure.

Refractory: ability of a material to retain its physical shape and chemical structure after being subjected to high temperatures.

Scale: a layer of material grown atop a substrate through intermetallic diffusion or through the transport of and reaction with oxygen. The layer may not have a uniform microstructure throughout and may consist of regions of different elemental composition.

Sinter: to create a compound through heating, but not melting of the reactant powders

Sintering Aid: compounds used in sintering to enable the binding of the various metallic powders to create a dense product. Typically the sintering aid liquefies during sintering.

Spalling: to chip away or break into fragments.

Stovepipes/wormholes: void channels, not necessarily of uniform length or diameter, formed randomly through a material due to outward diffusion of gases.

UHTC: Ultra high temperature ceramic

UHTC composite: A mixture of UHTC materials

INTRODUCTION

Ultrahigh temperature ceramics (UHTC) are a class of materials being considered for reusable atmospheric re-entry vehicles, hypersonic flight vehicles and rocket propulsion [1, 2]. In these applications, the materials are subjected to high temperatures and extremely reactive and high flow environments (e.g. O, O_2). Therefore, potential material candidates have to be mechanically, chemically and thermally stable.

Currently no one material exists that have all the properties required for these applications therefore composites have to be developed. However, materials choices are limited [3]. While some candidates have proven to be more suitable than others, the underlying mechanisms by which they withstand the environment and offer protection are still not understood [4]. For other materials, the processing method and the resulting properties of the starting materials can be a major contributor to preventing or promoting some of the microscopic processes [1].

One part of the inability to find suitable materials can be attributed to the fact that most of the work has been application driven. Recent reports on the progress of research in this field indicate that only if fundamental knowledge of the behavior each material in different regimes is obtained in a systematic process, can a solution be developed.

The first part of this work primarily focuses on the Hf-C system within the UHTC class of materials. It addresses the processing challenges in the synthesis of Hf-C based films such as oxygen dissolution, particulate and void formation, non-stoichiometric and non-uniform film formation. In Chapter II we explore the diffusion and reaction characteristics of these two elements through thermal treatment in an inert environment.

In Chapter III, the formation of hafnium carbide (HfC) by pulsed laser deposition and the inherent technique parameters that need to be considered are addressed. The efficacy of thus deposited HfC as a protective coating is then explored. In Chapter IV, using the PLD technique, oxygen dissolution into the Hf-C based films are controlled and the oxidation behavior of the resulting hafnium oxycarbide layer is studied and compared to data published in literature. The results from all three parts are thus used to provide a preliminary explanation at a fundamental level about the behavior of the Hf-C system and its suitability for hypersonic environments.

In the last part, the focus shifts from material synthesis to the importance of developing theoretical models to explain the oxidation behavior, in all temperatures and gas flow regimes, of UHTC materials after synthesis. As a first step the oxidation of silicon is addressed since results from theoretical computations and isotope tracer experiments are available. In Chapter V, the data are used to develop and test the more complex model for the oxidation of silicon at high temperatures in a partially dissociated oxygen environment.

References

1. Gasch M.J., Ellerby D.T., Johnson S.M., Ultra High Temperature Ceramic Composites, Handbook of Ceramic Composites, Vol. 2, Springer, US, 2005, p. 197-224.

2. Opeka M.M., Talmy I.G., Zaykoski J.A., *Oxidation-based materials selection for 2000 °C+ hypersonic aerosurfaces: theoretical considerations and historical experience*, J. Mater. Sci., **2004**, 39, 5887-5904.

3. Schwartz, M., New Materials Processes and Methods Technology, 1st ed., CRC Press, Taylor & Francis Group, 2006, p. 77-171.

4. Bongiorno A., Forst C.J., Kalia R.K., Li J., Marschall J., Nakano A., Opeka M.M., Talmy I.G., Vashishta P., Yip S., *A perspective on modeling material in extreme environments: oxidation of ultrahigh-temperature ceramics*, MRS Bulletin, **2006**, 31, 410-418.

CHAPTER I

BACKGROUND

1.1. The Development of Ultrahigh Temperature Materials

The search for high temperature structural materials has been driven by the development of three technologies: rocket propulsion systems, atmospheric re-entry vehicles, and hypersonic flight vehicles [1]. Materials used in these three technologies are exposed to extreme temperatures (greater than 1200 °C) and oxidizing environments.

The early space shuttle orbiters, with their relatively blunt nose cone and leading edges, experience a maximum temperature of 1650 °C upon re-entry. The blunt design, however, lowers the lift-to-drag ratio, thereby reducing the maneuverability and cross-range for the vehicle during atmosphere re-entry. The sharp leading edges of the new hypersonic aircraft designs provide overall vehicle safety but lead to aerothermal heating and the bow shocks that cause the dissociation of atmospheric oxygen and nitrogen. The monoatomic species can then recombine on the surface thereby shifting the thermal and chemical equilibrium. Degradation of leading edges and control surfaces due to this highly reactive environment would negatively impact the controllability of these vehicles [2].

Currently, carbon-carbon (C/C) composites are used on the leading edges and nose caps, however these materials oxidize at temperatures as low as 400 °C [3]. Also, previous research has shown that the presence of dissociated gas molecules alter the microstructure and behavior of the materials at the high temperatures experienced in

these applications [4, 5]. Therefore, two areas of research were initiated: (1) replacement materials for the C/C composites and (2) protective coatings for the existing C/C composites, with most of the emphasis being placed on the former [1].

1.2. The Alteration of Structural Material Used

The alternative to using a protective coating is to change the type of material used for the nose caps and leading edges. A typical response to the need for low structural weight materials is to use metals. Refractory metals were found to be suitable since they have high melting points, high thermal shock resistance and low fracture toughness but they could not offer protection by themselves because they underwent active oxidation [6, 7]. However, most metals have a high catalytic efficiency. Oxides of metals were considered for oxidation barrier use, but in general they had low thermal shock resistance, low fracture toughness and poor creep resistance at elevated temperatures [6].

Applications requiring temperatures between 2200 °C and 3000 °C and reactive environments mandated the creation of composites of refractory metal and other ceramics to form an ultrahigh temperature ceramic (UHTC) composite. The approach was to create a composite of materials that individually or combined could be load-bearing, structurally supportive, and act as a thermal and oxidation barrier [8]. The broad range of materials investigated is shown in the Figure 1.1 [6].

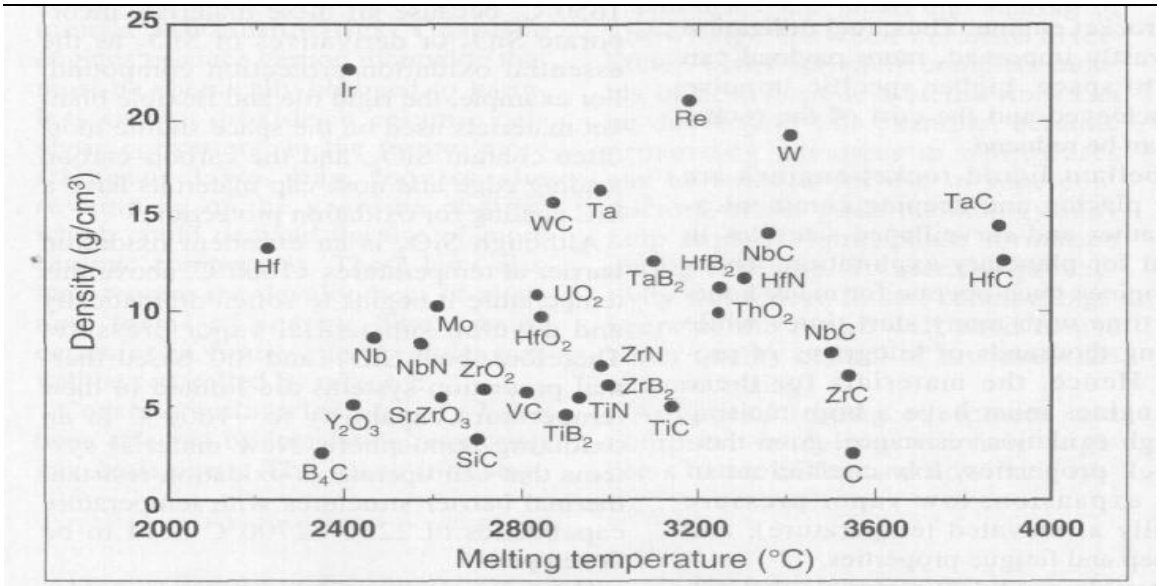

Figure 1.1: Density and melting points, compiled by Upadhya and co-workers., for the wide array of high temperature materials tested for potential use in UHTC applications [6].

1.3. Material Selection: Refractory Borides and Carbides

Figure 1.1 indicates that multiple options are available based on the thermal, chemical and physical properties necessary for these applications. However, in the last few years, it has become evident that further testing of the diboride and carbide UHTC composites was required since they showed the most potential to be used in such highly reactive, high temperature applications [7].

The very strong covalent bonding in diborides (HfB_2, ZrB_2) and the electronic nature of the boron atoms (i.e. high thermal and electrical conductivies) allow the materials to sustain high thermal loads.

Similarly, the strong bonds in the covalent carbides, eg. SiC, B_4C, which are used as additives in diboride composites, have excellent thermal and chemical stability.

Monolithic interstitial refractory carbides (HfC, ZrC) have strong carbon networks and are thus two of the most refractory binary compounds [8].

1.4. Issues Related to UHTC Fabrication and Use

The criteria for material selection were predominantly based on attaining materials of superior thermal, physical and chemical properties. Paradoxically, these same properties that made the above materials suitable presented challenges related to processing, characterization and evaluation of their performance [9].

In the fabrication of both refractory diborides and carbides, the challenges were in producing dense, uniform composites [1]. The starting powders are refractory materials of varying grain sizes therefore high thermal energy was required and the grain formation, occurrence of grain boundaries and voids have to be controlled. Oxygen contamination of the starting materials also has to be monitored in order to maintain the stoichiometry and chemical state of the UHTC required.

In these applications, materials are subjected to high temperatures and different oxidizing environments, therefore the material reaction with oxygen post fabrication is also important [1]. The material behavior varies in the different environments and, as described below, the microstructure and the phases formed in each are different. Any defect introduced in the processing stage can thus also adversely affect the high temperature and oxidation behavior of the materials.

Therefore, material fabrication and knowledge and control of its subsequent behavior in oxidizing environments are the primary interrelated challenges faced by researchers in this field.

1.5. Oxidation Behavior of UHTCs in Different Environments

1.5.1. Evaluation of oxidation resistance of diborides and their composites

Initial studies of the oxidation resistance of the transition metal diborides showed that the group IVb compounds were highly resistant to oxidation, up to 1500 °C [10]. Hafnium diboride (HfB_2) was the most resistant followed by zirconium diboride (ZrB_2) [7]. In some cases, aluminum for example, a surface oxide layer prevents further oxidation. However, in the oxidation of hot-pressed ZrB_2 and HfB_2, initially a surface layer of fluid B_2O_3 forms, which begins to vaporize rapidly at 1000 °C. Above 1400 °C the boria evaporation rate equals its formation rate [11, 12]. For HfB_2, the HfO_2 that forms is relatively compact but the evaporation of B_2O_3 creates large voids and stovepipes through the oxide layer [6].The ZrO_2 layer formed during ZrB_2 oxidation initially is not as compact as HfO_2 but eventually undergoes the same damage. At application temperatures both hafnia and zirconia are tetragonal but upon cooling to room temperature they revert to a monoclinic structure. This causes material volume changes, reducing the stability of the layer and causing more cracking and spalling to occur [11]. ZrO_2 and HfO_2 become nonstoichiometric also due to the formation of oxygen lattice vacancies under low partial pressures of oxygen, thereby increasing the rate of oxygen transport through the oxide layer [12].

Considerable research has been conducted to further improve the oxidation behavior of these materials through the inclusion of additives/reinforcing fibers. Some of the options for reinforcing fibers are shown in the diagram below (Figure 1.2) [6]. Each material proved to have disadvantages due to their inability to withstand the extreme

temperature or from having poor mechanical or other properties: (i) MgO had a high evaporation rate, (ii) BeO is toxic, (iii) Graphite and ACC-4 C/C have a high thermal resistance and a low thermal expansion coefficient but the release of CO_2 during oxidation increases the porosity of the existing and forming layers.

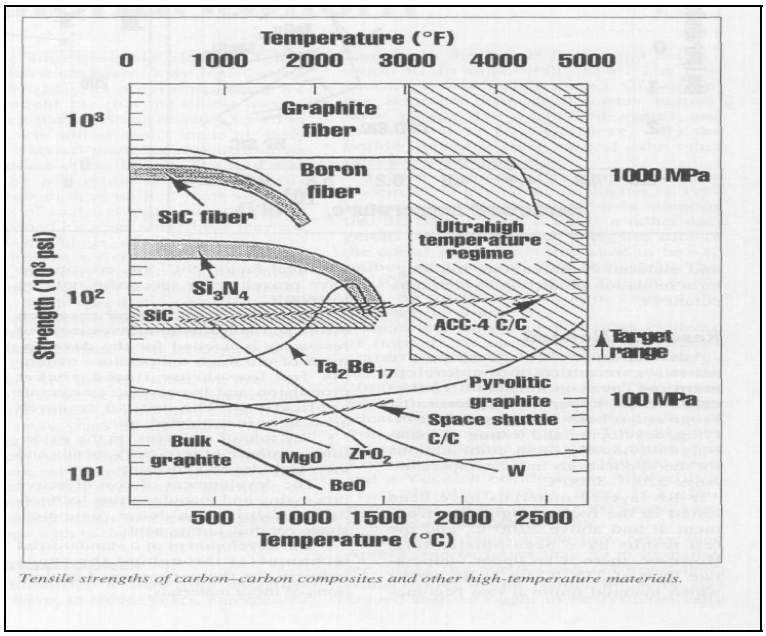

Figure 1.2: Tensile strength, at various temperatures, for fibers being considered as additives to improve oxidation resistance of refractory borides [6].

The most promising candidates were Si-based materials, primarily SiC at 20 vol% since it limits diboride grain growth during sintering [6, 13-15] and the carbon enhances thermal stress resistance [11]. Oxidation resistance is promoted through the formation of a borosilicate layer [10, 14]. However in conditions that are representative of a propulsion environment, i.e. higher oxygen pressures, the materials failed due to rapid oxygen transport rates and the phase transformations, from monoclinic to tetragonal at

1150 °C and 1650 °C respectively, of hafnia and zirconia. The protective silica that forms also softens at temperatures above 1600 °C and vaporizes creating more pores [8]. In addition, the processing of these materials is neither affordable nor reproducible and when tested under these extreme conditions there was a large scatter in mechanical property data [9, 13].

Levine and co-workers has studied the oxidation of composites of HfB_2-SiC. The composite consisted of a Zoltek Panex® 30 carbon fabric PWO6 plate with a HfB_2-AHPCS (allylhydridopolycarbosilane) coating on one side and a SiC/AHPCS coating on the other [11]. Figure 1.3 below shows the FESEM micrographs obtained, with the phases present, for both sides of the composite. The materials deteriorated through severe microcracking due to the thermal expansion coefficient mismatch between the matrix and carbon fibers. The predominant oxide formed was $HfSiO_4$ with isolated particles of SiO_2 and HfO_2. It was also evident that either a seal coat would be needed on the edges and the C/SiC side or an oxidation resistant coating for the UHTC side. These improvements, while necessary, cannot be easily identified or implemented.

1.5.2. The Importance of Dissociated Gases in the Performance of UHTC composites

Behavior of the proposed materials in molecular oxygen is just one aspect of the application. During hypersonic flight, high temperature shock waves, which have enough energy to dissociate molecular oxygen and nitrogen, form in front of the leading edges [9]. These atomic species can react with the vehicle's surfaces more readily than their molecular counterparts. If the atomic species recombine on a surface, the released energy can increase the surface temperature, again increasing the reaction kinetics.

Hence, a UHTC's performance is limited by both its catalytic recombination efficiency and by the kind of oxidant present.

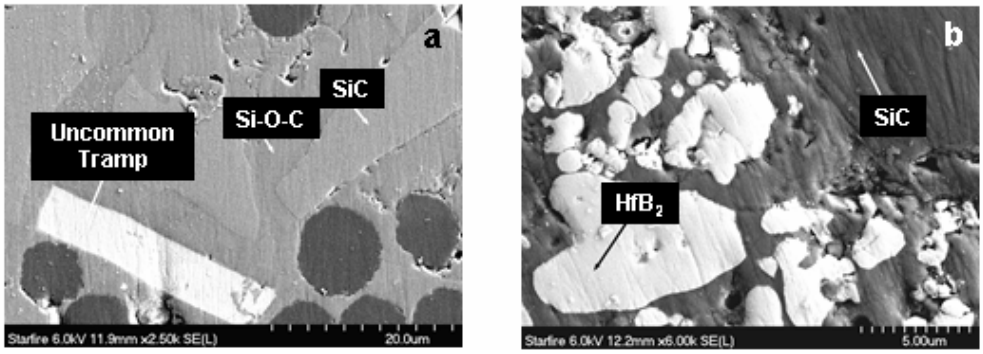

(a) (b)

Figure 1.3: A UHTC composite was created by adding a HfB_2 rich coating on one side of a carbon fiber and a C/SiC rich coating on the other. Both matrices also had an allylhydridopolycarbosilane polymer that acts a binding agent. These FESEM micrographs show the random and non-uniform phase distribution in the UHTC composite, prior to oxidation, for a) the C/SiC rich side and b) the HfB_2 rich side [11].

An enhanced oxidation rate was observed by Opila and co-workers [16] for pure SiC and Si_3N_4 which are the most common additives used in UHTC processing. It has been observed that for temperatures below 1500 °C, there is a slight difference in oxidation kinetics between SiC and Si_3N_4 due to the formation of a suboxide in the latter, but above that temperature the rates become equal again because the limiting step becomes the transport of oxygen through the silica that forms. These enhanced rates under atomic oxygen indicate possible formation of other protective layers and the possibility of a temperature range where the effect may be negligible.

Similar behavior was also observed when the silica formers are used in the UHTC composite. Preliminary oxidation studies were conducted by Marschall and co-workers

on pure spark plasma sintered HfB_2 and hot-pressed HfB_2-20vol% SiC provided by NASA Ames. The samples were run at 1250 °C for 3 hours, with and without partially dissociated oxygen, and the oxide thicknesses (compiled in Table 1.1) were determined from cross-sectional SEM micrographs. As indicated, the presence of oxygen atoms has significantly increased the oxide growth rate.

Table 1.1: Thickness of oxide formed on the diboride systems when exposed to partially dissociated oxygen environments for 3 hrs at 1250 °C.

Material system	Oxide thickness - Discharge on (μm)	Oxide thickness - Discharge off (μm)
HfB_2	25.1	13.6
HfB_2-20vol%SiC	10.3	8.7

Material behavior changes further as more atomic oxygen is present in the environment. Arc jet testing (100% dissociated oxygen gas) of the SiC reinforced Hf and Zr diborides have also been conducted to study the effect of dissociated oxygen and high heat flux onto the surface [2, 17]. For HfB_2-SiC, 3 distinct regions were identified: the substrate, a SiC depleted region and a porous surface oxide that was primarily HfO_2, while in ZrB_2-SiC an extra layer of molten SiO_2 and Zr- rich phase was detected between the outer surface and the SiC depletion region. The UHTC surface initially oxidizes to form a protective silica layer. At high conditions, the silica becomes unstable and is removed, and a refractory oxide forms. As the refractory oxide grows, there is an increase in surface catalycity and decrease in surface emittance and the surface temperature of the oxide increases. At longer times, the volatile species BO, B_2O_2 and SiO evolved and

there is continued oxidation of the SiC phase as evidenced by the SiC depleted region. The high heat flux in combination with the dissociated gases created a temperature and pressure gradient across the sample which impacted the oxidation kinetics.

The enhancement of oxidation rates in the presence of atomic oxygen does not pertain to just one material system. However, neither the role of dissociated gases nor the effect of stagnation pressure, on the diffusion and oxidation mechanisms, are understood for these model systems or their constituents. Before catalytic recombination efficiency for the composite material systems can be determined, it is imperative to obtain an extensive understanding of the mechanisms by which atomic oxygen enhances oxidation, how the kinetics differ from that for oxidation with molecular oxygen, for the individual components.

Si-based systems are an ideal starting point for our work since considerable research and models exist for the molecular oxidation of the same. These results can then be used to predict oxidation behavior of various UHTC composite systems, e.g. Hf-O-C, and to observe any differences between theory and experiment.

1.6. The Multilayer Thermal Protective Coating System

Much of the reported research done on modifying the diboride system, for example through the addition of Ta and $TaSi_2$ [12], in an attempt to improve their application potential, resulted in just a compilation of observed structural property changes. Thus far the mechanisms by which any of these changes occur or even how the oxidation process occurs have not been systematically investigated, and therefore, are not completely understood [7, 9]. For example, the very different oxidation behavior

observed between hafnium and zirconium based materials is contradictory to the theoretical claim that these two elements are chemically similar. The inconsistencies and observations made could also be attributed to the various processing methodologies used. Hot-pressing and sintering process parameters can affect the grain size, and uniformity, which are contributing factors to a material's performance. Even materials processed under the same conditions using different lots of raw materials have often resulted in composites with very different properties. In fact, samples on the test flight SHARP-B2 failed due to poor properties such as varying sized grains, defects and porosity [1]. Researchers are currently exploring non-conventional synthesis techniques such as reactive hot-pressing, pressureless sintering by liquid infiltration and reaction to address these problems, but as reported in the 2007 AFOSR workshop on UHTCs [9], most of the progress is limited by the lack of fundamental knowledge of the individual element or compound behaviors on the microscopic level and the inability to model the complex microstructure of materials synthesized from powders.

Given the complexities of replacement material fabrication through sintering and hot-pressing, a considerable interest has arisen in identifying potential protective coatings for the existing C/C composites. Coating processes, in general, are easier to control and can produce more uniform layers. An additional advantage is that using thin layers of the coatings in conjunction with the currently available characterization tools, the many dynamic thermal heating and oxidation processes can be identified and understood. This knowledge can therefore also be put forward to the bulk synthesis of the materials from powders. Also retaining the C/C composites as the main structural material is extremely

advantageous for these applications because they are stable, strong, lightweight and easy to machine.

As in the bulk replacement material studies, several technical challenges lie in identifying materials that can withstand multiple exposures to these extreme conditions. Most coatings created to protect these carbon based materials proved unsuitable at the high temperature the reactions took place at. Also, the mismatched thermal expansion coefficients created defects in the materials. One such composition was the zirconium diboride and silicon, at about a 50-weight percent basis, coating that was used on JTA-grade graphite [7]. Other additives included transition metal additions such as niobium, but while the overall oxidation resistance was improved at high temperatures, it was not so at lower temperatures [6, 7].

In line with both the thermal considerations and the reactive environments these materials are subjected to, there is only a limited selection of suitable materials available for immediate use. Also, there was no one structural material that could withstand all the different environments therefore a multilayer protection system design was proposed where the combined advantageous properties of each layer would bring about effective protection of the underlying carbon-carbon (C/C) composite.

An ideal multilayer protective system [3, 18] is described above in Figure 1.4 where each layer has a particular function. The outermost layer is the catalytic layer which reduces the recombination efficiency of dissociated gas and thus decreasing the heat absorbed into the structure. The emittance layer has a dual function, that of increasing the emittance and/or reducing the rate of oxidation. The oxidation barrier consists of the base layer and its adjacent coating that are similar in content but with a

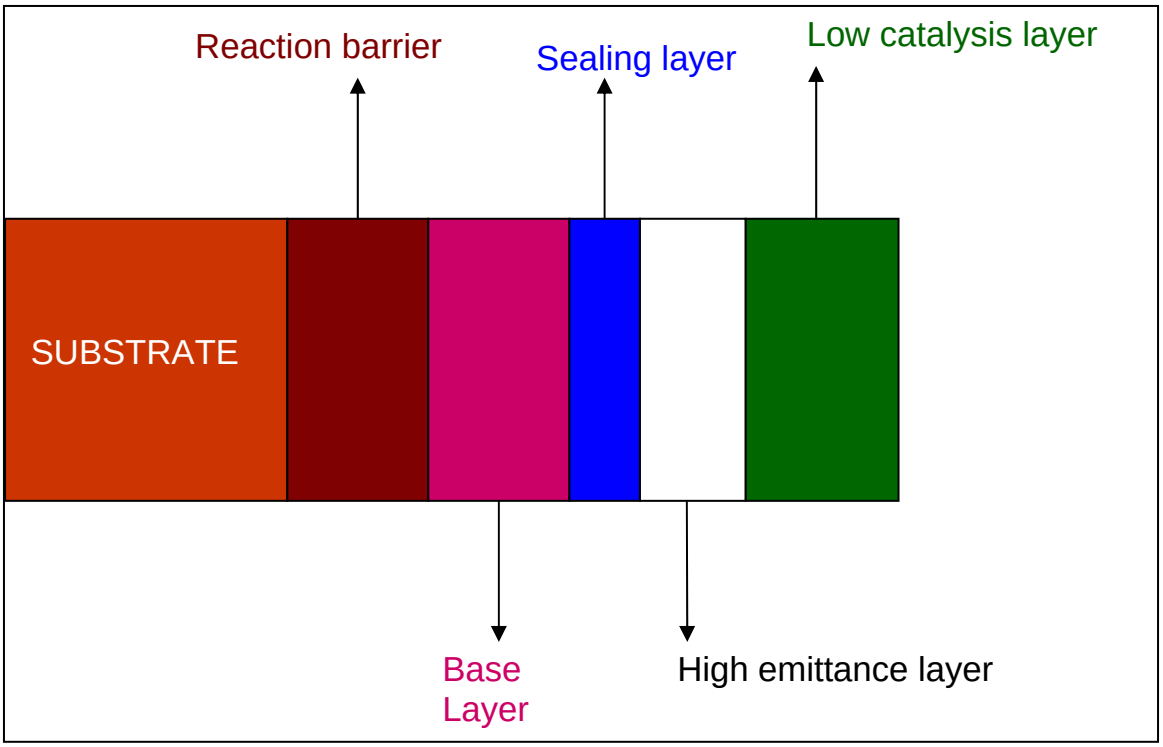

Figure 1.4: The ideal multilayer thermal protective system.

higher proportion of a low glass transition temperature phase in the latter which enables effective sealing. The reaction barrier layer can reduce the oxidation rate but mostly provides protection against reaction between the substrate and the subsequent layers.

The use of thin films helps reduce some of the thermal stress; however the inherent problem is the mismatch of the coefficient of thermal expansion between the various layers and the lack of knowledge of the material's behavior separately and as a composite in hypersonic environments. Therefore our first step in providing fundamental knowledge about the protection system was to focus on the first layer close to the C/C composite: the reaction barrier layer.

1.6.1. Evaluation of refractory carbides as a protective coating

Refractory carbides are the ideal reaction barriers for this application due to the same ideal properties, described above, that were needed for the bulk replacement composites. Additionally, the carbide acts as a diffusion barrier to carbon thereby reducing one of the inherent problems of using C/C composites at these high temperatures.

The use of refractory carbide as a potential coating was highlighted also in Black and Parekh's patent "Sublimitable Carbon-Carbon Structure for Nose tip for re-entry vehicles" [19]. In this design, the nose cap is coated in the outer and inner part with sublimitable materials with the latter sublimating at lower heat fluxes. The rate of erosion of both materials can thus be controlled and the nose cap is always maintained at the required temperature. While the inner material is to be a fluorocarbon, the choice for the outer material is partially carbonized refractory metal that would be converted completely into a carbide during atmosphere re-entry. As mentioned above, refractory carbide HfC and ZrC are the most ideal candidates and thus their oxidation behavior studies are highly relevant.

Refractory carbides, HfC and ZrC, can dissolve large quantities of oxygen into their lattice before converting into an oxide [20-22]. No long term protection against oxidation is offered because of the formation of a porous, outer oxide layer due to the evolution of CO and CO_2 gases but HfC does offer superior oxidation resistance to HfB_2 at 1440-2100 °C [7]. However, the oxide scale for HfC had a non-porous, amorphous interlayer that initially grew and then stayed at a constant thickness of a few micrometers [23]. The interlayer was an oxygen deficient oxide of hafnium with a carbon

impurity, $HfO_{2-x}C_y$, that adhered to both the underlying HfC and the outer HfO_2 forming sharp interfaces. It is hypothesized that the carbide first absorbs oxygen, and then transforms to an oxygen deficient oxide once there is insufficient oxygen to oxidize all the carbon to CO. The sharp interfaces indicate that because of the way HfC oxidizes, high interfacial vapor pressure of molecular vapor species will not disrupt the interfaces or the actual layers. This is in sharp contrast to the way hafnium diborides oxidize. Using the Danckwerts moving-boundary diffusion theory and assuming a discontinuous concentration for the diffusing species at the interfaces, it was determined that the oxygen diffusion constant was lowest for the interlayer [23]. Despite its optimal characteristics for high temperature applications, further investigation about the chemical state of this interlayer and its function as an oxygen diffusion barrier has not been conducted to date.

As with the diborides, another limitation in the use of refractory carbides lie in the processing. It has been reported [7] that the starting microstructure of the hafnium carbide is extremely important because the formation of the oxycarbide interlayer that protects the carbide from oxidation, which is the primary reason for its use in these applications, was not observed for hot-pressed or sintered samples. Studies done previously [9, 24, 25] have shown that oxygen contamination, excess carbon in the boundaries or carbon deficiencies are the common processing problems faced in coating processes. Oxygen dissolution into the carbide at the processing stage can only be beneficial if the process can be reproduced, controlled and the highly beneficial hafnium oxycarbide film is formed each time. If the oxygen atoms can easily displace the carbon atoms at the processing temperatures, then the carbides would not be of use at high temperatures and oxygen pressures because the carbide would be completely converted to an oxide.

All these processing and oxygen dissolution issues have to be addressed and understood in order for the layer to be used as a part of a multilayer system. Compared to work on diborides, the level of research on improving the refractory carbide coating processing methods and characterization pre and post oxidation is not adequate [1]. This provides several avenues for our research: (1) identifying new techniques to form hafnium carbide films that averts some of the processing challenges faced currently, (2) determining whether the carbide films can be synthesized without oxygen dissolution and (3) turning the oxygen dissolution to an advantage through the formation of oxycarbide layers and determining its efficacy as a stand-alone thermal and oxidation barrier coating.

References

1. Gasch M.J., Ellerby D.T., Johnson S.M., Ultra High Temperature Ceramic Composites, Handbook of Ceramic Composites, Vol. 2, Springer, US, 2005, p. 197-224.

2. Chamberlain A., Fahrenholtz W.G., Hilmas G.E., Ellerby D.T., *Oxidation of ZrB_2-SiC Ceramics under atmospheric and reentry conditions*, Refractories Applications Transactions, **2005**, 1(2), 1-8.

3. Schwartz, M., New Materials Processes, and Methods Technology, 1st ed., CRC Press, Taylor & Francis Group, 2006, p. 77-171.

4. Bongiorno A., Forst C.J., Kalia R.K., Li J., Marschall J., Nakano A., Opeka M.M., Talmy I.G., Vashishta P., Yip S., *A perspective on modeling material in extreme environments: oxidation of ultrahigh-temperature ceramics*, MRS Bulletin, **2006**, 31, 410-418.

5. Rogers B.R., Song Z., Marschall J., Queralto N., Zorman C.A., The effect of dissociated oxygen on the oxidation of Si, polycrystalline SiC and LPCVD Si_3N_4, High Temperature Corrosion and Materials Chemistry V, The Electrochemical Society Proceedings Series, Pennington, New Jersey, 2005.

6. Upadhya K., Yang J.M., Hoffman W.P., *Materials for ultrahigh temperature structural applications.* Am. Ceram. Soc. Bull., **1997**, 76(12), 51-56.

7. Opeka M.M., Talmy I.G., Zaykoski J.A., *Oxidation-based materials selection for 2000 °C + hypersonic aerosurfaces: theoretical considerations and historical experience*, J. Mater. Sci., **2004**, 39, 5887-5904.

8. Pierson, H.O., Handbook of refractory carbides and nitrides: properties, characteristics, processing, and applications, Noyes Publications, Park Ridge, New Jersey, 1996.

9. Fahrenholtz W.G., Hilmas G.E., NSF-AFOSR joint workshop on future ultra-high temperature materials, National Science Foundation, Arlington,VA, 2004, p. 1-34.

10. Monteverde F., Bellosi A., *Oxidation of ZrB_2-based ceramics in dry air*, J. Electrochem. Soc., **2003**, 150(11), B552-B559.

11. Levine S.R., Opila E.J., Robinson R.C., Lorincz J.A., Characterization of an ultra-high temperature ceramic composite, National Aeronautics and Space Administration, Glenn Research Center, Cleveland, Ohio, 2004, p. 1-20.

12. Levine S.R., Opila E.J., Tantalum addition to zirconium diboride for improved oxidation resistance, National Aeronautics and Space Administration, Glenn Research Center, Cleveland, Ohio, 2003, p. 1-13.

13. Levine S.R., Opila E.J., Halbig M.C., Kiser J.D., Singh M., Salem J.A., *Evaluation of ultra-high temperature ceramics for aeropropulsion use*, J. Euro. Ceram. Soc., **2002**, 22, 2757-2767.

14. Monteverde F., Bellosi A., *Microstructure and properties of an HfB_2-SiC composite for ultra-high applications*, Adv. Eng. Mater., **2004**, 6, 331-336.

15. Tripp W.C., Davis H.H., Graham H.C., *Effect of SiC addition on the oxidation of ZrB_2*, Cer. Bull., **1973**, 52, 612-616.

16. Ogbuji L., Opila E.J., *A comparison of the oxidation kinetics of SiC and Si_3N_4*, J. Electrochem. Soc., **1995**, 142(3), 925-930.

17. Gasch M.J., Ellerby D.T., Irby E., Beckman S., Gusman M., Johnson S., *Processing, properties and arc jet oxidation of hafnium diboride/silicon carbide ultra high temperature ceramics*, J. Mater. Sci., **2004**, 39, 5925-5937.

18. Bird R.K., Wallace T.A., Sankaran S.N., *Development of protective coatings for high-temperature metallic materials*, J. Spacecr. Rockets, **2004**, 41(2), 214-220.

19. Black W.E., Parekh E.M., (Lockheed Corporation, USA), Sublimitable carbon-carbon structure for nose tip for re-entry space vehicle, US Patent 5,413,859, May 9, 1995.

20. Constant K., Kieffer R., Ettmayer P., *On the pseudo-ternary system 'HfO'-HfN-HfC,* Monatsh. Chem., **1975**, 106, 973-981.

21. Barnier P., Thevenot F., *Synthesis and hot-pressing of single phase ZrC_xO_y and two-phase ZrC_xO_y-ZrO_2 materials*, Int. J. High Technol. Ceram., **1986**, 2, 291-307.

22. Berkowitz-Mattuck J.B., *High temperature oxidation: IV. zirconium and hafnium carbides,* J. Electrochem. Soc., **1967**, 114(10), 1030-1033.

23. Bargeron C.B., Benson R.C., Jette A.N., Phillips T.E., *Oxidation of hafnium carbide in the temperature range 1400-2060 °C,* J. Am. Ceram. Soc., **1993**, 76(4), 1040-1046.

24. Teghil R., Santagata A., Zaccagnino M., Barinov S.M., Marotta V., De Mari G., *Hafnium carbide hard coatings produced by pulsed laser ablation and deposition*, Surf. Coat. Technol., **2002**, 151-152, 531-533.

25. Spatenka P., Suhr H., Erker G., Rump M., *Formation of hafnium carbide thin films by plasma enhanced chemical vapor deposition*, Appl. Phys. A, **1995**, 60(3), 285-288.

CHAPTER II

ANNEALING BEHAVIOR OF HAFNIUM FILMS ON GRAPHITE IN THE TEMPERATURE RANGE 500-1045 °C

Introduction

At present reinforced carbon-carbon (C/C) composites are used for the nose caps and wing edges of hypersonic vehicles. C/C composites are materials systems where the fiber and matrix are composed of different forms and compositions of carbon. They typically combine the excellent properties of graphite, i.e. good electrical conductivity, high thermal conductivity, chemical inertness, and the mechanical strength of carbon fibers [1].

However, the reinforced C/C tends to oxidize at temperatures as low as 400 °C [1] and therefore its application is limited. Suitable films to protect the C/C composites and prevent carbon diffusion have been narrowed down for all temperatures of use. For temperatures below 1800 °C, inclusion of silicon and boron into the materials suffice due to the formation of a protective glassy borosilicate layer that prevents the oxidation of the C/C composite. However, above 1800 °C a multilayer protection system is necessary due to the evaporation of the glassy layer at these temperatures. Narrowing down all the available candidates, based on chemical compatibility and thermal stability, researchers proposed that a refractory carbide as the initial coating would work as a carbon barrier since carbon diffuses slowly in a refractory carbide and as an oxygen barrier since it forms a protective oxycarbide layer [1]. The type of refractory carbide used is also important. Of all the refractory carbides, hafnium carbide has the highest melting point of

3890 °C [2]. Therefore, obtaining knowledge of how to form a hafnium carbide thermal barrier coating for C/C composites is highly beneficial.

While several physical vapor deposition techniques, such as sputter deposition and chemical vapor deposition [2], exist for the formation of hafnium carbide coatings, a cost-effective method is highly advantageous. Studies on the heat treatment of niobium films on amorphous carbon and graphite have shown the possibility of carbide formation through solid state reactions in the temperature range of 400-1000 °C [3]. Since the bonding energies of NbC and HfC are comparable at 16.62 eV and 16.45 eV respectively [2], the formation of hafnium carbide should be possible through a similar method. In addition, Leroy and co-workers [4] have shown that hafnium carbide can be formed at temperatures as low as 710 °C by the annealing of amorphous hafnium and amorphous carbon layers. Forming a carbide through solid state reactions is also beneficial for eliminating any surface defects of the C/C composite [1].

No data are currently available on the possible formation of hafnium carbide at low temperatures from solid state reaction of hafnium thin films and bulk carbon substrates. Since graphite is often a major component of C/C composites [1], starting with studies on graphite substrates is a logical first step. The films were annealed for varying annealing temperatures and times for both bare hafnium and hafnium capped with amorphous silicon nitride that served as an oxygen diffusion barrier. The surface chemical state and the bulk composition were determined by x-ray photoelectron spectroscopy (XPS) and Rutherford backscattering spectrometry (RBS) respectively.

Experimental Setup

Film deposition and annealing

The graphite substrates (1" x 1/16") were purchased from Ernest F. Fullam Inc. The pre-polished side of the carbon planchet was polished further using a 600 mesh SiC paper to reduce the surface roughness. After polishing the substrates were ultrasonically degreased and cleaned in de-ionized water.

The hafnium films were deposited at the Microelectronics Research Center at the University of Texas, using a magnetron sputter system from KJL. A pure hafnium target was sputtered in argon (20 sccm) at a pressure of 30 mTorr, an input power of 30 W and current of 0.2 A. The substrate was kept at room temperature during the 40 minute process to deposit 1000 Å of the hafnium film.

The amorphous silicon nitride capping layers were deposited using a Trion Orion II plasma enhanced chemical vapor deposition reactor. The deposition was done under a pressure of 750 mTorr and a power of 50 W. The reactant gases used were silane and nitrogen with flowrates of 100 sccm and 120 sccm, respectively. The substrate was heated to 300 °C. The thickness of the silicon nitride layers, as determined by spectroscopic ellipsometry, was 123 nm.

For temperatures up to 900 °C, the samples were annealed to the temperature of interest at a ramp rate of 1 °C/min using an induction heater in a vacuum chamber. For the higher temperature of 1045 °C a tube furnace was used. The switch was done due to the limits of the substrate heater in the vacuum system. Annealing times from 30 to 60 minutes were used.

Film characterization

Microstructural analyses of the samples were performed using a Scintag X_1 θ/θ thin film X-ray diffractometer (XRD) with a Cu $K\alpha$ radiation.

The surface composition was determined through XPS analysis performed in a PHI 5000 Versaprobe using a monochromatic Al $K\alpha$ X-ray.

Bulk composition information was obtained from RBS data collected using 2 MeV He+ produced by a Van de Graaf accelerator. RBS spectra were collected pre- and post annealing at the same spot on the sample.

Results

Despite the deposition of the hafnium film in a vacuum system there was oxygen contamination within the film. The oxygen was distributed uniformly throughout the hafnium film as determined by RBS. During annealing, the residual oxygen present in the vacuum system diffused into the film thereby oxidizing the film further as seen by the decrease in the hafnium signal and the corresponding increase in the oxygen signal in the RBS spectra, for the pre and post annealed samples, in Figures 2.1 and 2.2. Computation of the hafnium to oxygen signal ratio value from the RBS spectra indicates the formation of hafnia.

The conversion to hafnia was seen at temperatures as low as 500 °C. The XRD spectrum (Figure 2.3) obtained from the film annealed at 500 °C for 30 minutes shows only HfO_2 and graphite peaks.

The conversion of the hafnium thin films to hafnia prevented the formation of hafnium carbide. However, the formation of a hafnium oxycarbide layer, i.e. free carbon

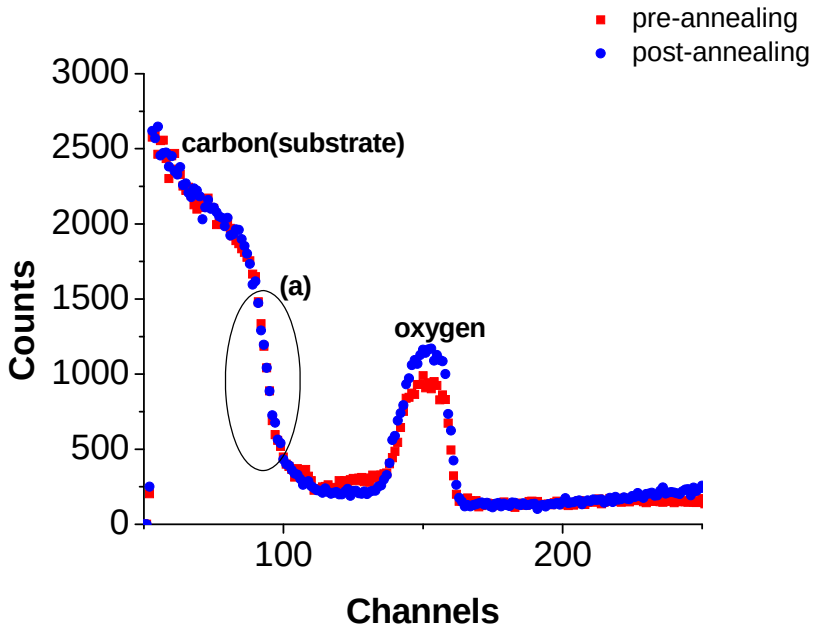

Figure 2.1: The RBS spectra with the C and O signals from the as-deposited Hf-C couple and after annealing at 900 °C for 30 min.

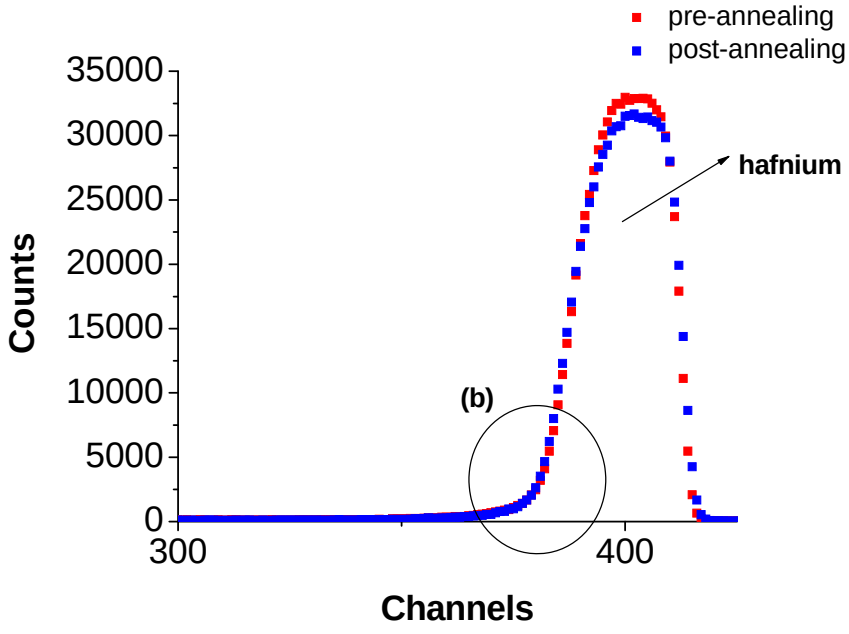

Figure 2.2: The RBS spectra with the Hf signals from the as-deposited Hf-C couple and after annealing at 900 °C for 30 min.

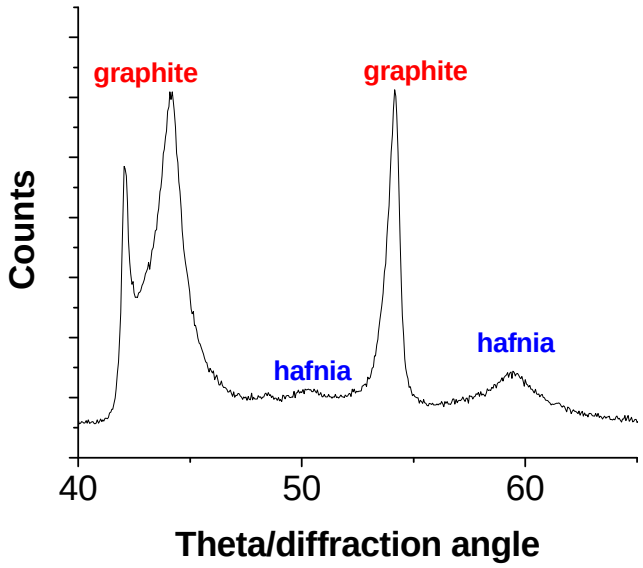

Figure 2.3: The XRD spectra for the Hf-C binary couple annealed at 500 °C for 30 minutes.

dissolved in hafnia, would also have been beneficial since theory indicates that the oxycarbide is a better oxidation barrier than either hafnium carbide or hafnia [5-9]. Analysis of the RBS spectra however shows that an oxycarbide layer did not form either since no intermixing occurred between the two layers. The region (a) in Figure 2.1 is the front edge of the carbon signal, while region (b) in Figure 2.2 is the back edge of the hafnium signal. Superimposing the spectra for the pre and post annealed samples show that no changes in region (a) and (b) are observed after annealing. If there had been intermixing between the layers, the back edge of the hafnium signal would have extended to lower channels. In the same way, if any carbon had diffused into the hafnium layer, an additional carbon peak would have been observed in region (a).

The RBS spectra (not shown here) for the annealed hafnium-graphite samples with the additional silicon nitride layer, were not different from those obtained for the

bare films except for the inclusion of the silicon and nitrogen signals. These results indicate that the diffusion of more oxygen through the film during annealing was prevented.

The front edge of the carbon signal and the back edge of the hafnium signal were analyzed in the RBS spectra collected from the capped samples. For the temperature range of 500-1045 °C no intermixing occurred between either the hafnium-silicon nitride interface or the hafnium-carbon interface. Also, no carbon was observed within the hafnium film. Both results indicate that even at these high temperatures, no carbide was formed at the hafnium-carbon interface.

Discussion

Three hypotheses are put forward for the lack of carbide formation in the annealing of a hafnium-graphite couple.

(i) The Gibbs free energies for formation of hafnia and hafnium carbide at these temperatures indicate that hafnium has a higher affinity to react with oxygen than carbon [10] therefore the diffusion of the former to the hafnium-graphite interface would inhibit the formation of the carbide. Hafnia can react with carbon to form hafnium carbide only at temperatures higher than 1000 °C and if excess carbon is present [11].

(ii) Despite the heat of formation and bond energy of hafnium carbide being lower than that for niobium carbide [2], niobium carbide could be formed from a niobium-graphite couple through annealing within the temperature range of 400-1000 °C. This suggests that the thermal energy supplied to the hafnium film may not have been high enough to induce a reaction.

(iii) In previous studies of metal-carbon interactions, the lack of carbide formation was explained by low diffusion rate of carbon in the metal [12]. Previous studies [13] have shown that the carbon diffusivity (cm^2/sec) in α-Hf metal is:

$$D_\alpha = 74\exp(-\frac{74600}{RT}) \qquad [1]$$

However, equation [1] did not hold true for carbon diffusion in amorphous hafnium films for the temperature range studied in these experiments. XPS analysis of the surface confirmed that for the 500-1045 °C temperature range, no carbon diffused to the silicon nitride/ambient interface or the hafnium/silicon nitride interface. This result was consistent even after sputtering the films in the XPS system.

However, while no carbon was detected in the hafnium films, carbon atom mobility was observed during annealing. Profilometer measurements of annealed bare graphite showed that as the temperature was increased, the surface roughness increased. This was attributed to the inherent problems of graphite substrates; the loosely bound grains and the weakening of the structure and defect formation due to the initial mechanical and chemical polishing done to reduce the surface roughness. This increase in the carbon roughness was also observed at the interface of the hafnium-graphite couple but no carbon diffused into the hafnium film. Therefore, another explanation for the lack of carbide formation is that the thermal energy supplied during annealing is used to reduce the grain defects in the graphite rather than to induce carbon diffusion into the hafnium or a reaction between the two materials.

Conclusions

The thermal treatment of a hafnium-graphite couple was studied for both a bare hafnium layer and a capped hafnium layer. Without a capping layer, the hafnium film oxidized by reaction with oxygen that had diffused into the film during the film deposition and the residual oxygen present in the chamber. Using a capping layer prevented further oxidation of the hafnium film, however oxygen was still detected within the hafnium films.

Both XPS and RBS results indicate that for the temperature range studied, 500-1045 °C, no interfacial carbide reaction occurred. The formation of the more protective hafnium oxycarbide layer from the thermal treatment of hafnium films converted to hafnia and graphite was not possible either. The lack of both reactions occurring could be due to a combination of (1) low thermal energy that could not induce a reaction between hafnium and polycrystalline graphite, (2) the presence of oxygen in the hafnium film, and (3) the hafnium-carbon interface roughness. Therefore a solid state reaction approach to forming the hafnium carbide protective layer on C/C composites is not feasible at low temperatures.

References

1. Schwartz M., New Materials Processes, and Methods Technology, 1st ed., CRC Press, Taylor & Francis Group, 2006, p. 77-171.

2. Pierson H.O., Handbook of refractory carbides and nitrides: properties, characteristics, processing, and applications, Noyes Publications, Park Ridge, New Jersey, 1996.

3. Barzilai S., Raveh A., Frage N., *Annealing of niobium coatings deposited on graphite*, Vacuum, **2005**, 79, 171-177.

4. Leroy W.P., Detavernier C., Van Meirhaeghe R.L., *Thin film solid-state reactions forming carbides as contact materials for carbon-containing semiconductors*, J. Appl. Phys., **2007**, 101, 0537141-05371410.

5. Shimada S., Yunazar F., *Oxidation of hafnium carbide and titanium carbide single crystals with the formation of carbon at high temperatures and low oxygen pressures*, J. Am. Ceram. Soc., **2000**, 83(4), 721-728.

6. Bargeron C.B., Benson R.C., Jette A.N., Phillips T.E., *Oxidation of hafnium carbide in the temperature range 1400-2060 °C*, J. Am. Ceram. Soc., **1993**, 76(4), 1040-1046.

7. Shimada S., Inagaki M., *Oxidation kinetics of hafnium carbide in the temperature range of 480° to 600 °C*, J. Am. Ceram. Soc., **1992**, 75(10), 2671-2678.

8. Shimada S., *Interfacial reaction on oxidation of carbides with formation of carbon*, Solid State Ionics, **2001**, 141-142, 99-104.

9. Shimada S., *A thermoanalytical study on the oxidation of ZrC and HfC powders with formation of carbon*, Solid State Ionics, **2002**, 149, 319-326.

10. Wang C.R., Yang J.M., Hoffman W., *Thermal stability of refractory carbide/boride composites*, Mater. Chem. Phys., **2002**, 74(3), 272-281.

11. Vodop'yanov A.G., Kozhevnikov G.N., Baranov S.V., *Interaction of refractory metal oxides with carbon*, Russian Chemical Reviews, **1988**, 57(9), 810-823.

12. Sinclair R., Itoh T., Chin R., *In-situ TEM studies of metal-carbon reactions*, Microsc. Microanal., **2002**, 8, 288-304.

13. Meshcheryakov G.Y.A., Andriyevskiy, Zagryazkin V.N., *Diffusion of carbon in hafnium*, Fiz. Metal. Metalloved., **1968**, 25(1), 189-191.

CHAPTER III

CHARACTERIZATION AND QUALITY OF $HfC_x(O)$ FILMS PRODUCED BY PULSED LASER DEPOSITION

Introduction

Refractory borides have been considered the prime replacement candidates for the structural materials used in hypersonic vehicles. However, oxidation studies of these materials indicate that even with the inclusion of additives and innovative processing techniques they cannot completely replace the existing materials. An alternative suggestion has been to create a multilayer protection system for the existing structural C/C composite materials [1]. In the multilayer system, refractory carbides have been proposed as the first layer of coating since they can also function as a barrier to carbon diffusion from the C/C substrate to the layers in the protection system. Hafnium carbide is an ideal candidate since it is the most refractory binary compound, having a high melting point of 3890 °C. The carbide also forms an oxycarbide layer during oxidation that appears to be an efficient oxygen diffusion barrier and prevents further oxidation of the underlying carbide [2-4]. These properties are highly beneficial towards its function as a protective coating and therefore focus on forming hafnium carbide coatings is needed.

All the coating deposition techniques studied previously produced films that are unsuitable as protective coatings since either HfC was produced with either carbon vacancies or oxygen inclusion or the films had non-uniform properties. The preparation of hafnium carbide thin films by plasma enhanced chemical vapor deposition of bis (η-

cyclopentadienyl) dimethylhafnium [5] and inductively coupled plasma assisted magnetron sputtering [6] produced contaminated, non-stoichiometric films with grain formation and carbon rich grain boundaries. These results indicate that an alternative technique for producing hafnium carbide films is much needed.

In this work, the results on the pulsed laser deposition (PLD) of amorphous HfC_x thin films are reported. PLD is a fast, efficient method used for materials with high melting points that can reliably reproduce the stoichiometry of the target material. Unlike sputtering and e-beam evaporation, which are the most common deposition techniques for refractory materials, PLD is far more complex and the method varies from material to material. Controlling PLD involves optimizing the laser-target interaction, which is material dependent, controlling the plume propagation to the substrate and controlling the film condensation on the substrate. The controlled plume shape and directon in PLD manipulates where species can deposit. Highly energetic gas phase species lead to dense layer-by-layer growth of a smooth film [7].

The deposition of hafnium carbide on Si(111) at various substrate temperatures and laser fluence energies using a 532 nm laser has been investigated by Teghil and co-workers [8]. The film had good adherence and coverage. However, clear HfC peaks were not present in their XRD spectra. Also, they did not explain the oxygen detected by time-of-flight mass spectroscopy. Additionally, the film quality was not extensively addressed. A more recent deposition done using a 529 nm laser with a shorter pulse duration of 250 fs, produced thin films that were smooth and compact but consisted of many nanoparticles [9]. Femtosecond laser deposition usually results in particle ejection from the target due to the longer penetration depth of the laser beam and its low absorption by

ceramics and hence a thin dense and uniform film cannot be grown [10]. Therefore, PLD studies that provide knowledge of important process parameters and the resulting film composition and quality is highly beneficial.

Two process parameters that are important in PLD are the laser wavelength and the microstructure of the target being ablated. If a suboptimal laser wavelength is used, in PLD from hot-pressed ceramic targets micron-sized particulates due to subsurface target boiling, splashing and exfoliation are produced and incorporated into the growing film [11-14]. Particulate formation in films used as protective coatings in environments of high temperatures and oxygen pressures is highly disadvantageous because the rates of oxidation of the film, the surface of the particulate and the area of contact between the particulate and film, would all be different and cannot be controlled. Also, the impact of the particulates as it deposits on the surface of the growing film can result in damage of the film.

Subsurface boiling occurs when the evaporation rate of the target surface layer is lower than the rate at which the laser energy is converted into heat and transferred into the target. For a hafnium carbide target, which is metallic in nature, this phenomenon is possible due to its high thermal conductivity. Therefore, the choice of laser fluence and pulse duration is important. For uniform target ablation of molecules with their bonds retained, the laser beam energy has to be higher than a threshold energy. If the energy is too low, the target is thermally evaporated, however if the energy is too high, the film quality is affected due to the highly energetic nature of the ejected species.

The splashing process takes place as the plume expands. The exerted recoil pressure causes the melting region of the target to be squeezed onto the solid bulk. Droplets are ejected to counteract this pressure.

Both splashing and subsurface boiling are events that are independent of the target morphology. Exfoliation is a hydrodynamic effect that causes the target surface to become rough as ablation occurs. The continuous melting-cooling cycles cause outgrowths to form which then break off during further heating. A non-uniform or non-compact target would then increase the likelihood of exfoliation to occur.

HfC can dissolve large quantities of oxygen into its lattice. If the oxygen is not uniformly distributed within the target, during ablation the plume species and the resulting bulk film composition would vary. Therefore oxygen contamination in the target must be controlled. The purification of Group 1V carbide hot-pressed targets requires heating at temperatures up to 2000 °C and often will increase the target's oxygen content if the vacuum is not better than 10^{-6} Torr [15].

In this work, the shadow mask technique is employed to physically block the highly ballistic particles present in the plume [16-18]. Collisions with background gas molecules enhance molecular diffusion around the mask and onto the substrate. The chemistry of the plume was also manipulated by varying the type of background gases used. The fluence energy on the target was also studied. Depositions were performed using two wavelengths to determine the influence of absorption depth on film properties.

In this chapter, the theory of pulsed laser deposition and the film growth mechanisms is presented. An extensive report on the film composition, quality and contamination in the deposition of HfC from a hot-pressed HfC target follows.

Theory of Pulsed Laser Deposition

The pulsed laser deposition technique consists of 4 different, complex, sequential physical processes: (1) Laser beam-target interaction, (2) Plume formation and propagation, (3) Mass transfer of the vapor species to the substrate, and (4) Nucleation and growth of a dense film on the substrate.

A laser beam is focused onto the target surface. How the beam then interacts, i.e. absorbed, transmitted or reflected, with the target depends on the frequency of the laser beam and the nature of the target atoms.

The target is a set of atoms that contain electrons bound to them. These bonds are often modeled as springs. The electrons and springs can only vibrate at a specific natural frequency. When the laser beam of a given frequency hits the target, the electrons that have the same vibrational frequency will absorb the energy of the beam and converts it to vibrational motion. The electrons then interact with the neighboring atoms thereby converting the vibrational energy to thermal energy. Additional to the thermal excitation are the collisional and electronic excitations that together bring about the evaporation of the target material.

Therefore in PLD, the laser wavelength, pulse energy, duration and repetition rate are parameters that must be controlled for good film quality. They depend on the target properties, i.e. morphology, thermal conductivity, absorption etc.

The above mechanisms occur within picoseconds of the laser beam hitting the target. Before the next pulse occurs, typical pulse durations are in nanoseconds, a plasma consisting of the species vaporized from the target forms. Typical estimations of the plume temperature lie within 10,000-20,000K. Due to Coulomb repulsion and recoil, the

plasma cloud then expands forming a forward peaking plume shape. The spatial extension of the plume follows a cosine flux distribution and the spread is dependent on how far the vapor species have to travel.

Through the different processes, the atoms and/or molecules reach and condense on the substrate. The ballistic particles travel straight to the substrate. The molecular clusters and/or atoms adsorb onto the surface of the substrate and with the incident kinetic energy travels across to the lowest energy site. The high energy adatoms interact and coalesce. A monolayer forms and serves as a template for additional species.

Experimental Setup

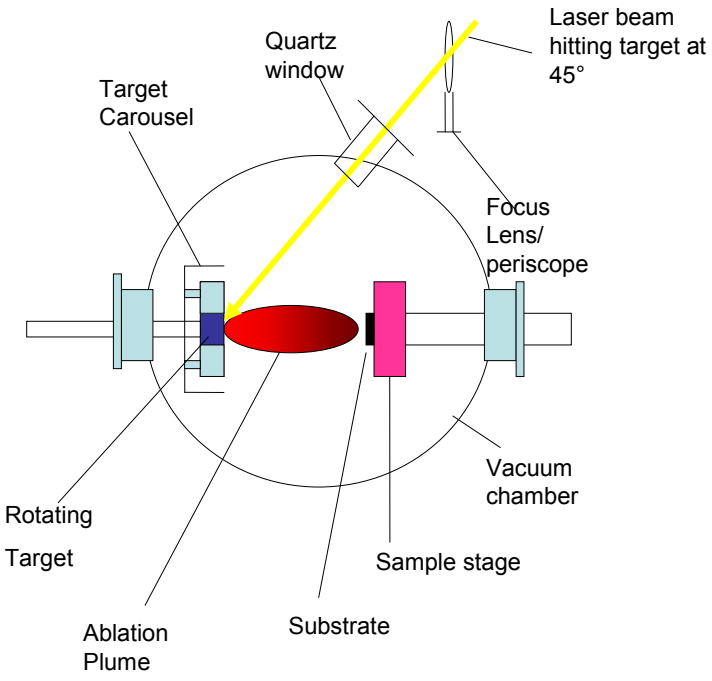

Figure 3.1: Schematic of the PLD system used to deposit hafnium carbide.

Depositions were performed in a "home-built" stainless steel chamber evacuated to a base pressure of 10^{-6} Torr. Any gas used was then introduced using a mass flow controller into the chamber. The pressure was held constant during the deposition.

The target was hot-pressed HfC made from 99.997% pure HfC powder using no sintering aid (Cerac Inc). The native oxide of the n-type Si (100) substrate (10-20 Ω-cm) was not removed since the small amount of oxygen present in this layer does not significantly contribute towards the film stoichiometry. The substrate was ultrasonically cleaned in acetone/methanol and dried with pure nitrogen.

A 308 nm XeCl excimer laser, with pulse duration of 18 ns and repetition rate of 10 Hz, was focused on the target by either a periscope or a quartz lens of 50 cm focal length creating a fluence of 3-5 J/cm^2. The beam hit the target at 45°. During deposition, the target was rotated at a rate between 60-120 rpm to avoid pitting. The substrate was held stationary. The substrate-target-shadow mask distances were varied as needed to optimize deposition rate and to minimize particulate formation.

For depositions using a 248 nm KrF laser (Epion PLD 3000), a pulse rate of 25 Hz and fluence energy of 4 J/cm^2 was used. The beam energy was held constant through a feedback control system. The laser was rastered across the diameter of the target. Additionally, the substrate was rotated.

Setups

The following five experimental configurations were used. Each setup addressed the resolution of one of the challenges of PLD described above, i.e. oxygen

contamination, reduction of particulate formation at the target and particulate elimination from the growing film.

(I) The substrate was placed with the polished side facing the target. The distance between the target and substrate was 30 mm. A periscope was used to focus the beam onto the target. A laser burn, i.e. laser beam hitting a burn paper, was used to obtain a qualitative description of the energy profile.

(II) The periscope was replaced by a focus lens. Two types of shadow masks were tested: a metal sheet and a helical conical copper wire [11]. The wire was optimized such that the base was the same size as the substrate and the transverse steps were smaller to the wire diameter. The metal sheet dimensions were varied to determine its effect on particular trajectory. The mask was placed parallel to the target, followed by the substrate (see Figure 3.2 below). A similar arrangement is used for the conical helical mask, with the larger diameter near substrate and the opposite end centered with the plume. The substrate was placed with the polished side facing the target. The target-mask-substrate distances, the size of the mask, the size of the substrate and background gas pressures were varied until the deposition rate and film quality was optimized. The target was rotated at 30-60 rpm and the substrate was maintained at room temperature. Argon was used as the inert carrier background gas. Deposition pressures between 1-100 mTorr were used.

(III) While retaining the optimum sized mask from the previous test, i.e. the mask that produced the film with the least amount of particulates, the type of background gas was varied. An inert gas of different mass, He, and a reactive gas N_2 were used to determine the effect of altering gas phase species collisions on the type of particulate

Figure 3.2: Target-shadow mask-substrate arrangement used to block out the ballistic particulates formed during target ablation.

formed and its number density.

(IV) C_2H_2 was introduced into the system at varying pressures. Acetylene is used in industry to carburize metals. Here it functions as a reactive gas, an additional carbon source, and an eliminator of oxygen present within the system, since it pyrolyzes at temperatures higher than 400 °C and becomes amorphous carbon at 900 °C. Unlike other hydrocarbons, the breaking of the triple bond between the carbon atoms is an exothermic process. A shadow mask was not used and the substrate was kept at room temperature. A periscope was used again to tightly focus the laser beam onto the target to obtain high fluence energies at the target.

(V) The PLD setup from part I was repeated with the 248 nm laser. The highest laser energy, 400 mJ, was necessary in order to maximize the deposition rate. The laser rastering distance and speed were set at ±4,000 cm and 50,000 cm/s respectively. A fixed number of laser shots (70-100K) were used for all the depositions. The target-substrate distance was set at about 20 mm. All depositions were done at room temperature.

The surface morphology of resulting films was observed, at SRI International, using a high-resolution field-emission SEM (JEOL 6100). The particulate number density

was then computed using the SEM images in conjunction with the Image J Analysis software (NIH) [19]. Atomic force microscopy measurements were acquired using a digital nanoscope for a maximum scanning range of 3 μm in tapping mode. The crystalline structure of the target and films were determined, at SRI International, by a Phillips X-ray diffractometer with a Cu *K*α source.

The surface chemical state was determined by XPS. The measurements were carried out in a PHI 5000 Versaprobe system using monochromatic Al *K*α X-rays (1486.6 eV). A beam spot size of 100 μm (25 W, 15 kV) was used. Survey spectra and individual core level spectra for Hf 4f, C1s, O1s and Si 2p peaks were collected. The survey spectra were collected using a pass energy of 117.4 eV (1.61 eV resolution). A pass energy of 23.5 eV was used for high resolution scans. Due to sample charging, a combination of Ar^+ ions and e- gun neutralization was used. The binding energy shifts were calibrated setting the C1s peak at 284.8 eV. After the initial analysis, the films were alternately sputtered with the 500 eV Ar^+ ions for a total time of 5 minutes.

Surface elemental composition can be estimated from the XPS data using the peak intensity ratios for the core shell peaks for each element following the relationship:

$$C_i = \frac{I_i S_i}{\sum_{i=1}^{n} I_i S_i} \qquad [1]$$

where I_i is the intensity area of the peak and S_i is the sensitivity factor of the element detected. The sensitivity factors were taken from the Handbook of X-ray Photoelectron Spectroscopy [20]. The individual core level spectra can be deconvoluted into peaks comprised of sums of Gaussian and Lorentzian functions that describe the various chemical states present within the film.

Bulk film elemental composition was determined by Rutherford backscattering spectrometry (RBS) and surface analysis by laser ionization (SALI).

Results & Discussion

(i) Reducing the number density of particulates formed

The films grown without either a shadow mask or background gas had good surface coverage and adherence to the substrate. However, the HfC films had a lot of oxygen contamination throughout the bulk of the film as well as nano- and micron- sized particulates on the surface. The particulates increased the surface roughness of the films as determined by AFM. The large particulates created voids in certain regions of the film either through the impact of collision or due to resputtering.

Nano-sized particulates are formed in three ways: (1) gas phase condensing on the condensed phase that was formed at the target upon ablation, (2) through the cooling of the vapor phase of the plume before it reaches the substrate, and/or (3) through the thermal difference between the gas phase and the substrate. This can be controlled by adjusting the target-substrate distance in order to increase the mean free path and decrease the residence time of the vapor species. The particulates that are formed at the target can be observed visually in the plume that forms. Figure 3.3 shows the "dirty" plume at the HfC target and for comparison the cleaner plume for HfO_2 created with the laser used in our system. The observance of sparks in the former is indicative of particulates forming at the target. The differences in the quality of the two plumes resulted in a marked difference in the films formed with both targets, as is shown in

Figure 3.4. The particulates formed at the target and in the vapor phase produce a HfC_x film that has a lot of surface defects and with the particulates embedded within.

Micron-sized particulates are the result of exfoliation of the target due to irregular heating by the laser beam, target sublimation or the characteristics of the target, i.e. its density, composition and morphological uniformity. With each high energy laser pulse shot, the microstructure of the target gets altered. The SEM images (Figure 3.5) of the target before and after deposition show the porous nature of the target, the melting of the target and how the surface defects increased after laser beam interaction. There is also a random distribution of melted phases within the target caused by the condensation of species in the plume or from splashing of the "melted" target due to high recoil pressure of the plasma plume. Spherical particles, akin to that on the substrate, are also present on the surface of the target. Visual inspection of the target after ablation indicated the formation of sharp cones. The degradation of the target is due to the highly energetic unidirectional laser beam created by the periscope used.

One way to deter the particulate condensation onto the substrate is to place a physical obstruction between the target and substrate. The masks created blocked out most of the ballistic particulates, i.e. high mass particles, since it was placed in the line of sight of the plume. The conical helical shadow mask provided a higher deposition rate since the lighter species in the plume were allowed to diffuse directly to substrate. The plane sheet blocked out the plume entirely and any diffusion was brought about by the collisions of the plume species with the inert background gas. With the conical helical mask, the number density of particulates, ~ 1-5 particles/μm^2, was significantly reduced but the film was non-uniform (Figure 3.6).

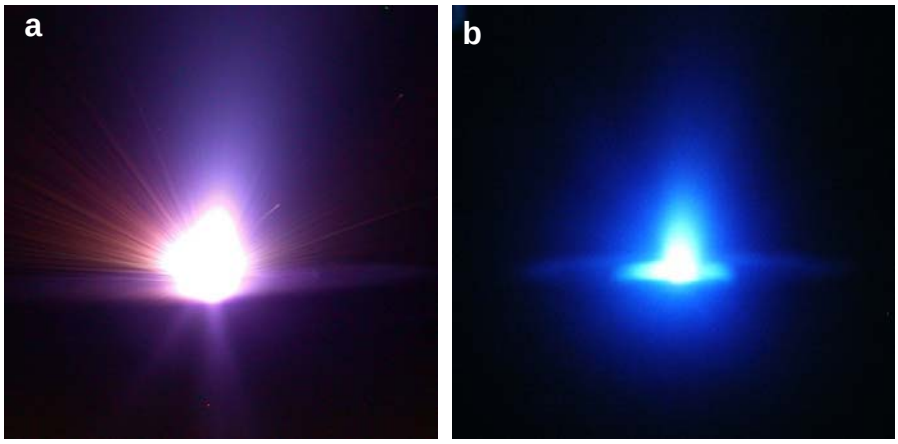

Figure 3.3: Comparison of the plumes created with a 308 nm laser at (a) the hafnium carbide target versus (b) the hafnia target.

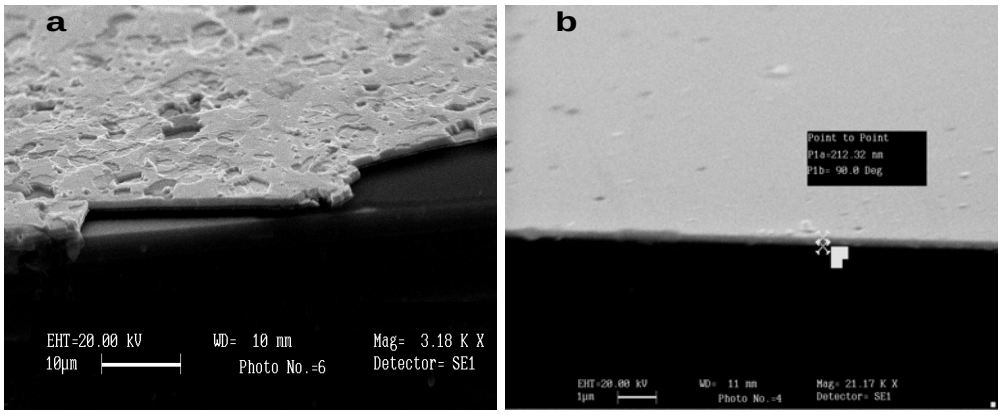

Figure 3.4: SEM images of (a) HfC_x and (b) HfO_2 films deposited with the same laser wavelength.

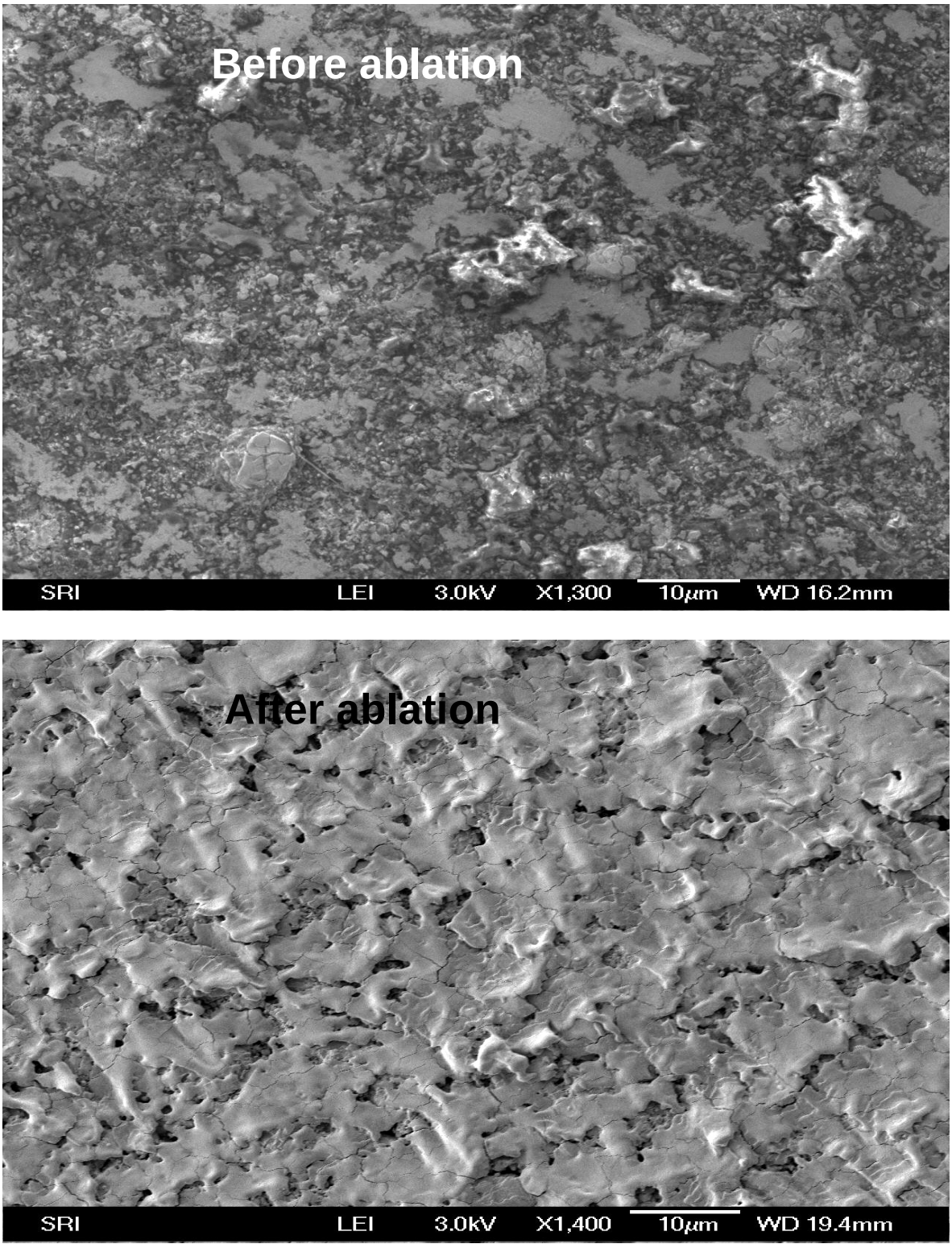

Figure 3.5: SEM images of the hot-pressed HfC target pre and post laser interaction.

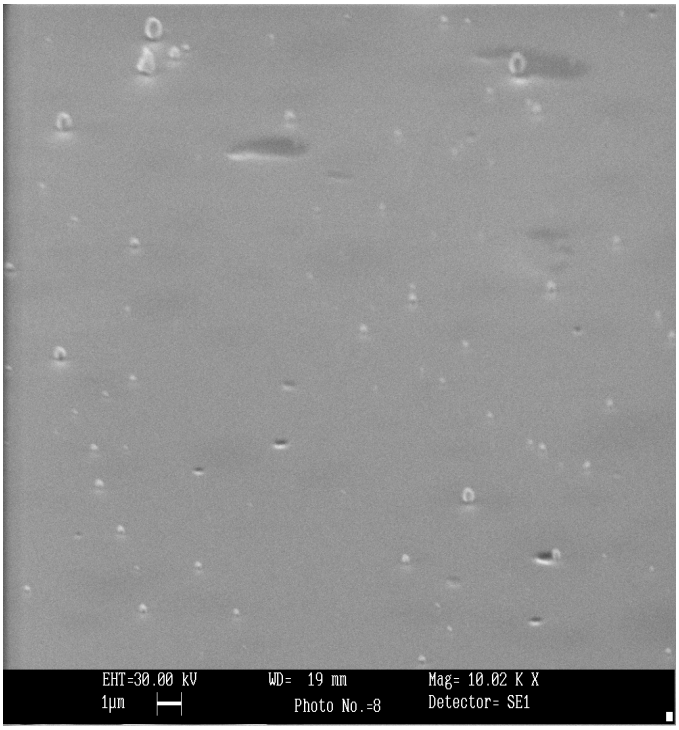

Total Area=350µm^2

Particle Count=1856

Average size=0.188µm

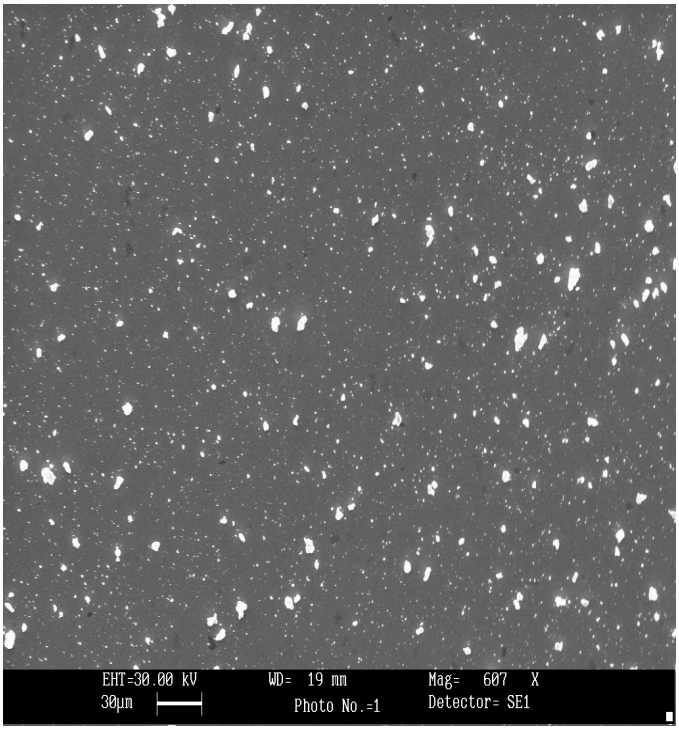

Total Area=4667µm^2

Particle Count=3031

Average size=1.54µm

Figure 3.6: Particle count and SEM images of two views of the HfC film deposited with a conical helical shadow mask and 40 mTorr of Ar.

For the plane sheet, it is optimal to have the size of the mask to be equal to that of the substrate both of which should equal the maximum width of the plume. This factor itself significantly reduces the possibility of high area deposition with this technique. The size of the mask affects the deposition rate since it alters the dynamic processes after the plume reaches the mask. Additionally the background gas affects the plume expansion, the kinetic energies and the spatial distribution of the plume species. The altered gas dynamic processes can change further as the plume approaches the substrate. Once the plume species are adsorbed on the surface, the varying energies cause particle movement. It was observed that the number density of particulates would increase as the substrate size was increased indicating particle movement from the edges of the substrate towards the center.

Changing the target-mask-substrate distances does not affect the number density but alters the size of the spherical particulates formed due to the diffusion effect. Below the optimum target-mask: mask-substrate distances of 20 mm: 10 mm, there is no significant effect on the size of the particulates. Increasing the distances increases the residence time of the gas phase molecules thereby allowing interaction with more oxygen that then diffuses into the film.

Since gas phase collisions/momentum transfer affect the number density of particulates, the type of background gas used can affect the kinetic energies of the plume species. Increasing the Ar background gas pressure increased the thicknesses of the film deposited, however, as indicated in Figures 3.7a-c, the number density of particulates and the size of particulates increase at higher gas pressures. At 5 mTorr of Ar, the number density of particulates was about 1 particles/μm^2. The number density increases to about

5 particles/μm^2 for 20 and 100 mTorr of Ar however for the latter the size of the particulates are much larger. This is due once again to (i) the alteration of the plume expansion and (ii) the high gas phase nucleation since an increase in gas phase collisions quenches the vapor species.

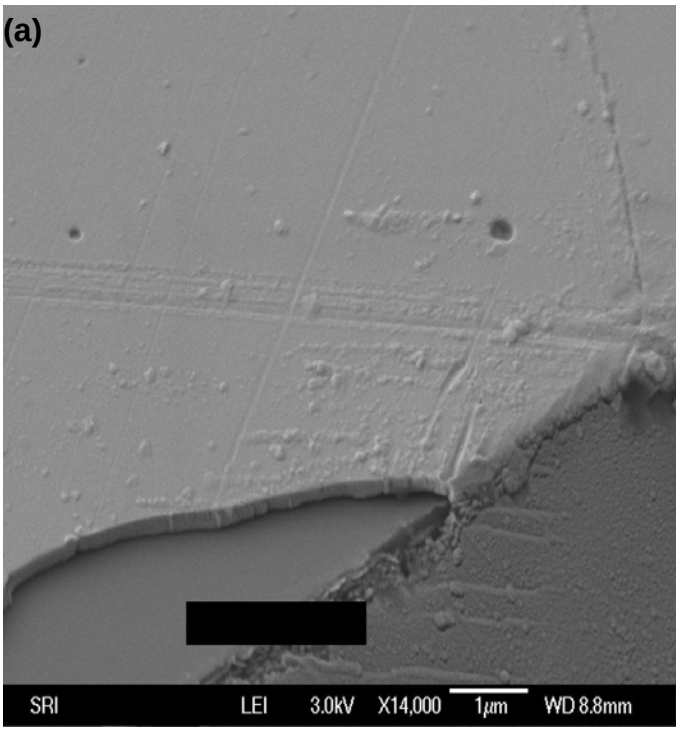

Figure 3.7a: Particle count and SEM image of HfC_x film deposited with only 5 mTorr Ar.

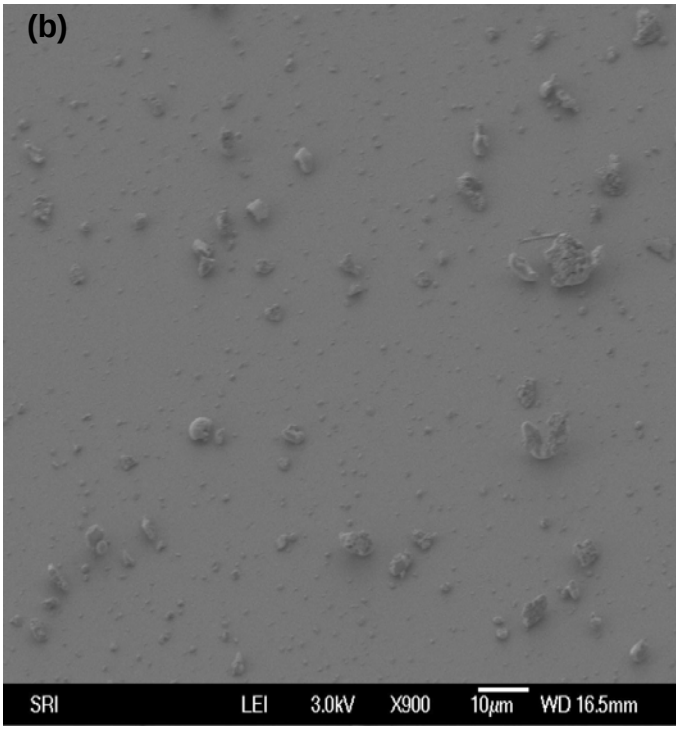

Total Area=1431μm^2

Particle Count=7494

Average size=0.19μm

Figure 3.7b: Particle count and SEM image of HfC_x film deposited with 20 mTorr Ar.

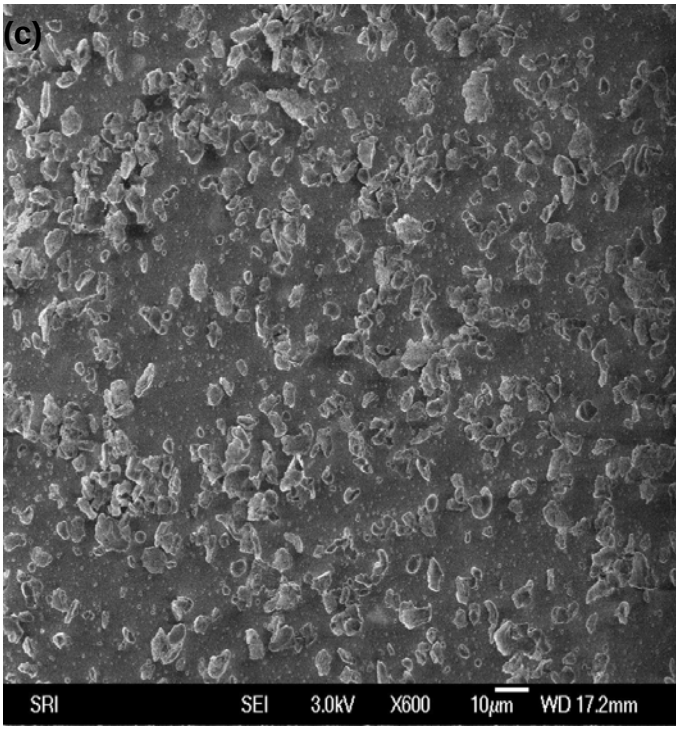

Total Area=7606μm^2

Particle Count=30226

Average size=0.252μm

Figure 3.7c: Particle count and SEM image of HfC_x film deposited with 100 mTorr Ar.

The use of a lighter gas, helium, did not alter the film composition or surface contamination from that deposited using Ar as the carrier gas. However the use of a reactive gas, N_2, significantly reduced the number density and size of the spherical particulates. This is further confirmation that most of the particulates formed are due to gas phase collisions. It can be speculated that some of the vapor phase atoms and ions transfer some of the energy to the nitrogen gas particles thereby enhancing the latter's chemical reactivity and help them to react with the plasma species. Since this reaction releases energy further vapor particulate quenching is inhibited.

No shadow mask is required when using a reactive gas, as seen by the reduction in the number density of particulates in the films deposited with acetylene and no shadow mask (Figure 3.8). AFM analysis showed using a reactive gas also considerably reduced the surface roughness of the films. This again confirms that most of the particulate formation and condensation occurs in the gas phase.

(ii) Film Composition

While the reduction in particulate contamination was addressed, the film composition was also monitored.

Without a shadow mask or inert background gas, the film was mostly hafnia as determined by RBS and XPS. The sources of oxygen contamination are: (1) the target, (2) the residual gas in the system, (3) oxygen in the atmosphere that the sample is exposed to when removed from the system.

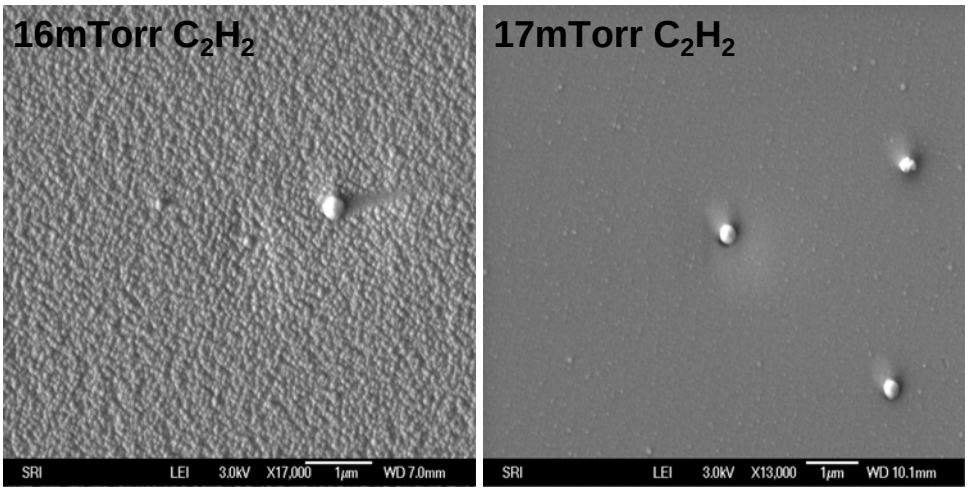

Figure 3.8: SEM images of $HfC_x(O)$ films deposited with varying acetylene pressures.

The XRD spectrum for the target (Figure 3.9) was compared to the XRD spectra obtained from the studies on carbon and oxygen ion implantation in hafnium [21, 22]. It indicates that there are no Hf-O bonds within the target but it does not negate the fact that a trace amount of oxygen may be dissolved in the lattice. However, there is no efficient way to remove the dissolved oxygen without high temperature heating of the target.

Oxygen present in the system can react with Hf atoms created in the gas phase, displace the carbon atom of HfC in the gas phase, or form an oxide layer on the substrate, through the mechanisms outlined below. Depending on the thermal heat at the target, carbon could preferentially vaporize from hafnium carbide [23]. The amount of energy absorbed or dissipated by the target depends on the laser wavelength used and the

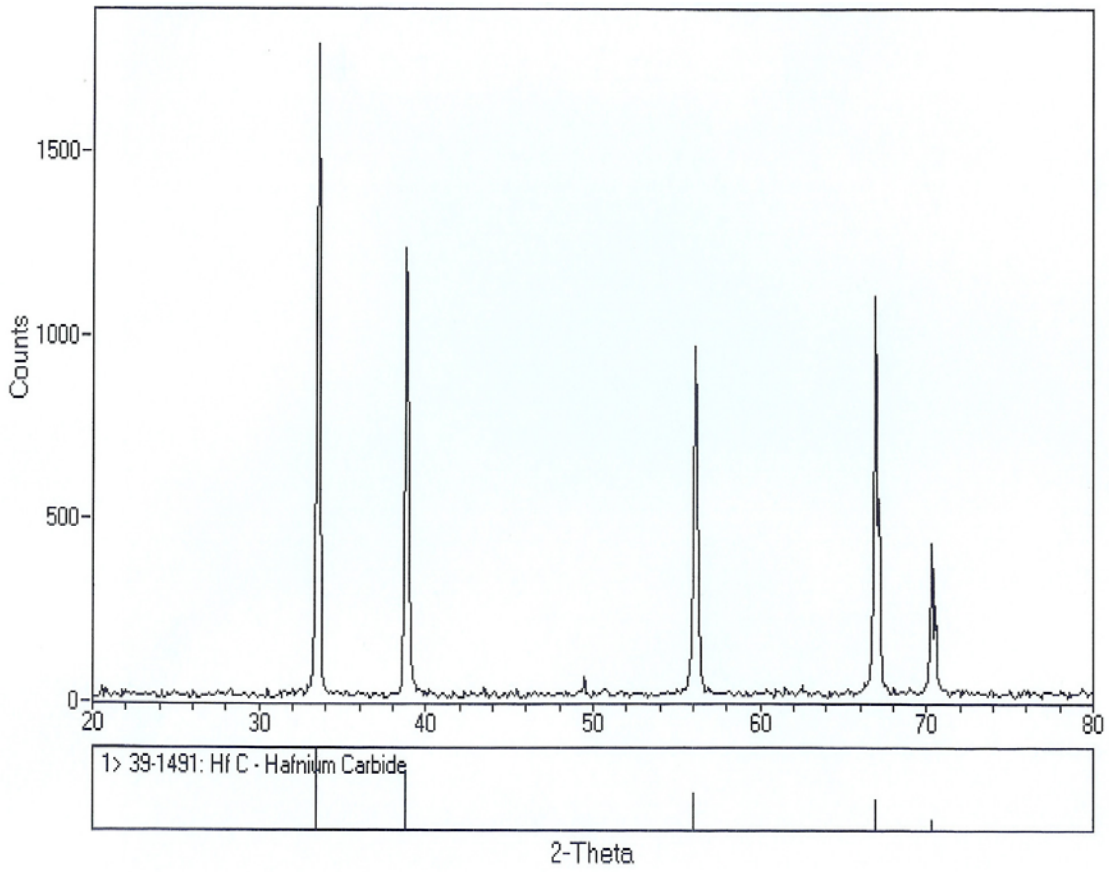

Figure 3.9: XRD spectra indicating the major HfC peaks for the pristine target.

resonant frequency required to cause thermal ablation of the atoms in the carbide. The vaporization creates vacancies that enable oxygen diffusion and reaction.

Density-functional theory calculations show that molecular oxygen can dissociate along two pathways on hafnium carbide surface [24, 25]. At a low temperature of 300 K, oxygen is adsorbed on the metal-metal bridge adsorption and at high temperatures (>1273 K) the oxygen is adsorbed on surface of the carbide, both lead to the oxygen atom moving into the 3 fold interstitial site, interacting strongly with the surrounding 1 carbon atom and 2 metal atoms. The inclusion of the oxygen atom, causes the outward displacement of the carbon atom.

Dissolution of oxygen into the film can occur at the substrate since residual oxygen can easily adsorb onto the substrate even at the low pressures. Assuming that there is no oxygen dissociation at the substrate surface, no surface reactions and that all the oxygen molecules stick to the Si surface, it takes 5 seconds for a monolayer of oxygen to cover a Si surface in a chamber evacuated to 1×10^{-6} Torr.

While theory states that hafnium oxycarbide, formed from oxygen diffusing into hafnium carbide, is a more effective protective coating than hafnium carbide, oxygen contamination of hafnium carbide films due to residual gas and atmosphere is a major problem for the following reasons. In the former, a fixed amount of gas is introduced into the system to oxidize the material, however in the PLD depositions, if the base pressure is not kept consistently at the same value for each deposition, the amount of oxygen available for reaction with plume species or diffusion into the growing film, be it hafnium carbide or hafnium oxycarbide, would differ with each run. Also if oxygen diffuses into deposited films, the surface composition would differ from the bulk composition and hence affect the efficacy of the hafnium carbide film. Hafnium carbide is one component of the proposed multilayer protection system, therefore if its composition itself differs before and after deposition, the protection capabilities of the entire system would be compromised.

The use of an inert background gas reduced the amount of oxygen in the deposited film and hence increased the carbon content in the film. RBS spectra (Figure 3.10) for a film deposited with 20 mTorr Ar and shadow mask at 20mm from the target indicates the presence of carbon, hafnium and oxygen with the ratio of C:Hf and O:Hf being 1.5 and 2.4 respectively. However, for a lower Ar pressure deposition, XPS

spectra (Figure 3.11) indicate that most of the carbon is present in the film as free carbon, while a very small percentage of the carbon is bonded to oxygen to form C=O bonds. Surface analysis by laser ionization (SALI) conducted on another film deposited under the same conditions indicated that the film is an inhomogeneous mixture of HfO_2, Hf and a small amount of HfC. Increasing the Ar pressure reduces the oxygen content in the film further but this advantage is counteracted by the increase in particulate formation.

The opposite effect was seen with the use of nitrogen. While the number density of particulates decreased with increasing gas pressure, SALI analysis confirmed the films contained nitrogen along with hafnium, carbon and oxygen.

Using Ar and N_2 did not remove all the oxygen content in the film and still produced carbon deficient films. Therefore, the use of acetylene served dual purposes: as the reactive gas and as an additional source of carbon. Acetylene could also react with HfO_2 to form HfC at the high temperatures produced by the laser interaction with the target, in the following reaction, provided that the ratio of carbon to hafnia is 3 to 1 [26].

$$HfO_2 + 2C \rightarrow HfC + CO_2 \qquad [5]$$

Element ratios deteremined from RBS spectra collected for the film indicate that for the same deposition time, as the acetylene pressure is increased, the carbon content in the film does increase. However as the pressure increases above 16 mTorr, there is a reduction in the film thickness.

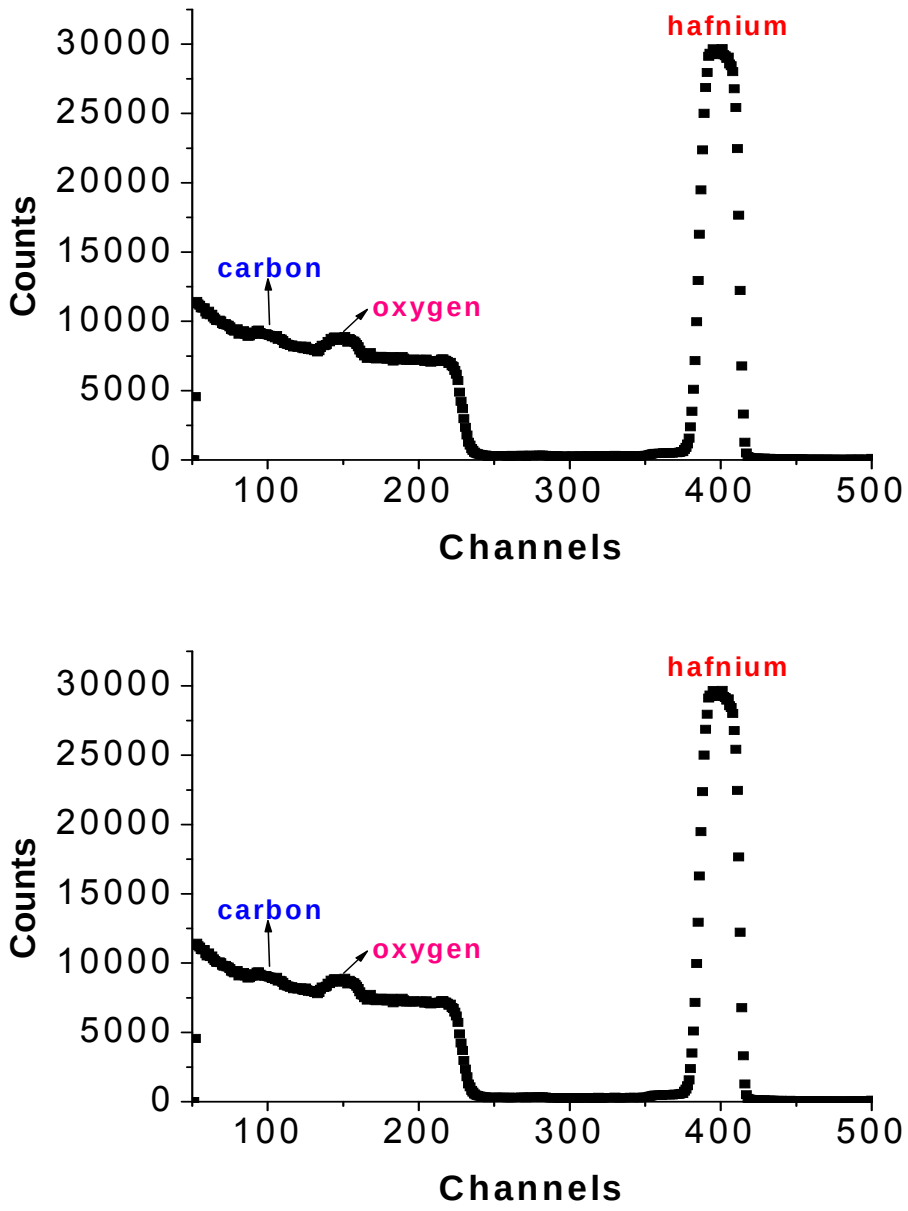

Figure 3.10: RBS spectra for a film deposited with the shadow mask and 20 mTorr Ar from which a ratio of C:Hf=1.5 and O:Hf=2.4 was determined.

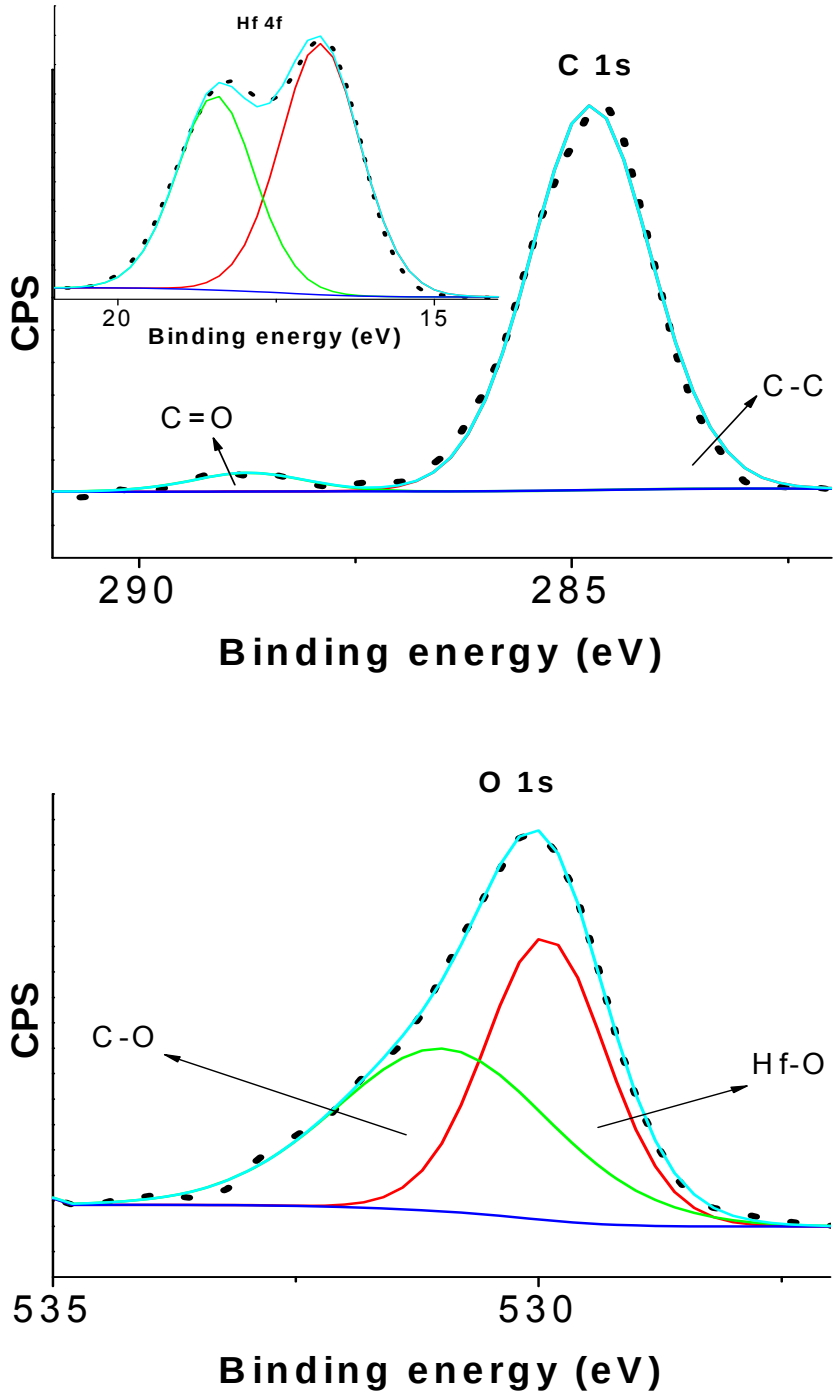

Figure 3.11: Hf 4f (inset), C1s and O1s core shell spectra; counts per second (CPS) versus binding energy, obtained by XPS for film deposited with shadow mask and 5 mTorr Ar.

The elemental composition was determined from the XPS data (Figure 3.12). For pressure less than 3 mTorr, the carbon content increases and the oxygen content decreases. Above 3 mTorr, a plateau is reached until a higher pressure of 17 mTorr. At 17 mTorr, the carbon content decreases while the oxygen content increases. Even though this decrease has been observed in the single set of pressure variation experiments, a plausible explanation can only be derived upon repetition of film deposition at each pressure.

The chemical states of the Hf, C and O atoms in the films were determined using XPS. The analysis indicates that an increase in carbon content in the film does translate into an increase in C-C bonds within the film. Figure 3.13 shows that increasing the acetylene pressure beyond 16 mTorr induced more carbon atoms to bond to the oxygen present in the residual gases in the chamber, however there is always more C-C bonds present within the film.

Ar^+ sputtering of the films removed some of the carbonyl bonds and Hf-C bond peaks emerged in the XPS spectra (Figures 3.14-3.15). However, even after 5 minutes of sputtering, the percentage of Hf-C bonds within the C1s spectra was only about 5%.

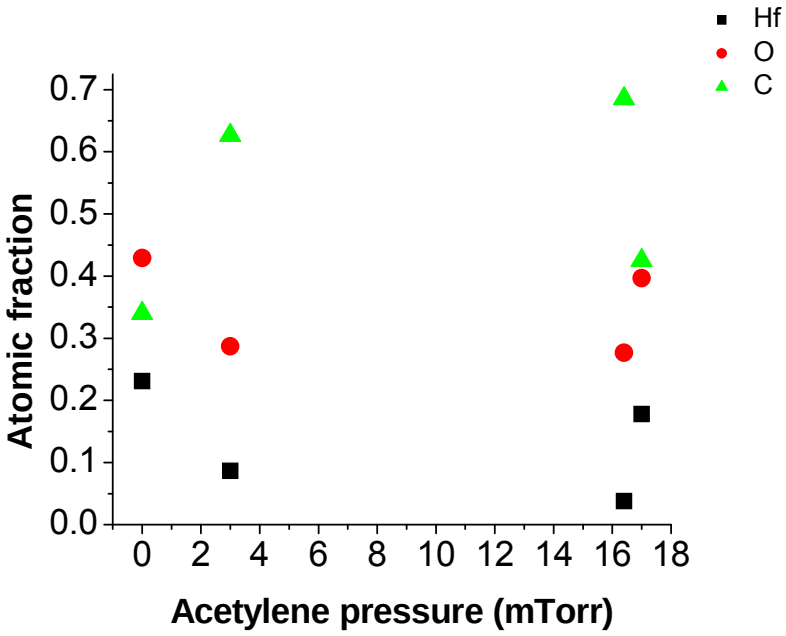

Figure 3.12: Atomic composition variation with pressure increase determined from XPS spectra.

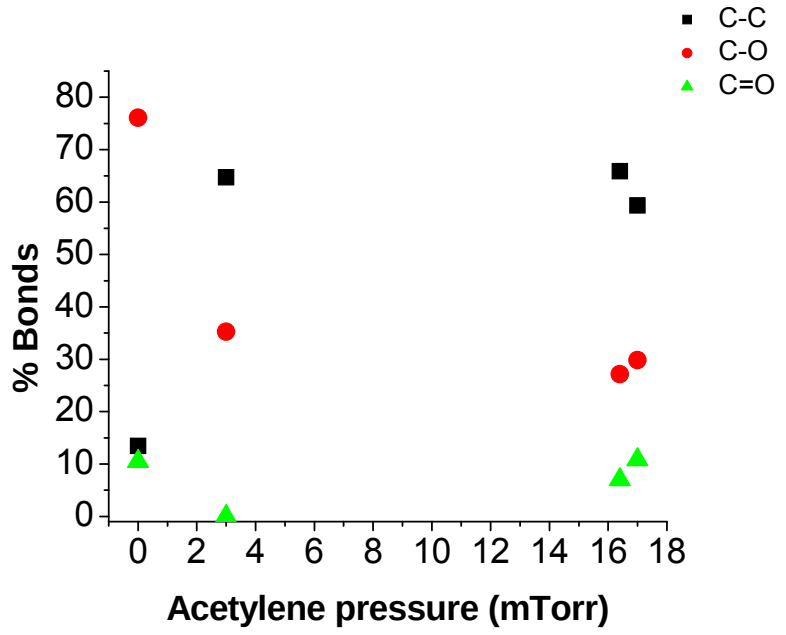

Figure 3.13: Using acetylene gas as an extra source of carbon is limiting for pressure less than 4 mTorr and higher than 16 mTorr.

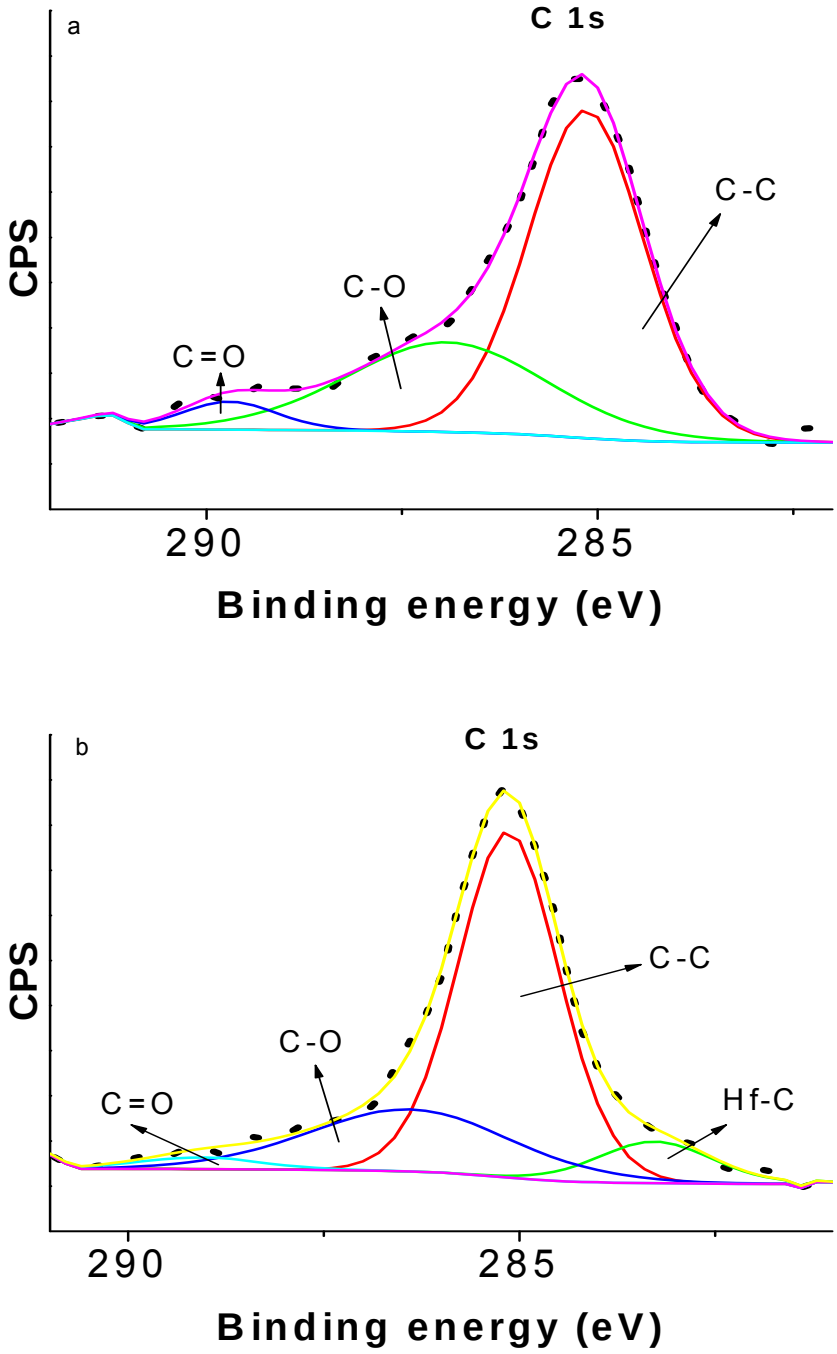

Figure 3.14: Core shell spectra for C1s (a) pre and (b) post sputtering with a 500 V Ar^+ ion gun.

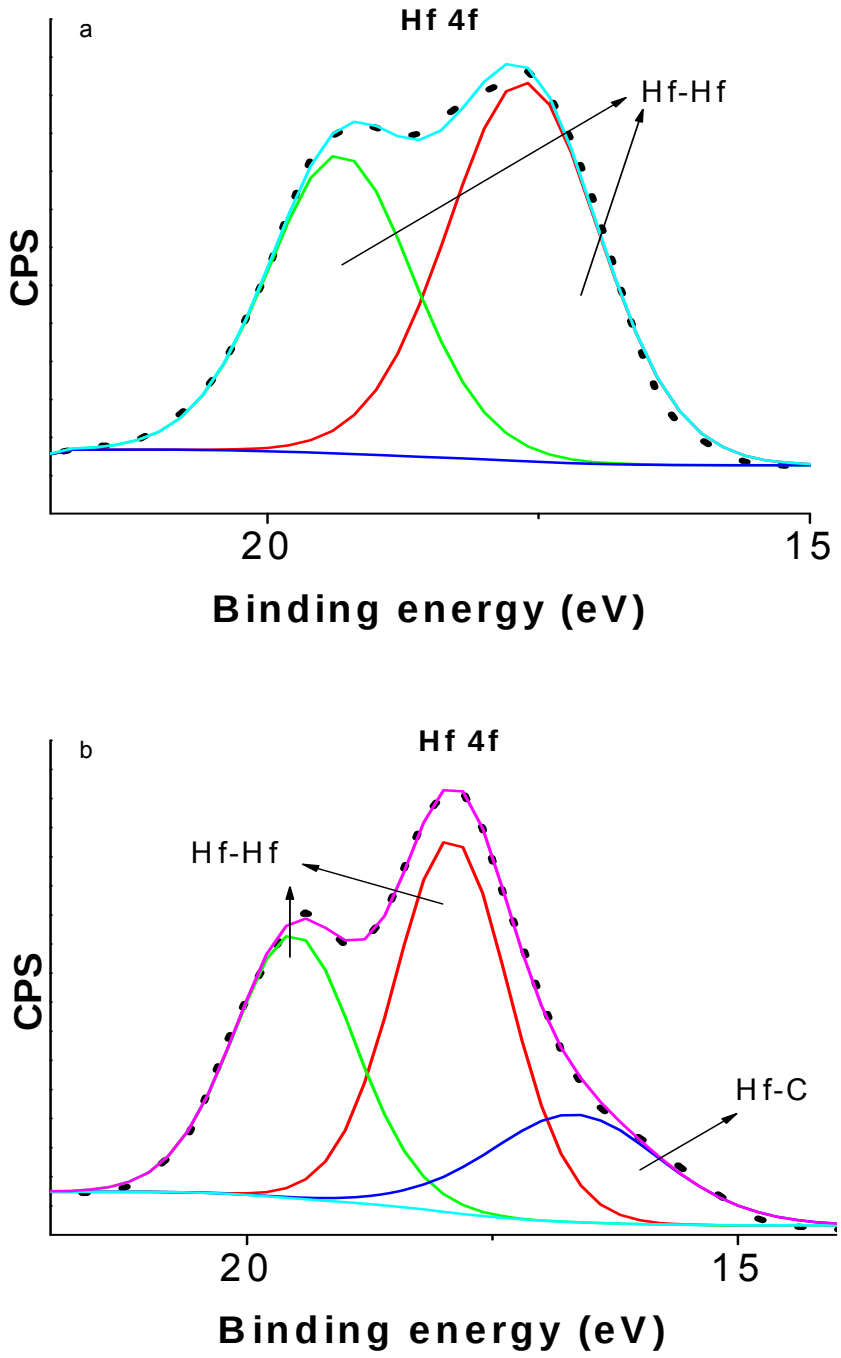

Figure 3.15: Core shell spectra for Hf 4f (a) pre and (b) post sputtering with a 500 V Ar^+ ion gun.

(iii) Altering fluence energy at and absorption characteristics of target

The effectiveness of the shadow mask and different background gases was brought about by the manipulation and alteration of the plume species kinetic energy and chemistry. The particulate formation was also controlled at the target level by varying the laser fluence energy at the target and the type of laser wavelength used.

Since the periscope produced a high energy beam that caused target damage, it was replaced with a focus lens. From the paper burn, it was deduced that the focus lens produced a Gaussian like intensity beam profile which uniformly ablated the target. By varying the position of the lens, the fluence energy at the target could be controlled. This setup was found to reduce the number density of particulates formed at the target level due to the more uniform heating process.

However, when using the acetylene gas, the fluence energy at the target was not high enough to induce a reaction between the vapor species and the gas. Therefore, the focus lens had to be replaced by the periscope lens again.

The depositions done using a 308 nm laser and a highly reactive gas, showed that that particular wavelength was not suitable for HfC because the fluence was still not high enough to retain the Hf-C bonds nor to cause the Hf atoms or ions to react with the acetylene gas to form HfC in the high temperature plume.

Using a 248 nm laser was advantageous for hafnium carbide, since a lower penetration depth of the UV photons is combined with a higher absorption. This caused only small fragments to be ablated off the target and it further fragmented in the plume. Reducing the gas phase particles led to smoother and denser film formation.

RBS spectra indicate a higher incorporation of carbon within the film as compared to the film deposited using the 308 nm laser, as seen in Figure 3.16. The amount of oxygen in the film increases with deposition time, indicating that the main source of oxygen is from residual gases within the chamber.

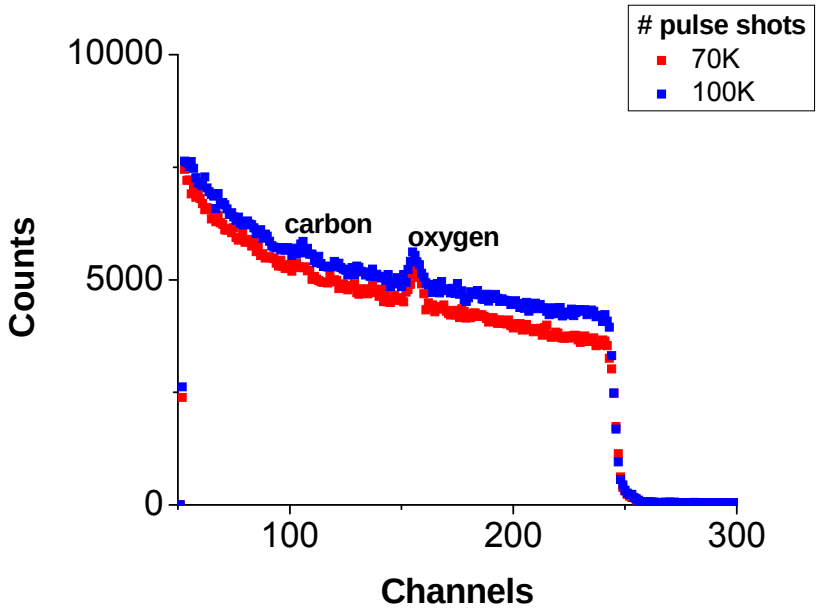

Figure 3.16: RBS spectra for HfCx(O) film deposited with a lower wavelength laser, for a varying number of pulse shots.

This is further confirmed by the deconvoluted XPS spectra shown in Figures 3.17-3.18. Initially, the oxygen bonds with the carbon atoms in the film. At longer deposition times, the oxygen reacts with the hafnium to form Hf-O bonds within the film. Compared to films deposited with the 308 nm laser there is still more C-C bonds present within these films.

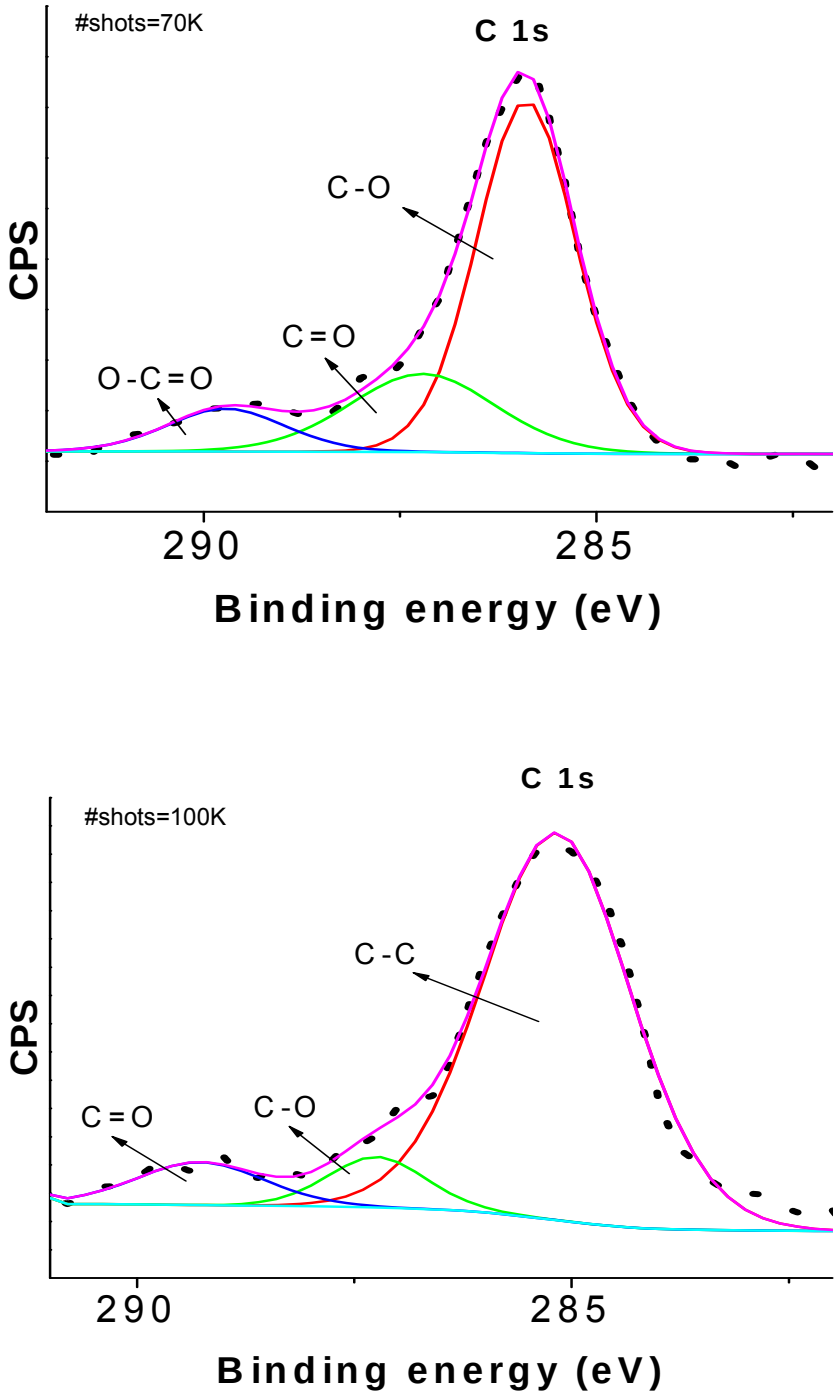

Figure 3.17: C1s spectra for the films deposited with the 248 nm laser ablation for varying number of pulse shots.

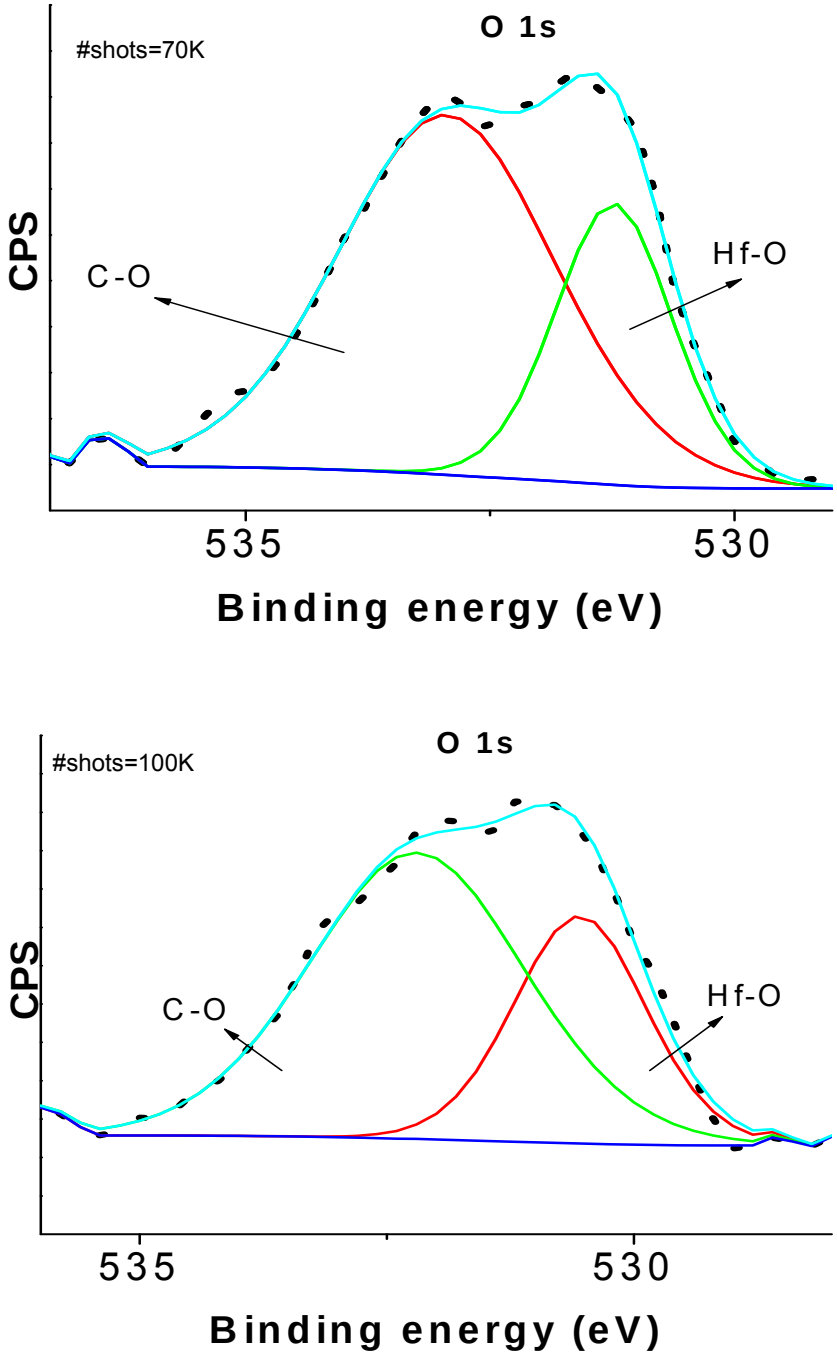

Figure 3.18: O1s spectra for the films deposited with the 248 nm laser ablation for varying number of pulse shots.

XPS spectra collected from the sputtered film (Figures 3.19-3.20), shows a significant presence of Hf-C bonds within the film (~25% within C1s spectra). However, the film still contains more hafnia and carbon segregates.

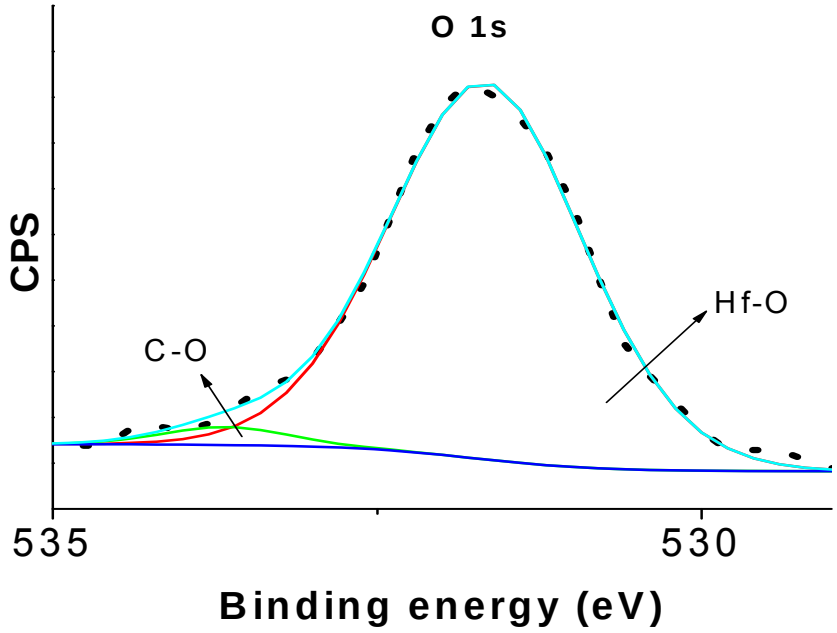

Figure 3.19: The O1s spectra after the films deposited with 248 nm laser were sputtered with a 500V Ar^+ ion gun.

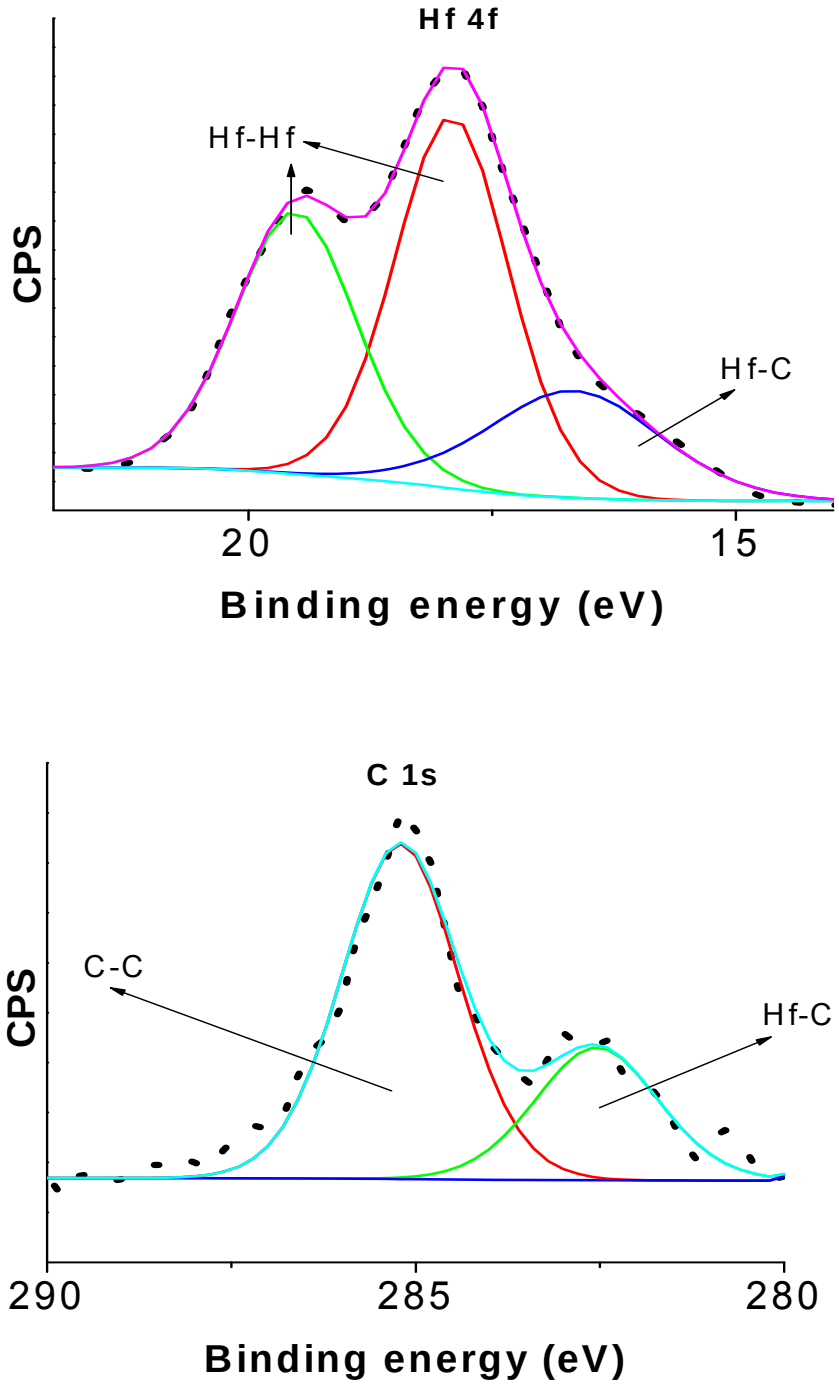

Figure 3.20: The Hf 4f and C1s spectra after the films deposited with 248 nm laser were sputtered with a 500V Ar^+ ion gun.

RBS and XPS results indicate that with the lower wavelength the Hf-C bond can be maintained. These tests helped conclude that the high absorption of the laser beam by the target did not preferentially vaporize off the carbon and that the 308nm laser was not suitable for the refractory carbide. If the plume consisted of just hafnium and carbon atoms, the former would have formed hafnia while the latter would burn off as carbon dioxide. However it will still react with oxygen through the following reaction:

$$HfC + O_2 \rightarrow HfO_2 + \text{free C} \qquad [6]$$

Conclusions

A variety of experimental parameters were tested to produce clean hafnium carbide films using a 308 nm XeCl. To our knowledge, the deposition of refractory hafnium carbide using a laser of this wavelength has not been conducted before.

While most ceramics can easily absorb light in the UV range, an optimum laser wavelength and absorption is important to produce particulate free film by pulsed laser deposition. Using a 248 nm laser for the ablation of hafnium carbide produced better results.

For the work done with the 308 nm laser, we found that using a reactive gas can significantly reduce the formation of particulates on the film surface. Using a gaseous carbon source provides the advantage of inducing reaction with any hafnium atoms or ions that form in the plume upon target ablation. Therefore, a combination of Ar/C_2H_2 background gas mixture with a 248 nm KrF laser could produce the optimum film

composition and quality. However, our studies have shown us that even in relatively high vacuum it is still hard to eliminate the oxygen dissolution and reaction within the carbide.

Our results show the even though the various species undergo reactions in a high temperature plume, the optimum film mixture is hafnia, free carbon segregates and hafnium carbide; with the first two components being dominant. This brings forth an interesting question of whether the oxycarbide formed during the oxidation of hafnium carbide is indeed just hafnia with free carbon dissolved within, as has been theoretically concluded in the past, or a mixture of hafnium carbide and hafnia with free carbon present in the solution.

References

1. Opeka M.M., Talmy I.G., Zaykoski J.A., *Oxidation-based materials selection for 2000 °C+ hypersonic aerosurfaces: theoretical considerations and historical experience*, J. Mater. Sci., **2004**, 39, 5887-5904.

2. Bargeron C.B., Benson R.C., Jette A.N., Phillips T.E., *Oxidation of hafnium carbide in the temperature range 1400° to 2060 °C*, J. Am. Ceram. Soc., **1993**, 76(4), 1040-1046.

3. Shimada S., Yunazar F., *Oxidation of hafnium carbide and titanium carbide single crystals with the formation of carbon at high temperatures and low Oxygen Pressures*, J. Am. Ceram. Soc., **2000**, 83(4), 721-728.

4. Shimada S., Inagaki M., *Oxidation kinetics of hafnium carbide in the temperature range of 480° to 600 °C*, J. Am. Ceram. Soc., **1992**, 75(10), 2671-2678.

5. Spatenka P., Suhr H., Erker G., Rump M., *Formation of hafnium carbide thin films by plasma enhanced chemical vapor deposition*, Appl. Phys. A, **1995**, 60(3), 285-288.

6. Nagao M., Sacho Y., Sato T., Matsukawa T., Kanemaru S., Itoh J., *Fabrication of polycrystalline silicon field emitter arrays with hafnium carbide coating for thin-film-transistor controlled field emission displays*, Jpn. J. Appl. Phys., **2004**, 43(6B), 3919-3922.

7. Willmott P.R., Spillmann H., Huber J.R., *Design and synthesis of novel tin films and structures by reactive crossed-beam laser ablation*, J. Mater. Chem., **2002**, 12, 397-402.

8. Teghil R., Santagata A., Zaccagnino M., Barinov S.M., Marotta V., De Mari G., *Hafnium carbide hard coatings produced by pulsed laser ablation and deposition*, Surf. Coat. Technol., **2002**, 151-152, 531-533.

9. Ferro D., Rau J.V., Albertini V.R., Generosi A., Teghil R., Barinov S.M., *Pulsed laser deposited hard TiC, ZrC, HfC and TaC films on titanium: hardness and an energy-dispersive x-ray diffraction study*, Surf. Coat. Technol., **2008**, 202(8), 1455-1461.

10. Teghil R., D'Alessio L., De Bonis A., Galasso A., Villani P., Santagata A., *Femtosecond pulsed laser ablation and deposition of titanium carbide*, Thin Solid Films, **2006**, 515(4), 1411-1418.

11. Marcu A., Grigoriu C., Jiang W., Yatsui K., *Pulsed Laser deposition of YBCO thin films in a shadow mask configuration*, Thin Solid Films, **2000**, 360(1-2), 166-172.

12. Blank D.H.A., IJsselsteijn R.P.J., Out P.G., Kuiper H.J.H., Flokstra J., Rogalla H., *High T_c thin films prepared by laser ablation: material distribution and droplet problem*, Mater. Sci. Eng., **1992**, B13, 67-74.

13. Gyorgy E., Mihailescu I.N., Kompitsas M., Giannoudakos A., *Particulates generation and solutions for their elimination in pulsed laser deposition*, J. Optoelectr. Adv. Mater., **2004**, 6(1), 39-46.

14. Thompson M., Chenery S., Brett L., *Nature of particulate matter produced by laser ablation - implications for tandem analytical systems*, J. Anal. At. Spectrom., **1990**, 5, 49-55.

15. Pierson, H.O., Handbook of refractory carbides and nitrides: properties, characteristics, processing, and applications, Noyes Publications, Park Ridge, New Jersey, 2006.

16. Trajanovi Z., Choopun S., Sharma R.P., Venkatesan T., *Stoichiometry and thickness variation of $YBa_2Cu_3O_{7-x}$ in pulsed laser deposition with a shadow mask*, Appl. Phys. Lett., **1997**, 70(25), 3461-3463.

17. O'Brien T.P., Lawler J.F., Lunney J.G., Blau W.J., *The effect of laser fluence on the ablation and depostion of $YBa_2Cu_3O_7$*, Mater. Sci. Eng., **1992**, B13, 9-14.

18. Morita E., Yamamuro K., Tachiki M., Kobayashi T., *Advanced eclipse pulsed laser deposition method for growth of perovskite crystals and relatives*, Nucl. Instrum. Methods Phys. Res. B, **1997**, 121, 412-414.

19. http://rsbweb.nih.gov/ij/.

20. Moulder J.F., Stickle W.F., Sobol P.E., Bomben K.D., Handbook of X-ray Photoelectron Spectroscopy: A Reference Book of Standard Spectra for Identification and Intrepretation of XPS Data, Physical Electronics Inc., USA, 1992.

21. Fujihana T., Taniguchi M., Okabe Y., Iwaki M., *Crystal structure of carbon-implanted Group 4 transition metals*, Surf. Coat. Technol., **1996**, 83, 120-123.

22. Okabe Y., Fujihana T., Iwaki M., Crist B.V., *Characterization of oxide layers induced by oxygen ion implantation into Ti, V, Cr, Zr, Nb, Mo, Hf, Ta and W*, Surf. Coat. Technol., **1994**, 66, 384-388.

23. Hansler, R.L., *Preferential vaporization of carbon from hafnium carbide*, J. Electrochem Soc., **1965**, 112, 881.

24. Vines F., Sousa C., Illas F., Liu P., Rodriguez J.A., *Density functional study of the adsorption of atomic oxygen on the (001) surface of early transition-metal carbides*, J. Phys. Chem. C, **2007**,111, 1307-1314.

25. Vines F., Sousa C., Illas F., Liu P., Rodriguez J.A., *A systematic density functional study of molecular oxygen adsorption and dissociation on the (001) surface of group IV-VI transition metal carbides*, J. Phys. Chem. C, **2007**, 111, 16982-16989.

26. Vodop'yanov A.G., Kozhevnikov G.N., Baranov S.V., *Interaction of refractory metal oxides with carbon*, Russian Chemical Reviews, **1988**, 57(9), 810-823.

CHAPTER IV

THERMAL AND OXIDATIVE STABILITY OF HfO_xC_y PRODUCED BY PULSED LASER DEPOSITION

Introduction

As discussed in Chapter III, pulsed laser deposition studies of hafnium carbide have shown that at high temperatures and low oxygen pressures, oxygen already dissolved in the carbide lattice can easily substitute for a carbon atom, and that the external oxygen molecules can bridge between the carbon and metal atoms. The interesting result was that despite the oxygen present in the system, the high plume temperature and the long deposition times, the carbide was never fully oxidized, i.e. the carbon was always incorporated in the film.

The PLD results are consistent with previous work done by Bargeron and co-workers on the oxidation of hafnium carbide which also showed that a very dense and amorphous oxycarbide interlayer forms between the carbide and the outer hafnium oxide [1-5]. Theoretical calculations [1] based on the Danckwert moving boundary theory indicated that the oxycarbide acts as a better oxidation barrier than the underlying carbide and outer oxide.

Very little is known about the properties of the oxycarbide layer that forms. Hafnium oxycarbide, $HfO_{2-x}C_{y,}$ is commonly considered to be free carbon within the hafnia interstitials and not carbon bonded to hafnium with oxygen dissolved in the interstitials [2, 3]. The latter would not be feasible for high temperatures. Both theoretical and our experimental work have demonstrated that oxygen dissolved in a carbide matrix

could displace the carbon easily. While the presence of excess carbon is typically thought of as limiting quality in an oxidation process, Blum and co-workers, discovered that carbon-enriched silicon oxycarbide was chemically and thermally stable up to 1200 °C [6].

These properties are advantageous for thermal barrier coatings hence exploring possible synthesis routes of stand alone amorphous HfO_xC_y thin films where the concentration of oxygen to carbon and the chemical state can be controlled, and then studying their behavior in a high temperature range is extremely important. To our knowledge, apart from one short paper on oxycarbide powders published in 1972 [7], no work on these materials has been reported. Refractory oxycarbides can be formed through the carburization of the respective metal oxides [8, 9]. This is the most efficient and cost effective method. However, to grow thin dense amorphous films with controlled stoichiometry, a physical vapor deposition process is necessary.

Pulsed laser deposition is a fast, efficient, reproducible technique that is typically used to grow congruent ternary films. Additional benefits include not having to heat the substrates to high temperatures to grow refractory materials and the avoidance of organic precursors that could contaminate the film.

In this work two methods of HfO_xC_y synthesis are described, using (i) a binary HfO_2/C target and (ii) a HfO_2 target with a carbon source gas in the background. The characterization of the resulting films and their subsequent oxidation behavior are also reported.

Experimental Setup

Films were deposited in a stainless steel vacuum chamber maintained at 10^{-6} Torr. A 308 nm XeCl excimer laser of 10 Hz repetition rate, τ = 18 ns, was used to ablate the various targets. The target was rotated while the substrate was held stationary. The substrates used were Si (100) wafers that have been ultrasonically cleaned in acetone and methanol.

(i) Direct synthesis

The target was formed in the lab by cold-pressing hafnia and graphite powders such that the mass ratio of HfO_2:C was 94.6:5.4. The films were deposited with the substrate at room temperature and placed at a distance of 26mm from the target.

(ii) Carbothermal reduction

The target was a sintered HfO_2 pellet (Cerac Inc). Acetylene gas was used as the carbon source and its pressure was varied from 0-28 mTorr. A sample from the run which introduced the most free carbon into the film was cut into equal sized pieces and capped with either an amorphous silica layer or an amorphous silicon nitride.

The preliminary oxidation behavior of the resulting films was determined using a simultaneous thermogravimetric analyzer and differential scanning calorimeter, SDT Q600, with a sensitivity of 0.1 μg (TA Instruments, Inc). Samples of equivalent nominal thickness were used so that differences in the oxidation behavior could be studied. The

oxidation experiments in the SDT and the tube furnace were performed at 600 °C and 700° C.

The procedure for SDT was as follows: In argon flow set at 30 ml/min, the sample was heated to oxidation temperature at 50 °C/min. The sample was then held at that temperature while the flow was switched to high purity compressed air set at a flowrate of 3 ml/min. The sample was then equilibrated to the oxidation temperature and held at this temperature for 60 minutes.

Films from the binary target were deposited on silicon carbide substrates at the same time as the deposition on Si. The samples were oxidized in a tube furnace after deposition at 1100 °C for 2 hours in 3.2 Torr of O_2/Ar.

The tube furnace used for the films deposited by reactive PLD was different from that used to oxidize the films on the silicon carbide substrates. The quartz tube inlet was connected directly to the gas lines while the outlet was sealed loosely with a quartz cap. High purity oxygen set at flowrates between 10-30 ml/min were used.

After the films were deposited and oxidized, their surface and bulk composition were determined using XPS and RBS respectively.

Results & Discussion

(I) Film Characterization

The films deposited from the binary target were strongly adhered to the substrate. However, the surfaces were not smooth due to the presence of particulates on the surface (Figure 4.1). From prior work done with our laser deposition system, it is known that the

hafnia target ablated with a 308nm XeCl excimer laser produces relatively droplet and particulate free films therefore the particulates observed here must be due to the graphite present in the binary target. RBS analysis also indicates excess carbon on the surface and a bulk composition of $HfO_{2-x}C_y$. The exfoliation of the graphite particulates is due to the poor quality of the target made. The difference in the grain sizes of the powders used and because cold-pressing does not induce a chemical reaction between the hafnia and carbon powders, results in a non-compact target.

The interlayer formed in the oxidation of hafnium carbide is free carbon dissolved in hafnia. This chemical composition has been theoretically determined to make the films efficient oxygen diffusion barriers. XPS analysis of the $HfO_{2-x}C_y$ films deposition in our studies however indicate that all the carbon, even the carbon particulates on the surface, is bonded to oxygen while some of the oxygen is also bonded to hafnium. No free carbon is present anywhere in the film. Therefore a difference in oxidation behavior of the $HfO_{2-x}C_y$ films can be expected.

Films deposited using the acetylene gas had no particulates present within or on the surface of the films. However, the film thicknesses were not uniform from the center to the edges of the substrate. The maximum thickness was at the center of the substrate, which coincides with the center of the plume. The film stoichiometry was determined by RBS and was found to be consistent within the center of the film.

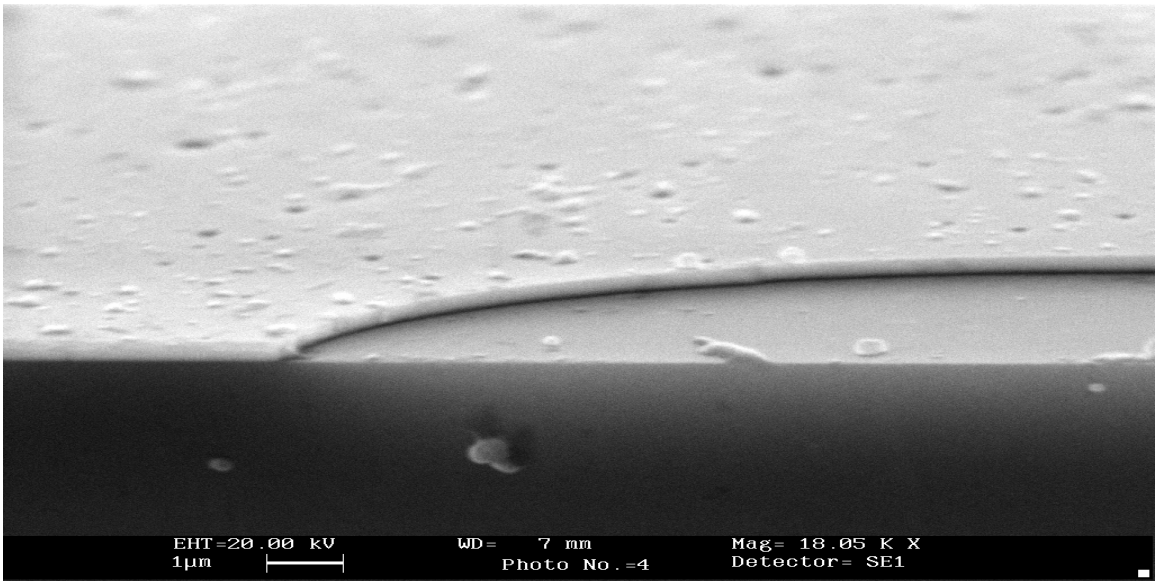

Figure 4.1: SEM image of the HfO_xC_y film deposited on Si(100) from a binary target. (*MPL, SRI International, Menlo Park, CA*).

The films were deposited using a range of acetylene pressures to control the introduction of carbon into the hafnia films. Table 4.1 has the elemental composition determined from RBS analyses. Below 28 mTorr, the carbon signal was below the detection limit of RBS. When 28 mTorr acetylene was used, a carbon signal was observed in the RBS data and the hafnium signal height and width decreases. This decrease suggests the deposition rate decreased.

Table 4.1: Film stoichiometry determined from RBS data.

PC_2H_2 (mTorr)	Hf	O	C
0	1	1.71	-
3	1	1.85	-
10	1	2.04	-
28	1	3.21	3.79

Unlike in RBS, carbon species were detected in XPS. Increasing the acetylene pressure did increase the carbon concentration, with more free carbon and more carbonyls forming (Table 4.2).

Table 4.2: The percentage of each type of carbon bonds present within each film.

Pressure of C_2H_2 (mTorr)	C-C	C-O	C=O
3	0	78.95	11.13
10	3.19	77.61	3.66
28	8.25	39.17	32.58

(II) Oxidation Behavior of HfO_xC_y films

The weight change (TG) curves obtained from the SDT analysis for films pre and post-oxidized at 600 and 700 °C are shown in Figure 4.2-4.4 below.

At 600 °C, the oxidation rate for the films deposited from the binary target was low but the mass steadily increased. No mass loss due to CO_2 evolution was observed. At 700 °C, an initial mass loss was observed followed by an increase, a plateau and then an increase again. The mass loss is attributed to carbon loss as CO_2. However, what is of interest is that despite the concentration of carbon present in the film, only a slight mass loss was observed at 700 °C. The two regions of increasing mass observed in the TG curves are harder to identify since the film is not homogeneous in composition. A hypothesis is that the initial increase is due to an intermediate metastable phase HfO_2C forming [5], followed by the increased growth of the hafnia. Since the graphite particulate production and distribution cannot be controlled with each deposition, the

oxidation behavior observed may not be reproducible and may differ from region where no particulates are present to regions where particulates are present.

The pure HfO_2 and the film with the highest carbon content introduced with the acetylene gas behaved differently. At 600 °C, a more significant mass loss was observed for the oxycarbide as a result of carbon evolution as CO_2. The slight mass loss for the pure hafnia is attributed to the removal of any adsorbed gas. At the higher temperature, the same mass loss behavior was observed. However both samples begin to oxidize at this temperature, with the onset of oxidation being earlier for the hafnia. The simultaneous DSC measurements for all four runs do not show any sharp reaction heat loss or gain hence are not shown here.

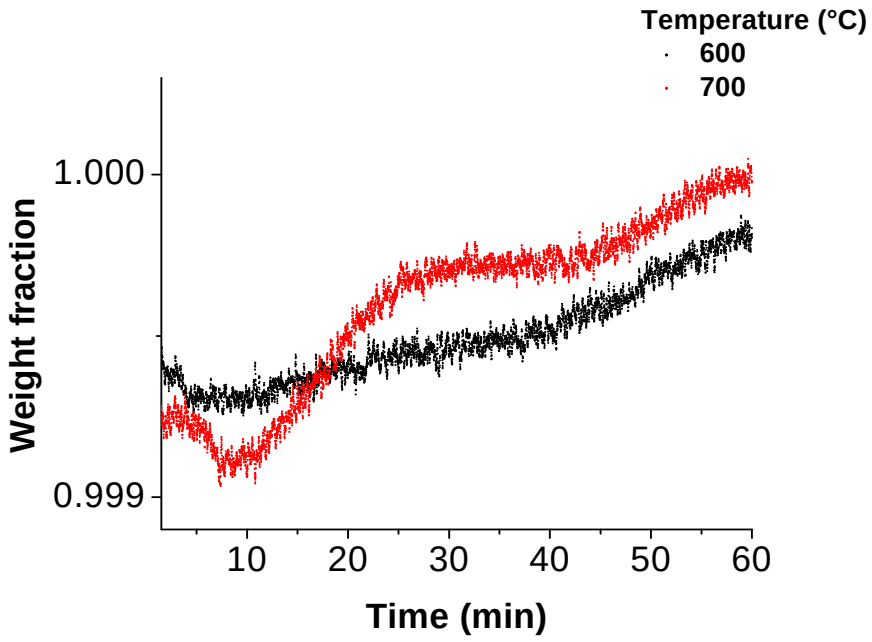

Figure 4.2: Thermogravimetric curves obtained during oxidation of hafnium oxycarbide deposited from the binary target for two different temperatures.

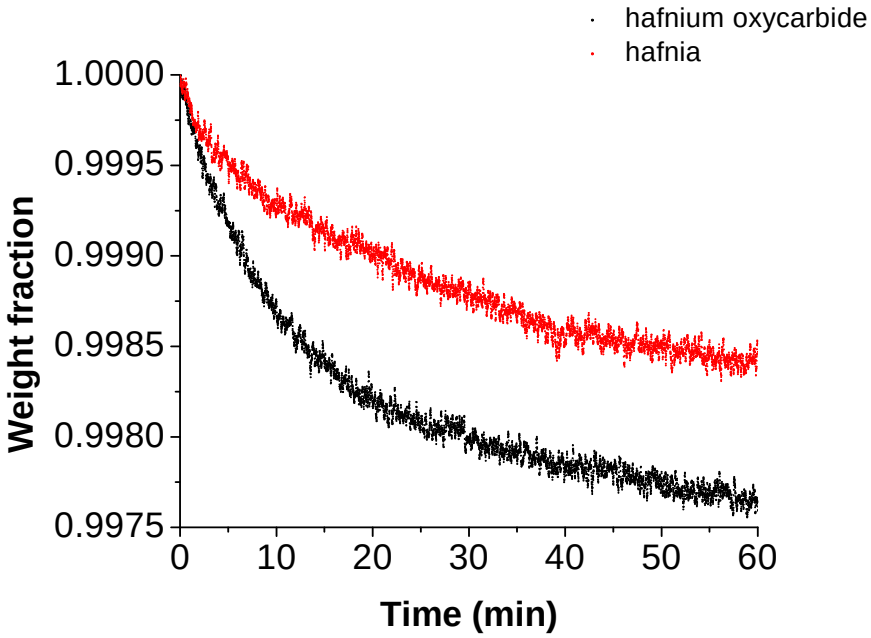

Figure 4.3: The thermogravimetric curves for hafnia and hafnium oxycarbide (28 mTorr) oxidized at 600 °C.

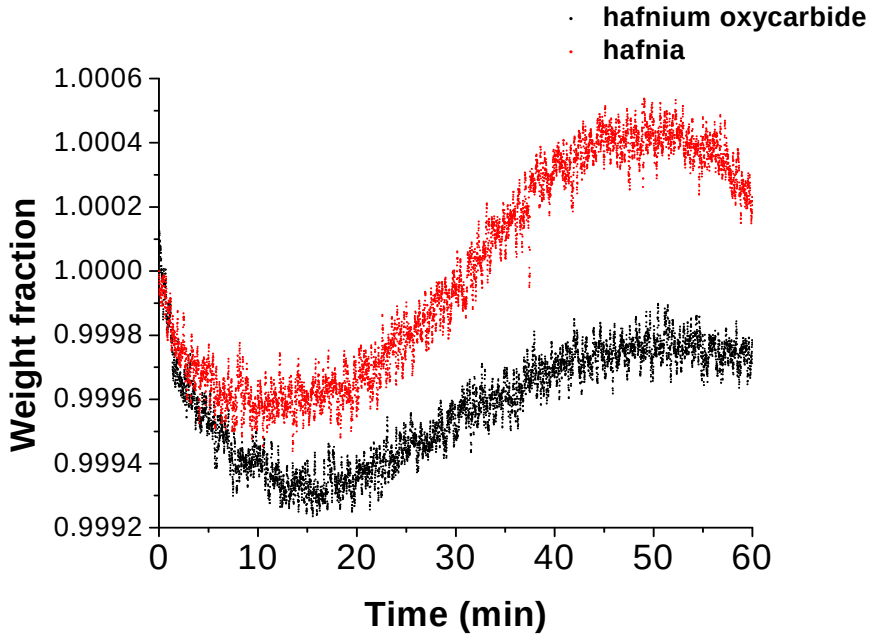

Figure 4.4: The thermogravimetric curves from the oxidation of hafnium and hafnium oxycarbide at a higher temperature of 700 °C.

RBS and XPS analysis of films oxidized in the furnace confirmed the oxidation mechanism suggested by SDT analysis. For all the films, the onset of oxidation is dependent on both the temperature and the oxygen pressure.

Figure 4.5 is the RBS spectra obtained for the oxycarbide film with free carbon before and after oxidation for 5 minutes in pure oxygen flowing at 30 ml/min. Most of the carbon was removed from the film. XPS analysis further confirms that no carbon was present in the film after the oxidation. The behavior of these oxycarbide films are different from that of the oxycarbide interlayer formed in the oxidation of hafnium carbide. In the latter, the free carbon is present at all times in the interlayer, even at high oxidation temperatures, and this chemical composition makes it a better oxidation barrier than either the underlying hafnium carbide or the outer oxide.

The oxidation mechanism for films deposited from the binary target did not involve complete carbon removal even at the low temperatures tested in the SDT. Since the films were also deposited on a SiC substrate, an oxidation run at a higher temperature was conducted to determine whether a significant loss of carbon would be observed. The survey and core shell spectra for Hf 4f, C1s and O1s were collected for pre- and post-oxidized films and are shown in Figure 4.6a-c. The XPS spectra were used to determine elemental composition. These results are given in Table 4.3. There is a loss of carbon during the oxidation, however most of carbon is still retained within the film. The free carbon bonds with the oxygen already present in the film and with the oxidant species. The multiplet splitting for the Hf 4f peak is broader after oxidation. This suggests some hafnium metal atoms reacted with the oxygen.

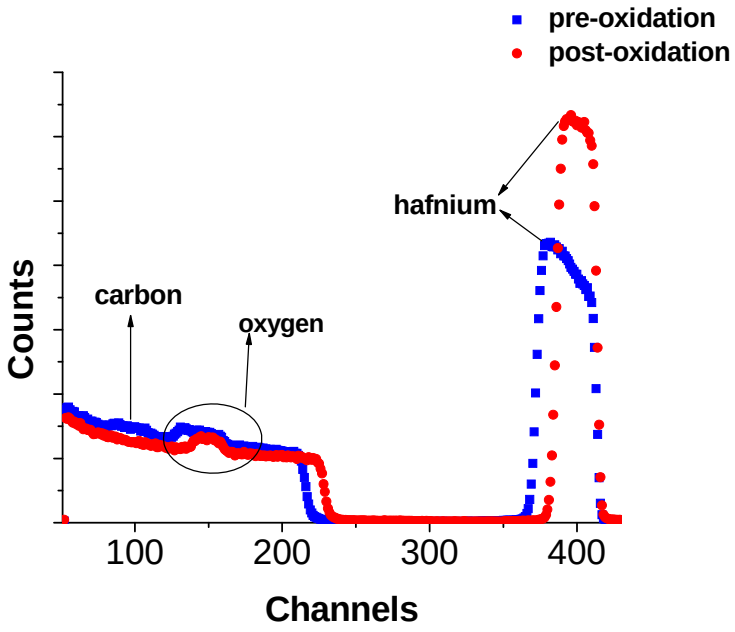

Figure 4.5: RBS spectra taken of the hafnium oxycarbide films show a significant loss of carbon upon oxidation.

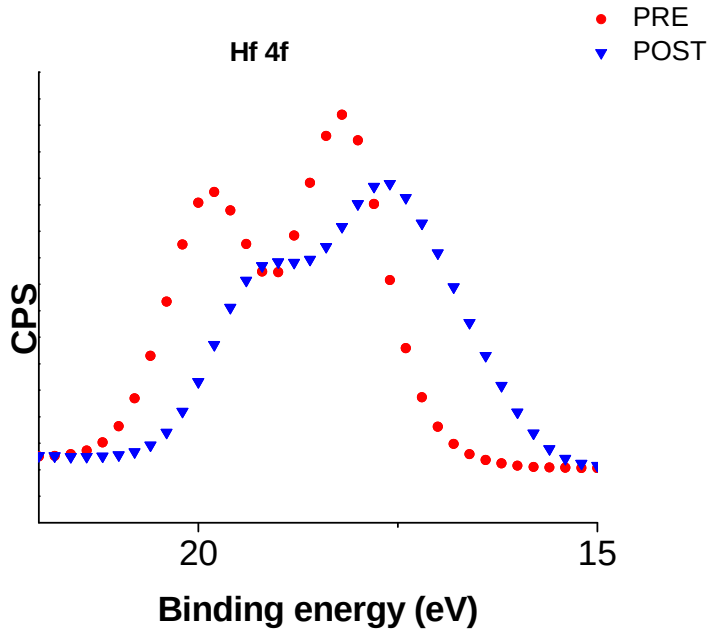

Figure 4.6a: The Hf 4f spectra collected from the as-received and oxidized film deposited from binary target.

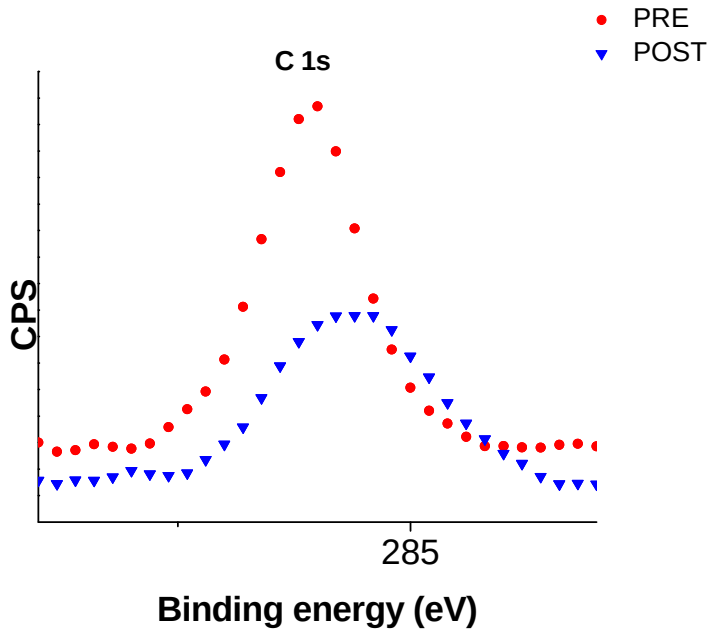

Figure 4.6b: The C 1s spectra collected from the as-received and oxidized sample film deposited from binary target.

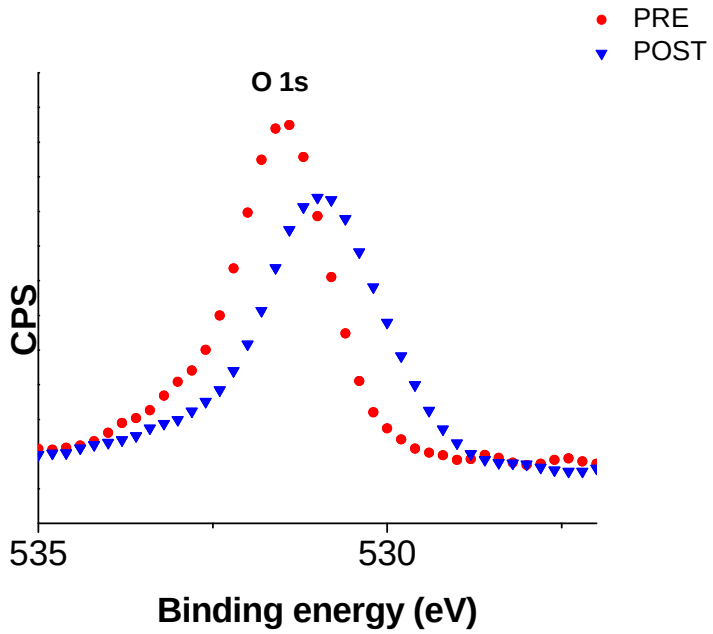

Figure 4.6c: The O 1s spectra collected from the as-received and oxidized sample film deposited from binary target.

Table 4.3: The chemical bonds deconvoluted from each of the core spectra indicated for the film deposited from the binary target.

Sample	C1s	O1s
Pre-oxidation	100% C-O	1.65% Hf-O 91.85% C-O 8.15% C=O
Post-oxidation	89.27% C-O 10.73% C=O	9.68% Hf-O 80.81% C-O 9.51% C=O

The oxidation experiments show that a stand-alone hafnia film with free carbon would not be a suitable oxidation barrier due to the carbon removal by oxygen. This result is different from that observed in the oxidation of hafnium carbide, where the formation of any interlayer of hafnia with free carbon that never burnt off, prevented further diffusion of oxygen to the underlying carbide. While the superior oxidation barrier properties of the oxycarbide interlayer has been accepted, our work highlights the fact no studies have been done to determine whether the enhanced properties are indeed due to the presence of the free carbon dissolved in hafnia. An alternative hypothesis is that initially the oxygen reacts with the carbon atoms at the surface of the hafnium carbide and those a few monolayers within. The oxygen atoms intermix with the carbon atoms to form the interlayer. Any more oxygen diffusing in will react at the surface of the intermixed region since no more carbon atoms are present for reaction. This results in the growth of an outer hafnium oxide which could then suppress the removal of the carbon by the oxygen diffusing into the film.

While free carbon is easily removed from the films, carbon bonded to oxygen in the films can be retained depending on the binding energy of the carbon-oxygen bond. Most of the carbon in the films produced with acetylene was lost upon oxidation while the carbon in the films produced from the binary target remained in the film. The processing issues associated with $HfO_{2-x}C_y$ films produced from the binary target render it unsuitable for use as is however it shows that the presence of the carbon bonded to oxygen in the hafnia makes the film resistant to oxidation and thereby still a viable candidate for use as protective coatings in hypersonic vehicles.

Conclusions

Previous studies have shown that hafnium oxycarbide formed during the oxidation of hafnium carbide served as a barrier to the further oxidation of the underlying carbide. The interlayer grows between the underlying carbide and the outer oxide. The oxycarbide layer is described as free carbon dissolved in a hafnia lattice [2-3]. In this work, the use of hafnium oxycarbide as a stand-alone thermal and oxidation barrier coating was explored. Two methods of oxycarbide deposition by pulsed laser deposition were tested. Both involved using a hafnia target with the inclusion of two different carbon sources.

The two different types of oxycarbide films each had limitations for their use as a protective coating. Using acetylene gas as the carbon source produced films where the concentration of carbon was high, i.e. $x \leq y$, and the carbon was removed at temperatures as low as 600 °C, followed by further oxidation of the remaining hafnia. Introducing

more carbon into the film, increased the rate of removal of the carbon and reduced the film barrier properties. Using graphite as a carbon source produced non-uniform films with many particulates embedded within the film. Films with such defects cannot perform as high temperature coatings since the oxidation behavior of the film, the defects and the particulates cannot be suitably controlled.

However an important observation is that, using graphite to produce films of composition $HfO_{2-x}C_y$, no free carbon was present initially and the carbon was bonded to the oxygen pre and post oxidation. The carbon-oxygen bond was stronger than those present in the film deposited with acetylene therefore most of the carbon was still retained within the film even after oxidation at high temperatures for long times. This chemical structure is different from that observed in the interlayer that forms during the oxidation of hafnium carbide. However, the oxidation behavior of the films indicates that it could still serve as a protective coating.

In conclusion, keeping the film substoichiometric i.e. $y < x < 2$, using graphite as the carbon source and having the carbon bonded to the oxygen, most of the carbon is retained in the films even after oxidation at high temperatures. Further investigation is necessary to determine if the elimination of the graphite particulates embedded into the $HfO_{2-x}C_y$ films would then provide coatings that are better oxidation barriers than hafnia or hafnium carbide at high temperatures and oxygen pressures.

References

1. Bargeron C.B., Benson R.C., Jette A.N., Phillips T.E., *Oxidation of hafnium carbide in the temperature range 1400 ° to 2060 °C*, J. Am. Ceram. Soc., **1993**, 76(4), 1040-1046.

2. Shimada S., Yunazar F., *Oxidation of hafnium carbide and titanium carbide single crystals with the formation of carbon at high temperatures and low oxygen pressures*, J. Am. Ceram. Soc., **2000**, 83(4), 721-728.

3. Shimada S., Inagaki M., *Oxidation kinetics of hafnium carbide in the temperature range of 480° to 600°C*, J. Am. Ceram. Soc., **1992**, 75(10), 2671-2678.

4. Shimada, S., *Interfacial reaction on oxidation of carbides with formation of carbon*, Solid State Ionics, **2001**, 141-142, 99-104.

5. Shimada, S., *A thermoanalytical study on the oxidation of ZrC and HfC powders with formation of carbon*, Solid State Ionics, **2002**, 149, 319-326.

6. Blum Y.D., MacQueen D.B., Kleebe H.J., *Synthesis and characterization of carbon-enriched silicon oxycarbides*, J. Eur. Ceram. Soc., **2005**, 25, 143-149.

7. Zhilyaev V.A., Zainulin Y.G., Alyamovskii S.I., Shveikin G.P., *High-temperature oxidation of zirconium and hafnium oxycarbides and oxycarbonitrides*, Powder Metall. Met. Ceram., **1972**, 11(8), 632-636.

8. Vodop'yanov A.G., Kozhevnikov G.N., Baranov S.V., *Interaction of Refractory Metal Oxides with Carbon*, Russian Chemical Reviews, **1988**, 57(9), 810-823.

9. Mazzoni A.D., Conconi M.S., *Synthesis of Group IVB Metals Oxicarbides by Carboreduction Reactions*, Mater. Res., **2002**, 5(4), 459-466.

CHAPTER V

THE OXIDATION OF SILICON IN AN O_2/O ENVIRONMENT

Introduction

Silica formers, i.e. Si, Si_3N_4, SiC, are major components of structural materials in hypersonic vehicles that are subjected to partially dissociated oxygen gas environments at high temperatures during use [1]. Previous studies have shown that the oxidation behavior of the materials in a dissociated environment is different from that observed in molecular oxygen [2] . Therefore knowledge of how these individual materials behave in these environments is crucial to material design development.

In this chapter, the oxidation behavior of silicon in partially dissociated oxygen, i.e. a gas mixture of molecular and atomic oxygen, is studied. The oxidation of silicon in molecular oxygen has been studied extensively in the past and therefore is used as a basis for comparison. While the Deal-Grove (DG) model [3] can predict the oxide growth in molecular oxygen, it cannot be extended to the oxide growth observed in atomic oxygen. A parallel oxidation model which incorporates the two types of oxidants, i.e. O_2 and O, was developed by Marschall and co-workers [4]. Based on results of recent computational predictions, two hypotheses are explored within this model: (1) where no interaction occurs between the oxidants as they diffuse/react in the growing oxide, and (2) where the atomic oxygen atoms recombine within the oxide to form molecular oxygen.

Experimental Setup

Experiments were carried out in a quartz tube furnace at temperatures between 910 °C and 1150 °C. A gas flow composed of 87 mole% O_2 and 13 mole% Ar, at a total pressure of 3.2 Torr was introduced. The oxygen is partially dissociated by an attached 6 kW microwave discharge. The discharge power was set at 80% for all experiments. Samples were characterized before and after oxidation using spectroscopic ellipsometry (MD 2000, J.A. Woollam) to determine the oxide thickness. A Cauchy layer model was used to describe the silica layer.

Results & Discussion

Oxidation predictions based on Deal-Grove model

Oxidation experiments were performed in molecular oxygen in order to compare the oxide growth rate with that predicted by Deal-Grove. The DG model [3] was developed to describe the oxidation of silicon in molecular oxygen. Figure 5.1 below outlines the transport processes included in the DG model. The main premise was that the molecular oxygen is the sole oxidant that diffuses through the growing oxide layer to react with the silicon/silica interface to form the oxide. *Ab initio*, first-principles molecular dynamics studies [5] and isotope tracer experiments [6] have since confirmed this assumption.

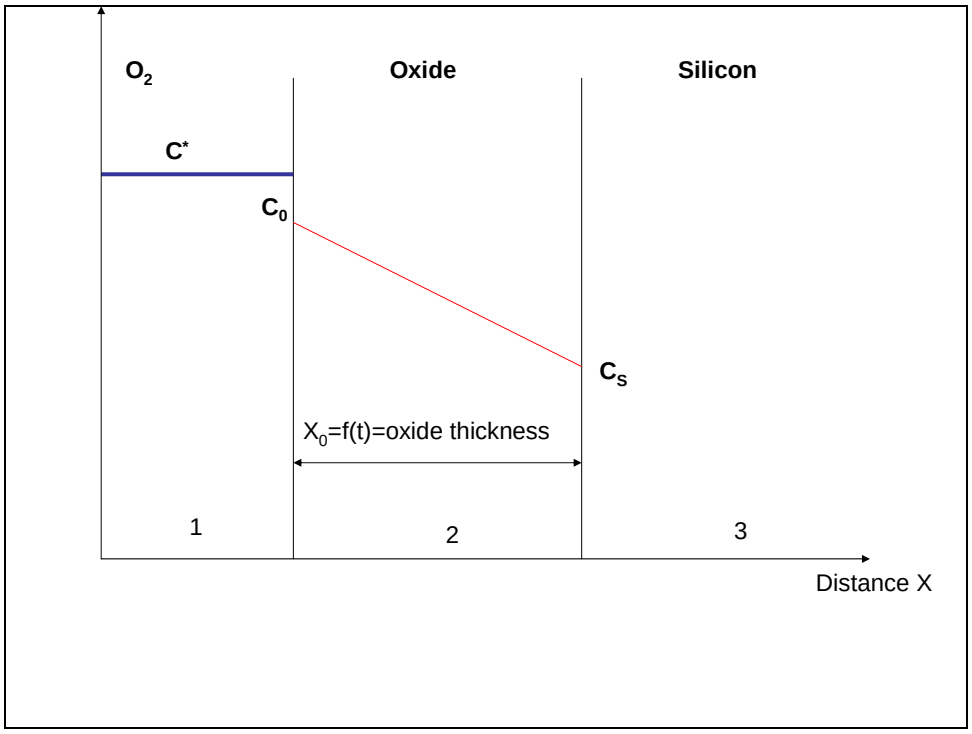

Figure 5.1: The Deal-Grove model for thermal oxidation of silicon.

The following equations describe the oxidant fluxes applicable within the regions marked above:

$$F_1 = h(C^* - C_0) \qquad [1]$$

$$F_2 = D(C_0 - C_S)/X_0 \qquad [2]$$

$$F_3 = k_S C_S \qquad [3]$$

where h is the gas transport coefficient, C^* is the equilibrium concentration of oxygen in the gas phase and is also equal to the maximum solubility in the oxide by Henry's law, C_0 is the concentration of oxygen at the oxide surface at any given time, D is the diffusivity, C_S is the oxygen concentration at the interface and k_S is the surface reaction rate constant.

Writing the above fluxes for molecular oxygen in the three regions and setting them equal (assuming steady state), Deal & Grove developed the following expression for the growth rate of silicon dioxide.

$$\frac{dX_0}{dt} = \frac{\frac{C^*}{N}}{\frac{1}{k_s} + \frac{1}{h} + \frac{X_0}{D}} \qquad [4]$$

where N is the number of oxygen molecules incorporated per until volume of oxide. The analytical form then can be written as,

$$X_0{}^2 + AX_0 - B(t + \tau) \qquad [5]$$

$$A = 2D(\frac{1}{k_s} + \frac{1}{h}) \qquad [6]$$

$$B = 2D\frac{C^*}{N} \qquad [7]$$

where τ is a parameter that takes into account any initial oxide present on the surface of the silicon.

The parameters B and $\frac{B}{A}$, determined from the experimental data, are the parabolic and linear reaction rate constants respectively. It was found that both sets of parameters change with temperature and A with pressure, and can be described by Arrhenius expressions.

The B and $\frac{B}{A}$ values for Si(100) oxidation in molecular oxygen were used to predict the oxide growth at the temperatures tested in our experiments. Figure 5.2a show

the oxide thicknesses obtained from one set of experiments in partially dissociated oxygen. Figure 5.2b plots those predicted by the DG model for oxidation of silicon in molecular oxygen. For all temperatures, the oxide growth rate is much higher in the dissociated environments than that in molecular oxygen.

A parabolic model similar to equation 5 can be used to model the experimental data for oxide growth in dissociated environments. However, the model coefficients A and B would no longer relate to the physical properties defined by Deal and Grove.

Oxidation in partially dissociated oxygen

The difference in oxide growth observed from that predicted by the DG model highlights the fact that for the oxidation of Si by atomic oxygen, the growth sequence is more complex. Recent computational and isotope tracer experiments have outlined some of the possible processes that could occur.

When in the gas phase, the O atoms recombine with other O atoms or O_2 molecules and/or absorbs onto the surface. Density functional theory (DFT) studies show that more reactive species like O atoms have a 85-90 % probability of absorbing onto a silica surface [7] and will only desorb upon further recombination.

Once adsorbed, O atoms incorporate into a surface Si-Si bond to form peroxyl or ozonyl linkages. Within the oxide network, O atoms can diffuse by two mechanisms. By maintaining equilibrium positions in the interstitial spaces [8] the oxygen atoms can recombine to form molecular oxygen which then out-diffuses or travels to the interface for oxide growth. The oxygen atom can also incorporate itself in the Si-O-Si network [8-

11], to form peroxyl or ozonyl linkage, followed by further diffusion through exchange within the network [11] which requires less energy than the removal of O atoms from the

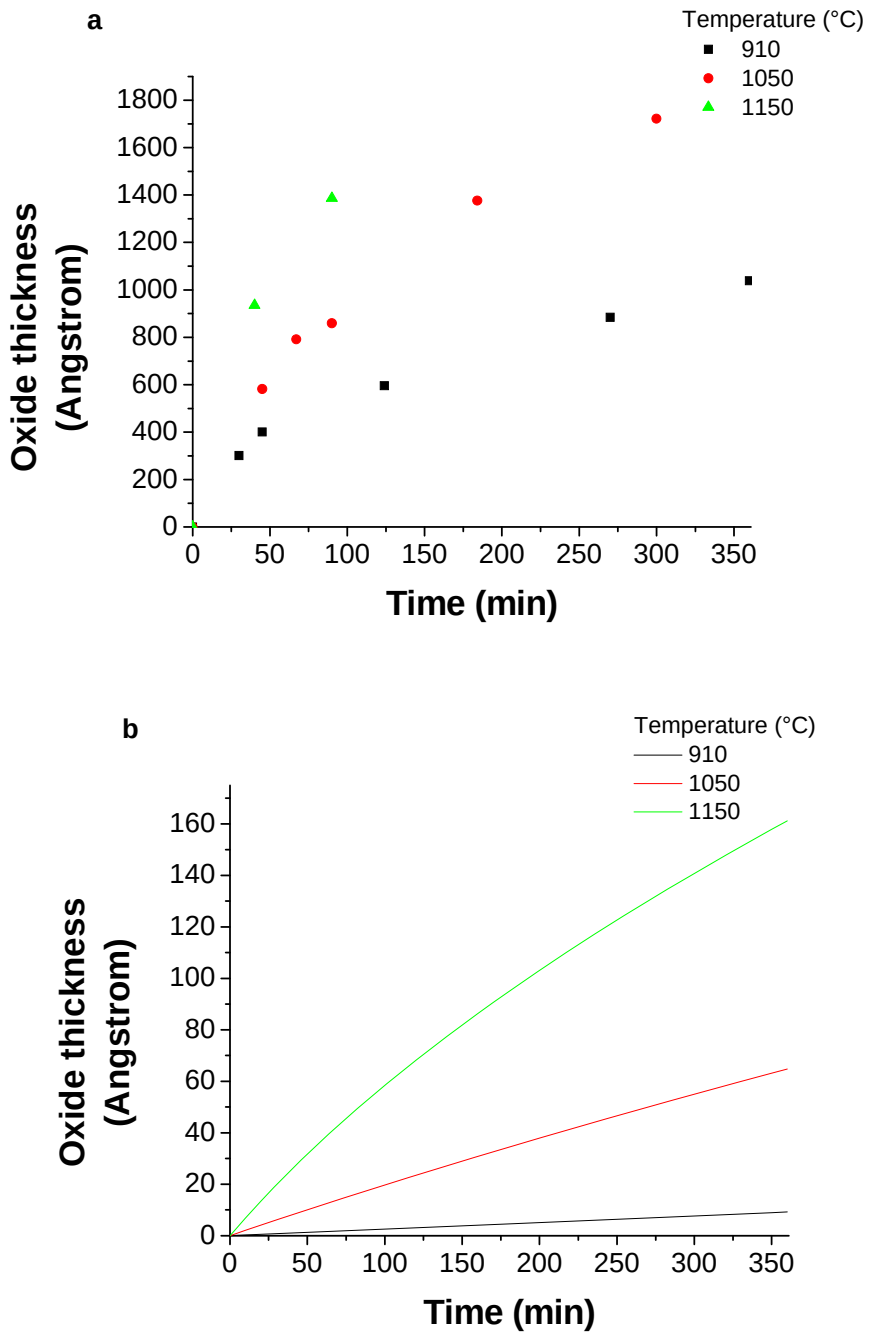

Figure 5.2: The oxide thicknesses for silicon (a) oxidized in partially dissociated and (b) those predicted by Deal-Grove model (DG) for oxidation in molecular oxygen at the same temperature and pressure.

linkages by breaking the bonds [10]. However, there have been conflicting reports as to the main O atom transport mechanism within the oxide network.

First principle studies on the energetics of oxygen species in quartz [12, 13] and amorphous silica [14] predicts that neutral interstitial molecular oxygen would be the lowest energy configuration in an oxide, and that if any oxygen atoms are present, they would bond to network species as peroxyls. However, theory also predicts that the separation of an interstitial molecular oxygen into two network defects is also energetically favorable. The latter statement is confirmed by isotope tracer studies of thermal oxidation of silicon in molecular oxygen that resulted in an uniform distribution of ^{18}O throughout the oxide network at temperatures higher than 1300 °C [6].

However, two different sets of isotope tracer studies [15-18] showed that either mechanism was plausible. In the $^{16}O_2/^{18}O$ sequential oxidation of Si in microwave discharge at 580 °C show the amount of ^{18}O initially at the surface equaled to that in gas phase. As the oxide grew, the ^{18}O migrated to the Si-SiO_2 interface, exchanging with O atoms in the oxide network. Eventually the ^{18}O became uniform through the oxide with the total concentration equal to that in gas phase. In a reverse oxidation sequence, that is $^{18}O_2/^{16}O$ the ^{18}O detaches from the oxide surface and diffuses to the ambient and/or migrates to an interface for further oxidation. Both experiments indicate that either of the mechanisms is possible.

Additionally, previous literature shows that catalytic recombination of oxygen atoms can occur on various silica surfaces [19-21]. This implies that more molecular oxygen could become available within the oxide to diffuse to and react at the silicon-silica interface.

One of the earlier models developed by Peeters and co-workers [22] describes this recombination of O atoms on silica surface as limiting since it produces the less reactive and mobile molecular oxygen. The model assumes the following: diffusion is negligible, atomic O is the only oxidant, recombination follows a first order kinetics with respect to gas phase composition and that the molecular oxygen formed out-diffuses rather than incorporating in the Si-O-Si bonds at the interface due to lower energy barriers for the former process.

The model adequately describes a range of experimental data; however the high magnitude of the recombination rate coefficients (k) holds no plausible mechanistic meanings. As suggested by Peeters, the presence of dopants in Si could create electron sites or dangling bonds that act as collision sites for the free O atoms. However the possibility of faster reaction rates due to rapid attachment to these sites cannot be justified when the rate of dissociation is unknown and because recent energetics calculations indicate that having more interstitially migrating O atoms than O atoms in the network is not feasible.

No model exists that can accurately predict the oxidation behavior of silicon in a dissociated environment. The results from computation work state that both molecular and atomic oxygen can play a role in the oxidation of silicon in a dissociated oxygen environment. A model has been developed using these theoretical findings in conjunction with the Han and Helms [15] parallel oxidation model. The oxidation process is described by taking into account both interstitial molecular oxygen and network oxygen defects, and their exchange/reaction within the oxide.

(i) The Parallel Oxidation model

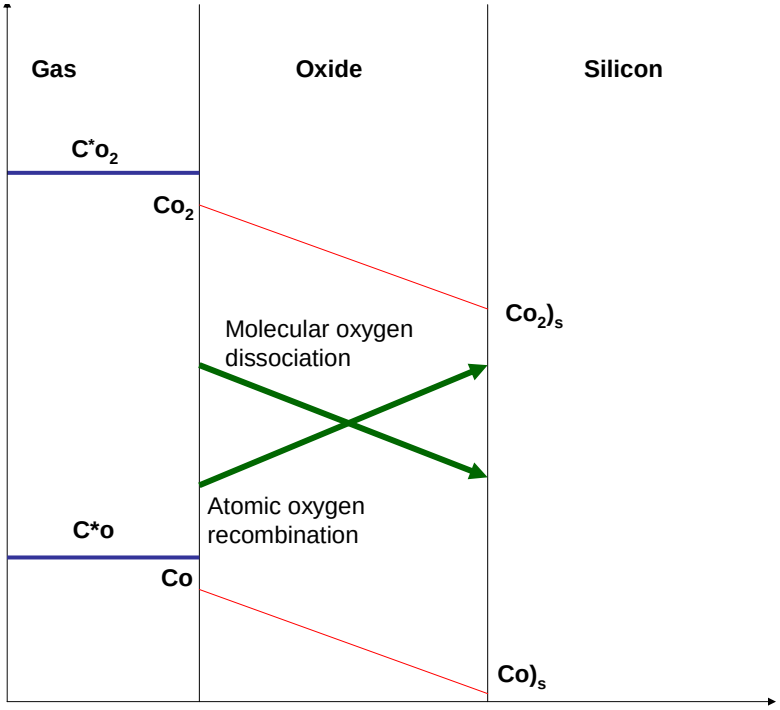

Figure 5.3: Parallel oxidation model for the oxidation of silicon with both atomic and molecular oxygen present in the gas phase.

As in the Deal-Grove model, both the oxidants, atomic and molecular oxygen adsorb unto the silica surface. The concentrations at the surface are determined by Henry's law which states that at a constant temperature, the amount of gas dissolved in a solid is proportional to the partial pressure of that gas in equilibrium with the solid.

$$C_{O_2}^{*} = C_{O_2} = \alpha_{O_2} \frac{P_{O_2}}{RT} \qquad [8]$$

$$C_{O}^{*} = C_{O} = \alpha_{O} \frac{P_{O}}{RT} \qquad [9]$$

where α_{O_2} and α_O are the molecular and atomic oxygen solubilities in the oxide respectively.

Once it dissolves into the oxide, the molecular oxygen diffuses interstitially with an effective diffusivity of D_{O_2}, while the atomic oxygen diffuses via peroxyl linkages with an effective diffusivity of D_O. During the transport through the oxide, the molecular oxygen can dissociate via a first order reaction at a rate constant of K_2 to produce oxygen atoms. Network atomic oxygen can recombine via a second order reaction with a rate constant of K_1. Once both oxidants reach the silica/silicon interface, they both react to form an oxide via a first order reaction with rate constants k_{O_2} and k_O respectively. $C_O\big|_S$ and $C_{O_2}\big|_S$ are the concentrations of atomic and molecular oxygen respectively at the silicon-silica interface.

The mass conservation equations for the two species are:

$$D_O \frac{\partial^2 C_O}{\partial x^2} = K_1 C_O{}^2 - 2K_2 C_{O_2} \qquad [10]$$

$$D_{O_2} \frac{\partial^2 C_{O_2}}{\partial x^2} = K_2 C_{O_2} - 0.5 \times K_1 C_O{}^2 \qquad [11]$$

The initial and boundary conditions at the silicon-silica interface for atomic and molecular oxygen are:

$$C_O(0) = C_O{}^* \qquad [12]$$

$$C_{O_2}(0) = C_{O_2}{}^* \qquad [13]$$

$$-D_O \frac{\partial C_O}{\partial x} = k_O C_O\big|_S \qquad [14]$$

$$-D_{O_2} \frac{\partial C_{O_2}}{\partial x} = k_{O_2} C_{O_2}\big|_S \qquad [15]$$

Equations 9-15 were converted to a dimensionless form and numerically solved by the second order forward finite difference method, using a FORTRAN code [23].

The analysis was divided into two parts: (1) dissociation and recombination reactions in oxide are negligible, and (2) atomic oxygen recombines to form molecular oxygen within the oxide.

The parameters for molecular oxygen are known from literature and are listed in Table 5.1 below.

Table 5.1: Molecular oxygen transport and reaction parameters.

Temperature (°C)	D_{O_2} **(m²/s)**	k_{O_2} **(m/s)**	α_{O_2}
910	3.5e-13	1.5e-6	0.01
1050	1.3e-12	1.2e-5	0.01
1150	2.7e-12	4.0e-5	0.01

Since the reaction rate constant, diffusivity and solubility for atomic oxygen are unknown, a range of values were studied for these parameters. This was done by incorporating the following dependencies between the parameters for molecular and atomic oxygen: D_O = Rd* D_{O_2}, k_O = Rk* k_{O_2} and α_O =Ra* α_{O_2} where Rd, Rk and Ra are the ratios of diffusivity, reaction rate constant and solubility of atomic oxygen to molecular oxygen respectively.The reaction rate constant for atomic oxygen was

constrained to be greater than that for molecular oxygen, while the diffusivity value was varied from atomic oxygen diffusion being dominant to the molecular oxygen diffusion being dominant.

The input parameters into the code were the temperature, the pressure, the gas composition for argon, molecular and atomic oxygen, the diffusivity, the reaction rate constant and solubility for molecular oxygen, and values for Rd and Rk.

The oxide thicknesses determined from our experiments are also input into the program. The program uses the inputted parameters, computes an oxide thickness for those parameters and oxidation time, compares it to the experimental data and outputs a value for the least square error (LSE) and for Ra.

Contour plots, for each temperature, which include the ratio of diffusivity and ratio of reaction rate constants studied, with the resulting solubility ratios and LSE values predicted, were developed.

(ii)The effect of no reactions within the oxide

In the analysis, the dissociation and recombination rates are taken to be negligible, i.e. the oxidation would occur primarily due to atomic and molecular oxygen diffusion to and reaction at the silicon/silica interface. Figures 5.4a-c are the contour plots developed for these conditions.

For each temperature, two plots are shown; one has the least square error value regimes for the range of diffusivity and reaction rate ratios studied. The right hand side plot is the solubility ratio values determined for the same combination of parameters in

the complementary plot. The horizontal and vertical lines in Figure 5.4a show how the values for each parameter can be determined using the contour plots.

The grey region in each contour plot indicates the range of parameter values that best fit the experimental data. An example of how this was done is shown below for oxidation temperature of 910 °C.

From the contour plot for 910 °C, point A is taken within the grey region and point B is taken outside the grey region. Table 5.2 gives the parameter values obtained at those points. The plots in figure 5.5 show the experimental oxide thicknesses and those predicted by the model using the parameters at point A and point B. By observation one can conclude the parameters within the grey region, Point A, provide a better fit than those outside the grey region, Point B.

Table 5.2: Parameter values determined from two regions within the 910°C contour plot.

Identification	Log(Rk)	Log(Rd)	Log(Ra)	Boundary
Point A	1.66	-0.25	>4.2	w/in 6.9
Point B	0.83	-0.24	>4.2	13

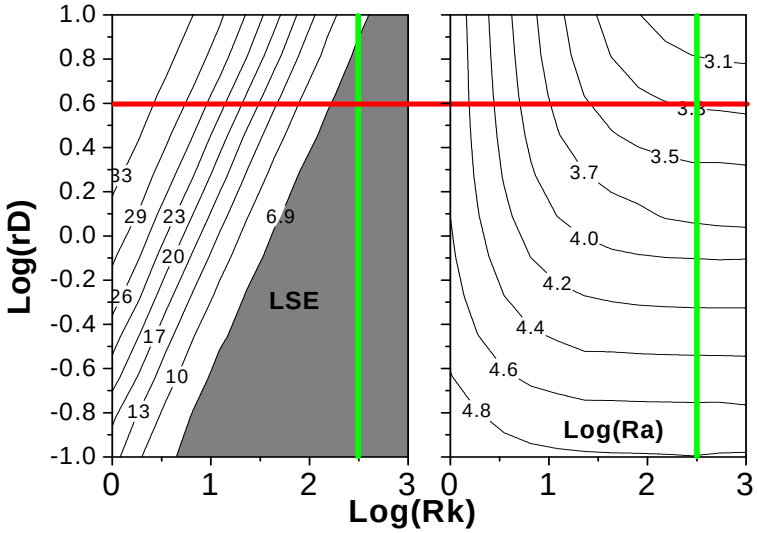

Figure 5.4a: Contour plots developed for 910 °C for the range of parameter values studied. The plots are used in conjunction with each other. The vertical lines mark the same reaction rate constant ratio of 2.5, the horizontal line a value for the diffusion rate ratio of 0.6 and the point were the two lines meet in the right hand side plot is the ratio of solubility value (3.3)for that set of parameters.

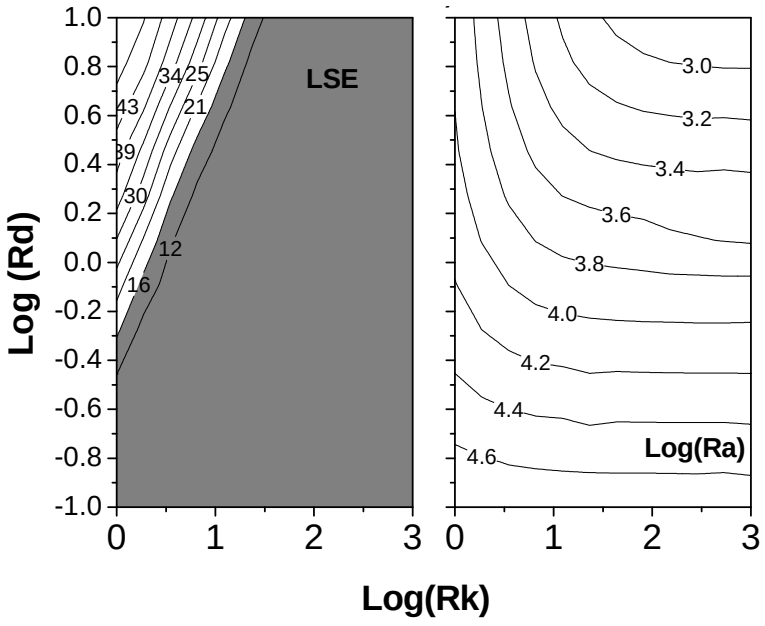

Figure 5.4b: Contour plots developed for 1050 °C for the range of parameter values studied.

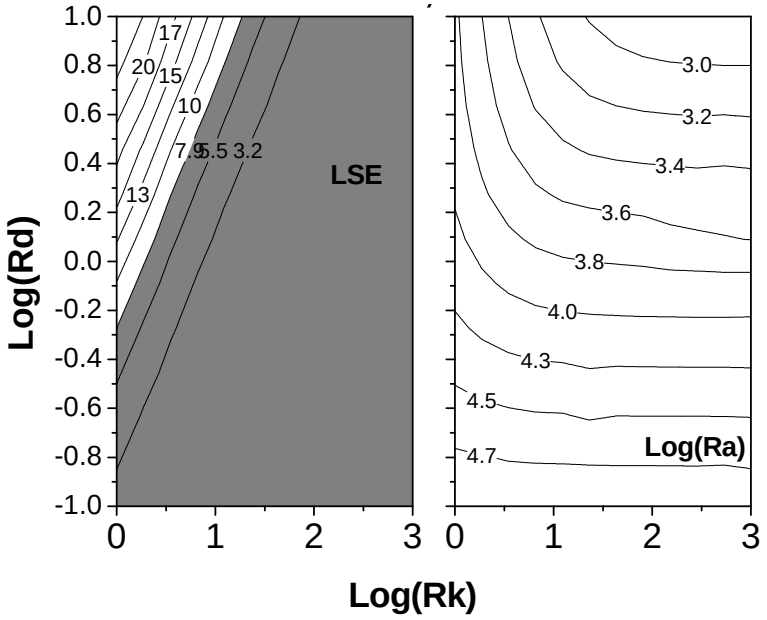

Figure 5.4c: The contour plots for 1150 °C which indicate only a small change from that at T=1050°C in the range of acceptable parameter values.

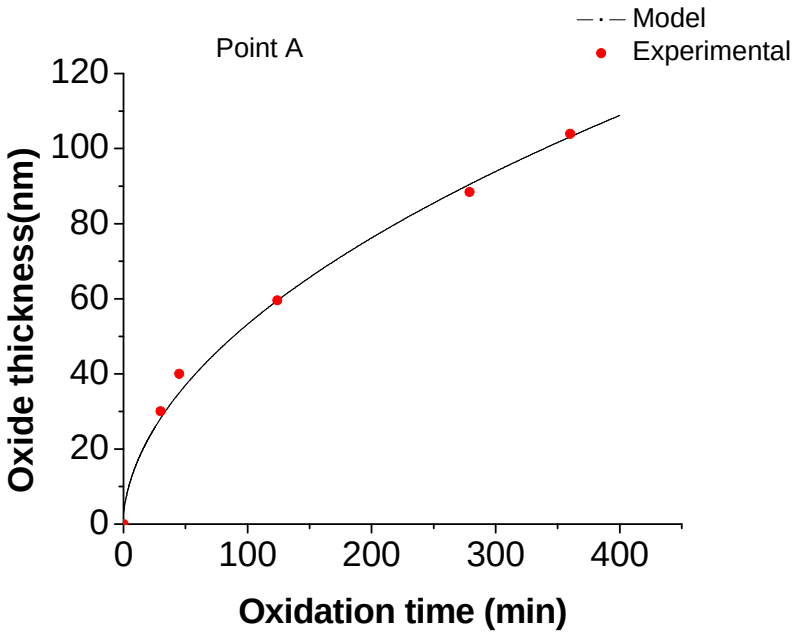

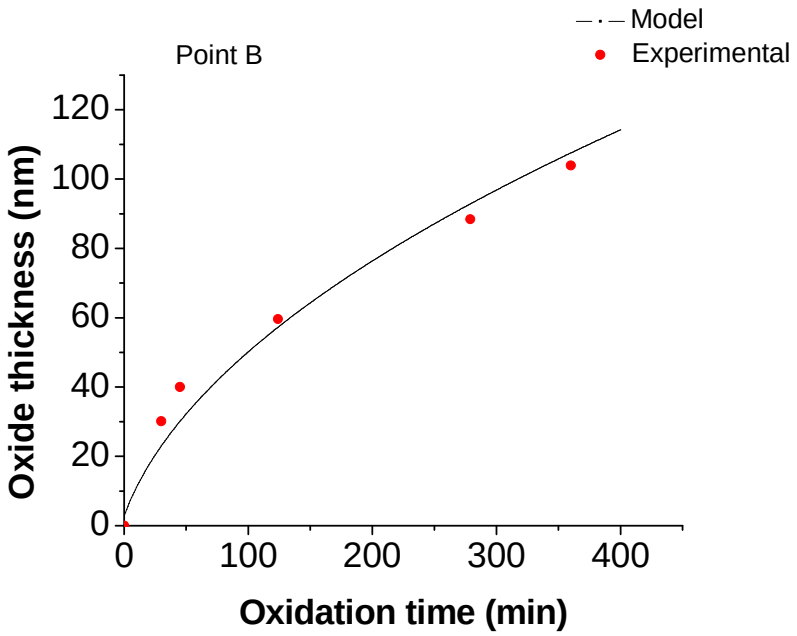

Figure 5.5: Experimental oxide thickness and thicknesses predicted by parameters taken from within and outside the grey region in the contour plots for 910 °C.

Based on our computations, for the range of diffusivity and reaction rates tested, the solubility of atomic oxygen is always greater than that of molecular oxygen.

At 910 °C, as the ratio of atomic to molecular oxygen solubility decreases, the diffusivity of the atomic oxygen is seen to increase, with a faster reaction rate predicted at the Si/SiO_2 interface. This means that whatever oxygen atom is adsorbed on the silica surface is immediately transported to the silicon-silica interface for reaction. The parabolic growth observed at longer times can then be accounted for by the increase in diffusion length as the oxide gets thicker.

If most of the oxygen atoms do dissolve into the oxide, the model predicts that the range of possible reaction rates at the interface remains unchanged, but the diffusivity of the oxygen atom is lower than that for molecular oxygen. Since there is no interaction between the molecular and atomic oxygen atoms, the results indicate that the oxide growth is primarily through the molecular oxygen reaction.

At higher temperatures, theoretically the diffusivity, solubility and the reaction rate constants of both oxidants should increase. However, at 1050 °C, the model predicts that the reaction rate constant ratio decreases from that predicted for 910 °C. This implies that either the reaction rate of oxygen atom decreases or only the reaction rate of molecular oxygen increases. Neither scenario is physically plausible.

Within the range studied there is no change, compared to 1050 °C, in the acceptable parameter values for 1150 °C. The same limitations as at 1050 °C hold true and therefore the model would not adequately predict the enhanced growth rates observed in a dissociated environment at the higher temperatures.

These results indicate that the model based on the assumption that no reaction occurs between the atomic and molecular oxygen as they diffuse through the oxide cannot adequately describe the enhanced oxidation rate observed experimentally.

(iii)Molecular oxygen as the dominant defect

In this analysis, the possible reactions between the two oxidants within the oxide was included since calculations assuming no reactions in the oxide indicate that a wide range of parameters can describe the oxidation of silicon.

Using the results derived from computational studies, the following are proposed as the main transport mechanisms. The molecular oxygen dissociates at the surface and recombines within the oxide. Simultaneously, some of the gas phase oxygen atoms will interact with an oxygen atom in the lattice, abstract a nearby oxygen atom to then desorb as molecular oxygen or the abstracted oxygen atom would recombine with the gas phase oxygen atoms. In this way the oxygen atoms would be distributed evenly through the oxide. This scenario was observed in the isotope tracer experiments conducted by Costello. The dominant defect is then the interstitial molecular oxygen. Therefore in terms of the model, K_2 is negligible while K_1 is important.

The presence of molecular oxygen as the dominant defect for the temperature range of interest, can be verified by examining the equilibrium relationship between the vacancy (created by O atoms) and the interstitial (molecular oxygen) within a silicon oxide.

The equilibrium relationship between the concentration of neutral interstitial molecular oxygen and the neutral network oxygen atoms, was formulated based on the Schottky process of interstitial and vacancy generation in a crystal.

A vacancy is generated by moving an oxygen atom in the bulk to the surface whereas interstitials are generated by moving an adsorbed surface oxygen atom into the bulk of the lattice.

The free energy change with the formation of N_{O_2} interstitials and N_O network vacancies is given by [24]:

$$\Delta G_{O_2} = \Delta G_I = H_I - S_I T = N_{O_2} H_{O_2} - k_B T \ln\left(\frac{N_I}{[N_I - N_{O_2}]N_{O_2}!}\right) \qquad [16]$$

$$\Delta G_O = \Delta G_V = H_V - S_V T = N_O H_O - k_B T \ln\left(\frac{N_V}{[N_V - N_O]N_O!}\right) \qquad [17]$$

where N_I and N_V are the total number of interstitials and vacancies within the oxide lattice, H_{O_2} and H_O are the enthalpies of formations, and k_B is the Boltzmann's constant. The minimum of the free energy sum $\Delta G_{O_2} + \Delta G_O$ is determined by differentiation with respect to N_{O_2} and N_O.

After simplifying the logarithmic terms, the equilibrium concentration ratio can be reduced to:

$$\frac{C_O{}^2}{C_{O_2}} = \frac{C_V{}^2}{C_I} \exp\left(-\frac{2H_O - H_{O_2}}{k_B T}\right) \qquad [18]$$

Assuming that all the interstices and the network sites can generate defects, C_V and C_I are 1.46*10^5 moles/m^3 and 8.30*10^3 moles/m^3 respectively. The enthalpy formation of each defect in amorphous silica has been theoretically determined by Richard and co-workers [25] and provides an enthalpy difference value of about 3.0 eV.

Equation 18 indicates that for the temperature range studied in this set of experiments, the concentration of network oxygen (vacancies) is far less than the concentration of molecular oxygen. This result, i.e. that the molecular oxygen is the dominant defect, is used in tandem with the general model developed above. The dissociation rate is considered to be negligible (since the concentration of atomic oxygen is very low) while the recombination rate is set to an arbitrary, yet physically possible, high rate of 1e5 m^3/(mole-s). Using the methods described in part (ii), the range of plausible parameters (Figures 5.6a-c) was determined. Table 5.3 shows two points that were taken from the contour plots for oxidation temperature of 910 °C that were then used to obtain the best fit region. Figure 5.7 are the oxide thickness plots developed based on the parameters from Table 5.3. The same procedure was performed for the contour plots computed at each oxidation temperature.

Table 5.3: Parameter values determined from two regions within the 910 °C, K1=1E5 contour plot.

Identification	Log(Rk)	Log(Rd)	Log(Ra)	Boundary
Point A	1.73	0.13	>4.3	w/in 8.9
Point B	0.68	0.13	>4.3	20

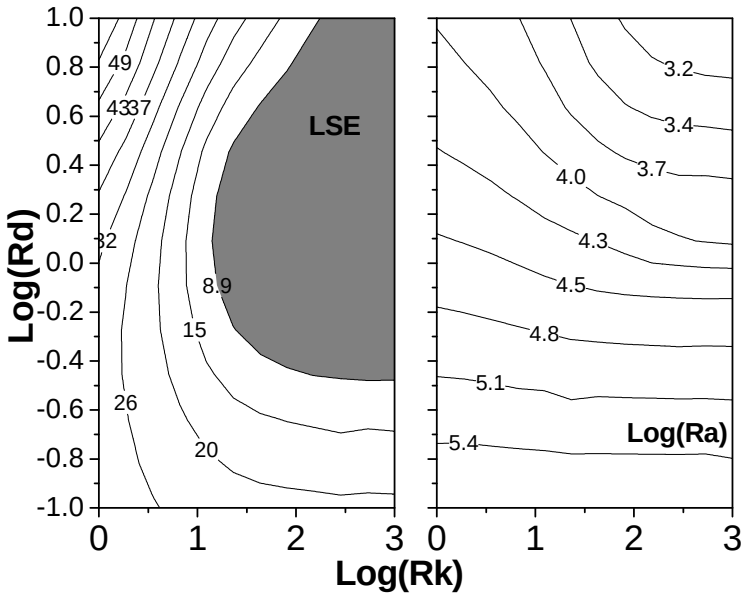

Figure 5.6a: Contour plots developed for 910 °C for the range of parameter values studied.

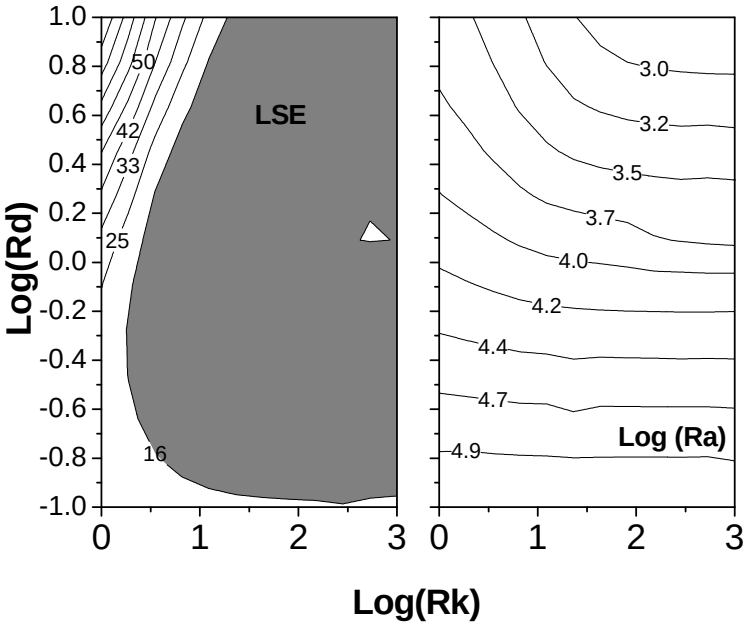

Figure 5.6b: Contour plots developed for 1050 °C for the range of parameter values studied.

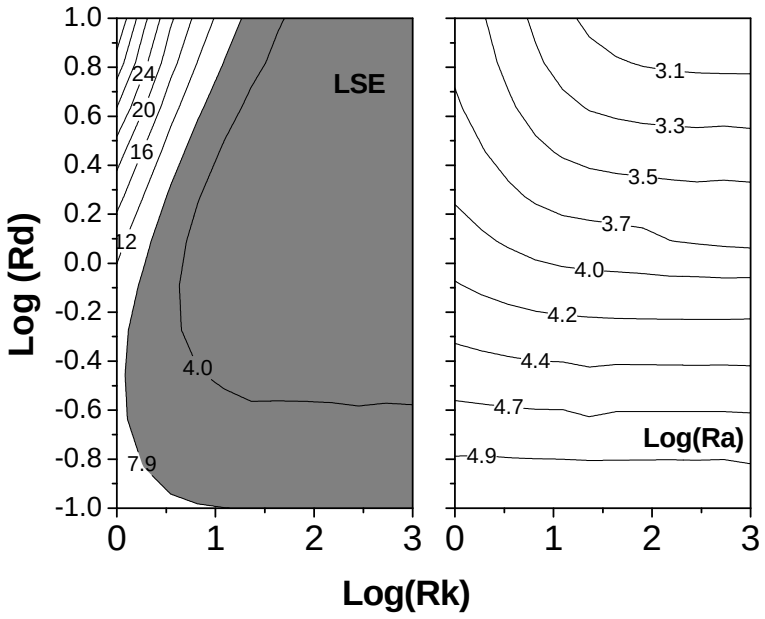

Figure 5.6c: Contour plots developed for 1150 °C for the range of parameter values studied.

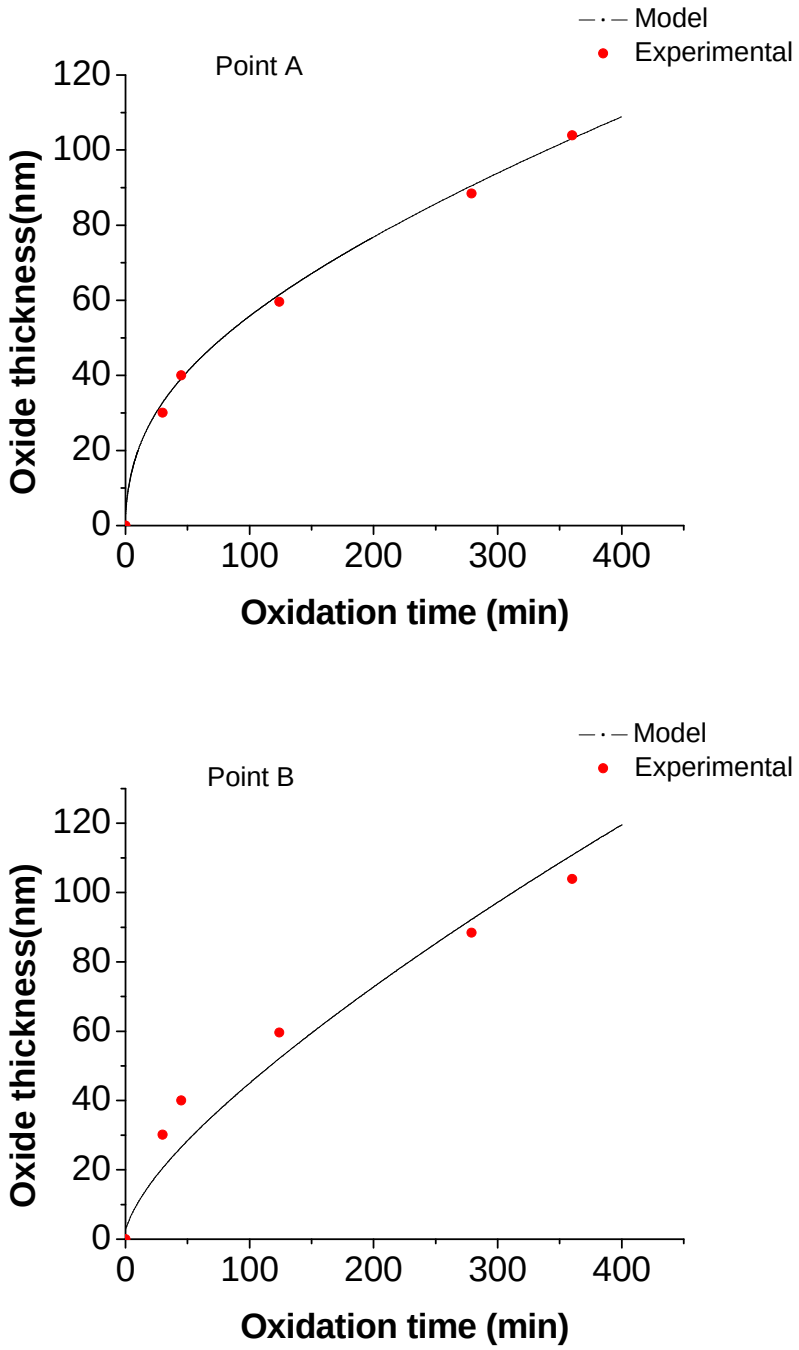

Figure 5.7: Experimental oxide thickness and thicknesses predicted by parameters taken from within and outside the grey region in the contour plots for 910 °C and K1=1E5.

A transport model developed by Vora and co-workers [26] for the dissociated gas flow in the tube furnace, predicts that the concentration of oxygen atoms near the sample decreases by 1% as the temperature is increased from 910°C to 1050 °C. Therefore the high solubility of oxygen atoms predicted by the calculations, as the temperature increases, is instrumental to the oxide growth. The atomic oxygen reaction rate decreases but is always equal to or greater than the molecular oxygen reaction rate. The oxygen atom diffusion rate decreases as observed in experiment.

While the trends observed could explain the enhanced oxide growth rate observed with time and increasing temperature, inclusion of an increase in interstitial oxygen formation within the oxide, has not considerably restricted the range of plausible parameters from those predicted for no reactions taking place within the oxide.

In the same way, a wide range of parameters would be predicted if the theoretically determined energetics of oxygen species within an amorphous silica is disregarded and the network oxygen formation (vacancy) is considered as the dominant defect in the model, i.e. K_1 is negligible while K_2 is a high value.

(iv)The Dual Vacancy-Interstitialcy Diffusion Mechanism

The parallel oxidation model, based on the equilibrium vacancy and interstitial concentration values predicted, cannot explain in entirety the enhanced oxidation observed. This leads to the conclusion that a sole dominant defect theory does not hold true for a high temperature reactive environment.

A more likely hypothesis is a dual mechanism of generation and annihilation of nonequilibrium point defects as predicted by Hu [24]; i.e. the diffusion of one type of point defect into the bulk brings about the generation of another type of point defect to the surface to annihilate the creation of the former.

This is observed in the oxidation of silicon in water vapor [27] where its predicted that the diffusion of water molecules through the oxide is facilitated through the formation of a loose oxide layer, i.e. when the hydroxyl group reacts with the oxygen in the network, the interstitial spaces widen to incorporate the extra atoms.

In the oxidation of silicon in a dissociated oxygen environment, defects are formed continuously. Surface vacancies are created as atomic oxygen reacts with the surface Si-Si bonds. Within the lattice, the incorporation and/or removal of oxygen atoms can alter the strain energy. Also, studies have shown that the microstructure of the oxide grown in dissociated environments is different from that grown in molecular oxygen [28]. Therefore, a model incorporating this dual mechanism may more accurately describe the enhanced oxide growth rate.

Conclusions

The oxide growth rate of silicon in a dissociated oxygen gas environment is much higher than the rate predicted for silicon in molecular oxygen. While the Deal-Grove model can describe the transport process for molecular oxygen very well, it cannot be extended accurately to describe the enhanced growth observed when two oxidants are present.

Recent theoretical DFT studies have provided a lot of information on the formation energies, migration pathways and the most stable form of the oxidants. Using the new information, a parallel oxidation model, which included the diffusion and reaction of both oxidants at the surface, through the oxide and at the interface, was developed. The model was extended to include the recombination of atomic oxygen within the oxide. The calculations indicate that while a range of diffusivities, reaction rate constants and solubilities for atomic oxygen can numerically describe the process, they do not support the observations made in previous experimental and theoretical studies.

A combined and more rigorous formulation of the transient surface kinetics, bulk diffusion of the various defects in amorphous silica, the microstructural changes, and the energetics of the species, is essential to better understand the enhanced oxidation rate observed.

References

1. Bongiorno A., Forst C.J., Kalia R.K., Li J., Marschall J., Nakano A., Opeka M.M., Talmy I.G., Vashishta P., Yip S., *A perspective on modeling materials in extreme environments: oxidation of ultrahigh-temperature ceramics,* MRS Bulletin, **2006**, 31, 410-418.

2. Ogbuji L., Opila E.J., *A comparison of the oxidation kinetics of SiC and Si_3N_4,* J. Electrochem. Soc., **1995**, 142(3), 925-930.

3. Deal B.E., Grove A.S., *General relationship for the thermal oxidation of silicon,* J. Appl. Phys., **1965**, 36, 3770-3778.

4. Marschall J., George M.R., Rogers B.R., *Reaction-diffusion model for passive oxidation of silicon in partially-dissociated oxygen (in prep)*, **2008**, SRI International, Vanderbilt University.

5. Bongiorno A., Pasquarello A., *Reaction of the oxygen molecule at the Si(100)-SiO_2 interface during silicon oxidation,* Phys. Rev. Lett., **2004**, 93(8), 086102.

6. Costello J.A., Tressler R.E., *Isotope labeling studies of the oxidation of silicon at 1000° to 1300 °C,* J. Electrochem. Soc., **1984**, 131(8), 1944-1947.

7. Arasa C., Gamallo P., Sayos R., *Adsorption of atomic oxygen and nitrogen at β-Cristobalite (100): a density functonal theory study,* J. Phys. Chem. B, **2005**, 109, 14954-14964.

8. Bongiorno A., Pasquarello A., *Oxygen species in SiO_2: a first-principles investigation,* Microelectron. Eng., **2001**, 59, 167-172.

9. Choi C., Liu D.J., Evans J.W., Gordon M.S., *Passive and active oxidation of Si(100) by atomic oxygen: a theoretical study of possible reaction mechanisms*, J. Am. Ceram. Soc., **2002**, 124, 8730-8740.

10. Hamann, D., *Diffusion of atomic oxygen in SiO_2,* Phys. Rev. Lett., **1998**, 81(16), 3447-3450.

11. Tatsumura K., Shimura T., Mishima E., Kawamura K., Yamasaki D., Yamamota H., Watanabe T., Umeno M., Ohdomari I., *Reactions and diffusion of atomic and molecular oxygen in the SiO_2 network,* Phys. Rev. B, **2005**, 72, 045205.

12. Chelikowsky J.R., Chadi D.J., Binggeli N., *Oxygen configurations in silica,* Phys. Rev. B, **2000**, 62, R2251-2254.

13. Szymanski M.A., Stoneham A.M., Shulger A., *The different roles of charged and neutral atomic and molecular oxidising species in silicon oxidation from ab initio calculations,* Solid-state electron., **2001**, 45, 1233-1240.

14. Bongiorno A., Pasquarello A., *Energetics of oxygen species in crystalline and amorphous SiO_2: a first-principles investigation,* Solid-state electron., **2002**, 46, 1873-1878.

15. Han C.J., Helms C.R., *^{18}O tracer study of Si oxidation in dry O_2 using SIMS,* J. Electrochem. Soc., **1988,** 135(7), 1824-1832.

16. Rochet F., Agius B., Rigo S., *An ^{18}O study of the oxidation mechanism of Si in dry oxygen,* J. Electrochem. Soc., **1984**, 131(4), 914-923.

17. Trimaille I., Rigo S., *Use of ^{18}O isotopic labelling to study thermal dry oxidation of silicon as a function of temperature and pressure,* Appl. Surf. Sci., **1989**, 39, 65-80.

18. Kimura S., Murakami E., Warabisako T., Mitani E., Sunami H., *An ^{18}O study of oxygen exchange phenomena during microwave discharge plasma oxidation of silicon,* J. Appl. Phys., **1988**, 63(9), 4655-4660.

19. Bedra L., Balat-Pichelin M.J.H., *Comparative modeling study and experimental results of atomic oxygen recombination on silica-based surfaces at high temperatures*, Aerosp. Sci. Technol., **2005**, 9, 318-328.

20. Pallix J.B., Copeland R.A., *Measurement of catalytic recombination coefficients on quartz using laser-induced fluorescence,* J. Thermophys. Heat Transfer, **1996**, 10, 224-233.

21. Linnett J.W., Marsden D.G.H., *The kinetics of the recombination of oxygen atoms at a glass surface,* Proc. Royal Soc. Lond. A, **1956**, 234, 489-504.

22. Peeters J., Li L., *Oxidation of silicon in plasma afterglows: new model of oxide growth including recombination of diffusing O atoms,* J. Appl. Phys., **1993**, 73(5), 2477-2485.

23. Marschall, J., **2006**, SRI International, Menlo Park, CA.

24. Hu, S.M., *Vacancies and self-interstitials in silicon: generation and interaction in diffusion,* J. Electrochem. Soc., **1992**, 139(7), 2066-2075.

25. Richard N., Martin-Samos L., Roma G., Limoge Y., Crocombette J.P., *First principle study of neutral and charged self-defects in amorphous SiO_2,* J. Non-Cryst. Solids, **2005**, 351, 1825-1829.

26. Vora N.D., Marschall J., Rogers B.R., *(in prep.)*, Vanderbilt University.

27. Arslambekov V.A., Kazarinova I.D., Gorbunova K.M., *Oxidation of silicon,* Russian Chemical Reviews, **1972**, 41(1), 36-46.

28. Kisa M., Li L., Yang J., Minto T.K., Stratton W.G., Voyles P., Chen X., Benthem K., Pennycook S.J., *Homogeneous silica formed by the oxidation of Si(100) in hyperthermal atomic oxygen,* AIAA J. Spacecr. Rockets, **2006**, 43(2), 4315-435.

CHAPTER VI

CONCLUSIONS/FUTUREWORK

6.1. Conclusions

The development of a multilayer protection coating system for use with the existing C/C composites is imperative. Material for each layer has been selected based on its thermal and chemical properties [1, 2] but before the composite can be developed and studied, it is important to investigate if the materials are indeed suitable, what the associated processing challenges are for each layer and how they behave in oxidizing environments.

In this work the focus was on the reaction barrier layer of the multilayer system. This layer is adhered to the C/C composite and should prevent the diffusion of the carbon into the adjoining layers and serve as an oxidation barrier [2]. Hafnium carbide meets the requirements for this first layer [2]. Existing coating processes for hafnium carbide have not produced uniform, stoichiometric and defect free films [3-5] therefore alternative synthesis routes had to be explored.

In Chapter 2, the formation of hafnium carbide through the thermal treatment of hafnium thin film on graphite is studied. Unlike other refractory carbides , of equivalent bond energy and heats of formation, such as NbC and TiC [6-8], HfC could not be formed using this low cost technique. Possible explanations are that as the temperature was increased, oxygen diffusion into the film and carbon diffusion from the graphite substrate to the hafnium-graphite were the predominant processes over carbide formation

or that adequate thermal energy was not supplied. Oxygen diffusion was suppressed through the use of silicon nitride as a capping layer, but no carbide formation was observed. These results highlight the fact that the inherent problems of the C/C composite, i.e. defects, density, are as important as the problems associated with a coating process. The thermal treatment of the oxidized hafnium film with the carbon substrate did not produce hafnium carbide. While the Gibbs free energy value for the reaction of hafnium with carbon to produce hafnium carbide is negative, the Gibbs free energy value for the reaction of hafnia with carbon to form hafnium carbide is positive, indicating that the latter is not a spontaneous reaction [9].

An alternative thin film technique, pulsed laser deposition of hafnium carbide, was also studied. In this method the problem with the diffusion of carbon can be eliminated. The depositions were done using a HfC target and lasers of two wavelengths. The major processing problem associated with this technique was particulate formation. We identified that the 248 nm KrF laser is ideal for HfC depositions since the combination of low penetration depth and high absorption eliminates this problem. However, despite the use of various background gases, oxygen contamination and the loss of carbon from the film could not be prevented. The films were composed of free carbon, HfC and HfO_2. The presence of the HfC bonds in the film is the only difference from the oxycarbide layer that forms during the oxidation of chemical vapor deposited HfC at high temperatures. The main conclusions from this section were that even though theoretically HfC is the best reaction barrier material, it is very hard to synthesize it without oxygen contamination or excess carbon formation.

Irrespective of the temperature or the deposition technique, oxygen dissolution in hafnium carbide is an issue. One way to combat it while retaining the advantageous properties of hafnium carbide is to develop hafnium oxycarbide films. Theory states that for oxycarbides, the presence of free carbon in the oxide can be an obstacle to oxygen diffusion [10-14]. In Chapter IV, two methods of hafnium oxycarbide synthesis by PLD of HfO_2 target with varying carbon source inclusions were explored. The role of the free carbon was then investigated through oxidation experiments of the films. Preliminary investigation demonstrated that free carbon dissolved in lattice is burnt away even at low temperatures. Comparison of the oxidation behavior of hafnia to hafnium oxycarbide indicated that there is no major difference between the two. However if the carbon in the film was bonded to oxygen before oxidation, the carbon was retained in the film after oxidation. This may be due to difference in the bonds and structure of the carbon used; amorphous carbon versus graphite. This work indicated that the role of carbon varies depending on the type of process used to form the oxycarbide.

The studies on HfC thin film synthesis demonstrated that the oxidation behavior of hafnium carbide and its oxycarbides varies from technique to technique and is different from that observed in literature. Also, the quantity of oxygen present in the environment affects the final composition of the film.

While the influence of the quantity of oxidant on UHTC materials is important, the form of oxidant is equally important. Previous oxidation studies of UHTC materials in dissociated oxygen showed that the oxidation rate is enhanced and the types and the sequence in which oxides form and disappear are vastly different from the oxidation sequence in molecular oxygen [15]. However, a theoretical description for the oxidation

mechanism for these composites is not fully understood [15]. In the second part to this work, studies were initiated to understand this phenomenon for a subset of UHTCs; silica formers. Silicon oxidation was chosen as the starting point since considerable experimental and theoretical work on silicon oxidation is available to build upon.

In Chapter V, the oxidation behavior of silicon in molecular oxygen is compared to that in atomic oxygen in the temperature range of 910-1150 °C. Silicon oxide growth in atomic oxygen is enhanced compared to oxidation in molecular oxygen. A possible explanation is that the processes that transport these species through the oxide layer are different. Theory and isotope tracer experiments [16-27] have shown that molecular oxygen diffuses through interstitials while atomic oxygen through networks. However, the concentration of each defect and the interrelationship between the two are unknown. The experimental data are used along with the theoretical findings to develop a transport and reaction model. The parameters associated with atomic oxygen, solubility, diffusivity and reaction rate constants, were unknown and therefore a wide range of values for each were tested. Two hypotheses were explored: (1) no interaction between the oxidants occurs as they diffuse through the oxide, and (2) atomic oxygen recombines within the oxide to form molecular oxygen which then becomes the predominant defect present. However, neither model could adequately describe the enhanced oxide growth rates. The computations indicate that a more complex interdependency between the point defects exist and that the alteration of the microstructure of the growing oxide should be included into the model for a more complete and accurate description of the oxidation process.

6.2. Futurework

6.2.1. Synthesis of hafnium carbide

There are multiple avenues that still need to be explored to determine the suitability of hafnium carbide and its resulting oxycarbide for hypersonic applications. These are outlined below.

(i) The formation of HfC_x thin films

Solid state reactions of Hf with C to form HfC are still an advantageous route due to the low costs and reproducibility of the technique. Also, such studies would help confirm whether the theoretically identified function of the HfC layer as a barrier to the carbon diffusing from the C/C composites holds true. Studies should be conducted on altering the microstructure of the deposited hafnium film such that oxygen can interact with the atoms on the surface to form a native oxide but no oxygen diffuses to the carbon and hafnium interface. More annealing studies should then be done with these hafnium films in order to determine whether hafnium carbide films can form at the interface between the two materials. Repeating the experiments with the dense and highly ordered pyrolytic graphite (HOPG) substrate is also beneficial and will help answer the question of whether the interface roughening was more dominant than the carbide formation.

(ii) The formation of HfO_xC_y films

The retention of the carbon in the oxycarbide film produced by PLD from the binary target is opposite to what was observed in the oxycarbide film deposited using a

gaseous carbon source. This demonstrates that technique used to develop the oxycarbide plays a role in its behavior. Therefore alternative synthesis routes have to be explored.

Previous studies have been done by Blum and co-workers [28], where carbon enriched silicon oxycarbide was formed from the dehydrocoupling and hydrosilylation reactions of polyhydridomethylsiloxane (PHMS). The oxidation studies of these polymer-derived ceramics indicated that the presence of free carbon in the domains made the material more resistance to oxidation. These results are similar to that observed in the oxidation of hafnium carbide. Therefore, investigations of whether hafnium oxycarbide could be developed following a similar synthesis process would be highly beneficial. Study of the oxidation behavior of hafnium oxycarbides should then follow.

6.2.2. Oxidation Studies

While material synthesis is one aspect of UHTC development, understanding the oxidation behavior of the materials studied in this work, silicon and hafnium carbide, is equally important.

(i) Understanding the role of bound and unbound carbon in HfO_xC_y upon oxidation

Previous oxidation studies of HfC have shown that the hafnium oxycarbide layer always forms between the underlying carbide and the outer hafnium oxide; thereby protecting the carbide from further oxidation [10-14]. However, our oxidation studies of the stand-alone hafnium oxycarbide films formed by PLD show that compared to the hafnia film, during oxidation the only delay to the onset of oxidation is the removal of carbon from the oxycarbide before the film converts to an oxide. The question of whether

the outer hafnia layer aids in the role of oxidation barrier to the oxycarbide itself has not been explored. Therefore, the use of the deposited hafnium oxycarbide in a composite: silicon/hafnium oxycarbide/ amorphous capping layer should be explored. Possible capping layers are amorphous silicon nitride and silica thin films. Amorphous silicon nitride functions as an oxygen diffusion barrier. Therefore any mass loss or gain observed in the TG curves upon oxidation could be attributed to the appropriate layer. Both materials are also commonly used as additives during the sintering of UHTC composites [29], therefore obtaining knowledge of the materials interaction with hafnium oxycarbide is useful. An oxide capping layer could mimic the composite that forms during the oxidation of hafnium carbide and could help in determining whether the presence of excess oxygen would increase or decrease the rate of oxidation of the hafnium oxycarbides at the temperatures of interest.

While the studies outlined above can provide more experimental data on whether oxycarbide films developed by PLD can be effective oxidation barrier coatings, it does not entirely provide insight on both the oxycarbide formation and the role of the carbon upon oxidation. Annealing and oxidation studies of carbon implanted hafnia should be performed. Using this method, the quantity and distribution of carbon in the oxide can be controlled.

(ii) The effect of atomic oxygen on the oxidation behavior of silicon

The oxidation behavior of silicon in molecular oxygen has been thoroughly explored and understood. However, the behavior of silicon in atomic oxygen cannot be physically explained. In this work, the currently available experimental and theoretical

study results [16-27] were used towards building a model however it failed to accurately describe the enhanced oxide growths observed.

Since the oxide growth in molecular oxygen is also larger than that predicted by Deal-Grove [30], one hypothesis is that the flow dynamics in the tube furnace may also play an important role in the transport of oxidants to the surface of the silicon. As a first step, a more complete model incorporating the gas phase chemistry, the silicon surface kinetics along with the oxide transport and reaction processes should be developed. Information on the first two components can be determined from the model developed by Vora and co-workers [31] to characterize the flow of molecular and atomic oxygen in the tube furnace used in these experiments.

The interdependency of vacancy and interstitial formation and annihilation and how these processes alter the microstructure of the growing oxide is another facet that has to be theoretically modeled. Developing such a model is complex and would involve using advanced materials modeling knowledge and large-scale computing capabilities.

References

1. Bird R.K., Wallace T.A., Sankaran S.N., *Development of protective coatings for high-temperature metallic materials,* J. Spacecr. Rockets, **2004**, 41(2), 214-220.

2. Schwartz, M., New Materials Processes, and Methods Technology, 1st ed., CRC Press, Taylor & Francis Group, 2006, p. 77-171.

3. Spatenka P., Suhr H., Erker G., Rump M., *Formation of hafnium carbide thin films by plasma enhanced chemical vapor deposition,* Appl. Phys. A, **1995**, 60(3), 285-288.

4. Pierson, H.O., Handbook of refractory carbides and nitrides: properties, characteristics, processing, and applications, Noyes Publications, Park Ridge, New Jersey, 1996.

5. Teghil R., Santagata A., Zaccagnino M., Barinov S.M., Marotta V., De Mari G., *Hafnium carbide hard coatings produced by pulsed laser ablation and deposition,* Surf. Coat. Technol., **2002**, 151-152, 531-533.

6. Leroy W.P., Detavernier C., Van Meirhaeghe R.L., *Thin film solid-state reactions forming carbides as contact materials for carbon-containing semiconductors,* J. Appl. Phys., **2007**, 101, 0537141-05371410.

7. Barzilai S., Raveh A., Frage N., *Annealing of niobium coatings deposited on graphite*, Vacuum, **2005**, 79, 171-177.

8. Viljoen P.E., Lambers E.S., Holloway P.H., *Reaction between diamond and titanium for ohmic contact and metallization adhesion layers*, J. Vac. Sci. Technol. B, **1994**, 12(5), 2997-3005.

9. Wang C.R., Yang J.M., Hoffman W., *Thermal stability of refractory carbide/boride composites*, Mater. Chem. Phys., **2002**, 74(3), 272-281.

10. Shimada, S., *A thermoanalytical study on the oxidation of ZrC and HfC powders with formation of carbon,* Solid State Ionics, **2002**, 149, 319-326.

11. Shimada, S., *Interfacial reaction on oxidation of carbides with formation of carbon*, Solid State Ionics, **2001**, 141-142, 99-104.

12. S. Shimada, Inagaki M., *Oxidation kinetics of hafnium carbide in the temperature range of 480° to 600 °C*, J. Am. Ceram. Soc., **1992**, 75(10), 2671-2678.

13. S. Shimada, Yunazar F., *Oxidation of hafnium carbide and titanium carbide single crystals with the formation of carbon at high temperatures and low oxygen pressures*, J. Am. Ceram. Soc., **2000**, 83(4), 721-728.

14. Bargeron C.B., Benson R.C., Jette A.N., Phillips T.E., *Oxidation of hafnium carbide in the temperature range 1400-2060 °C*, J. Am. Ceram. Soc., **1993**, 76(4), 1040-1046.

15. Bongiorno A., Forst C.J., Kalia R.K., Li J., Marschall J., Nakano A., Opeka M.M., Talmy I.G., Vashishta P., Yip S., *A perspective on modeling material in extreme environments: oxidation of ultrahigh-temperature ceramics*, MRS Bulletin, **2006**, 31, 410-418.

16. Bongiorno A., Pasquarello A., *Oxygen species in SiO_2: a first-principles investigation*, Microelectron. Eng., **2001**, 59, 167-172.

17. Bongiorno A., Pasquarello A., *Oxygen diffusion through the disordered oxide network during silicon oxidation*, Phys. Rev. Lett., **2002**, 88(12), 125901.

18. Bongiorno A., Pasquarello A., *Energetics of oxygen species in crystalline and amorphous SiO_2: a first-principles investigation*, Solid-state electron., **2002**, 46, 1873-1878.

19. Bongiorno A., Pasquarello A., *Reaction of the oxygen molecule at the Si(100)-SiO_2 interface during silicon oxidation*, Phys. Rev. Lett., **2004**, 93(8), 086102.

20. Bongiorno A., Pasquarello A., *Multiscale modeling of oxygen diffusion through the oxide during silicon oxidation*, Phys. Rev. B, **2004**, 70, 195312.

21. Han C.J., Helms C.R., *^{18}O tracer study of Si oxidation in dry O_2 using SIMS*, J. Electrochem. Soc., **1988**, 135(7), 1824-1832.

22. Rochet F., Agius B., Rigo S., *An ^{18}O study of the oxidation mechanism of Si in dry oxygen*, J. Electrochem. Soc., **1984**, 131(4), 914-923.

23. Trimaille I., Rigo S., *Use of ^{18}O isotopic labelling to study thermal dry oxidation of silicon as a function of temperature and pressure*, Appl. Surf. Sci., **1989**, 39, 65-80.

24. Costello J.A., Tressler R.E., *Isotope labeling studies of the oxidation of silicon at 1000° to 1300 °C*, J. Electrochem. Soc., **1984**, 131(8), 1944-1947.

25. Ganem J.J., Battistig G., Rigo S., Trimaille I., *A study of the initial stages of the oxidation of silicon using $^{18}O_2$ and RTP*, Appl. Surf. Sci., **1993**, 65/66, 647-653.

26. Imai K., Yamabe K., *$^{18}O_2$ isotope labeling studies of stress effect on oxidation kinetics*, J. Appl. Phys., **1998**, 83(7), 3849-3855.

27. Kimura S., Murakami E., Warabisako T., Mitani E., Sunami H., *An ^{18}O study of oxygen exchange phenomena during microwave discharge plasma oxidation of silicon*, J. Appl. Phys., **1988**, 63(9), 4655-4660.

28. Blum Y.D., MacQueen D.B., Kleebe H.J., *Synthesis and characterization of carbon-enriched silicon oxycarbides*, J. Euro. Ceram Soc., **2005**, 25, 143-149.

29. Gasch M.J., Ellerby D.T., Johnson S.M., Ultra High Temperature Ceramic Composites, Handbook of Ceramic Composites, Vol. 2, Springer, US, 2005, p. 197-224.

30. Deal B.E., Grove A.D., *General relationship for the thermal oxidation of silicon*, J. Appl. Phys., **1965**, 36, 3770-3778.

31. Vora N.D., Marschall J., Rogers B.R., *(in prep.)*, Vanderbilt University.